Department of Physics and Astronomy
Georgia State University
Atlanta, GA 30303-3083

**Support:**

# Nanoplasmonics: Fundamentals and Applications

**Mark I. Stockman**

Department of Physics and Astronomy and
Center for Nano-Optics (CeNO)
Georgia State University, Atlanta, GA 30303, USA

# •CONTENTS

Department of Physics and Astronomy
Georgia State University
Atlanta, GA 30303-3083

Meet the Author in his natural habitat:

# CONTENTS OF THE COURSE

- Lecture 1: **Introduction to Nanoplasmonics**
- Lecture 2**: Spaser: Fundamentals and Applications**

# LECTURE 1

**•Introduction to Materials for Nanoplasmonics**

1. Introduction
    - 1.1. Problem of nanolocalization of optical energy
    - 1.2. Surface plasmons and enhanced optical fields
    - 1.3. Applications of surface plasmonics

Department of Physics and Astronomy
Georgia State University
Atlanta, GA 30303-3083

# PROBLEMS IN NANOOPTICS

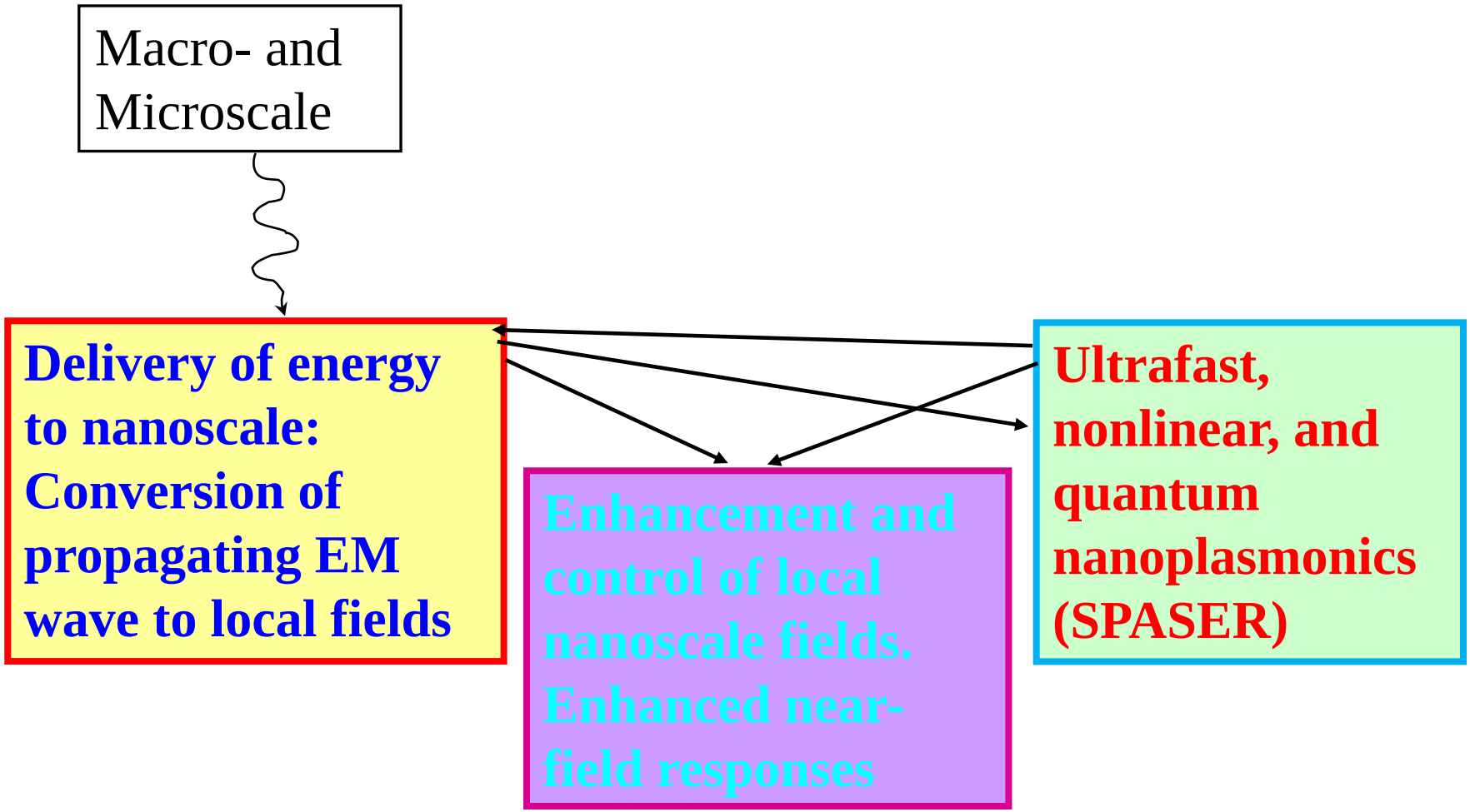

Department of Physics and Astronomy
Georgia State University
Atlanta, GA 30303-3083

M. I. Stockman, *Nanoplasmonics: The Physics Behind the Applications*, Phys. Today **64**, 39-44 (2011).

# Nanoplasmonics in a nano-nutshell

## Concentration of optical energy on the nanoscale

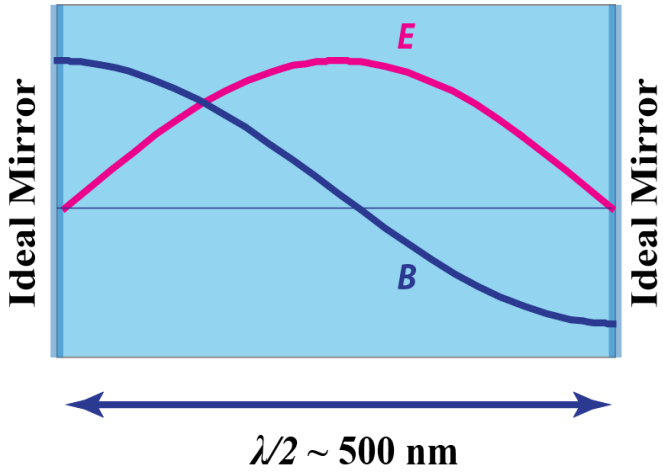


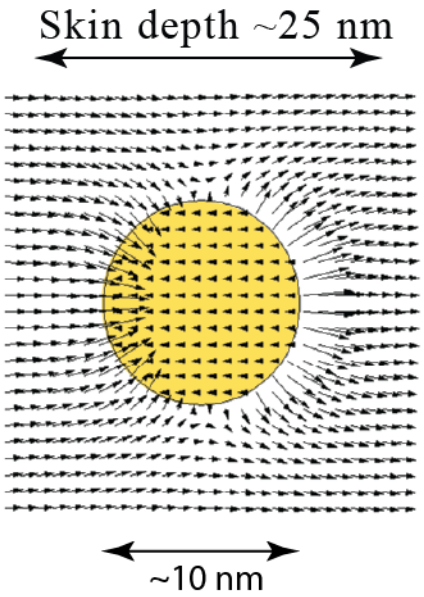


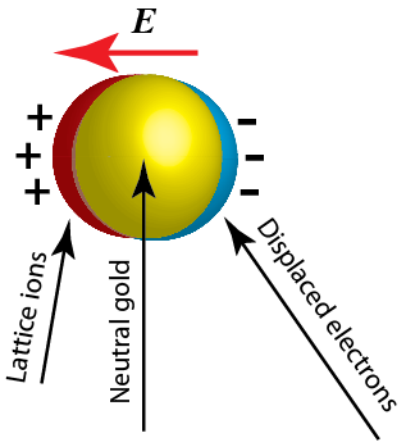


Photon: Quantum of electromagnetic field

Surface Plasmon: Quantum of electromechanical oscillator

# Nanoplasmonics in a nano-nutshell

Enhanced Local Fields in Proximity of Metal Nanoparticle are Nanoscale-Localized

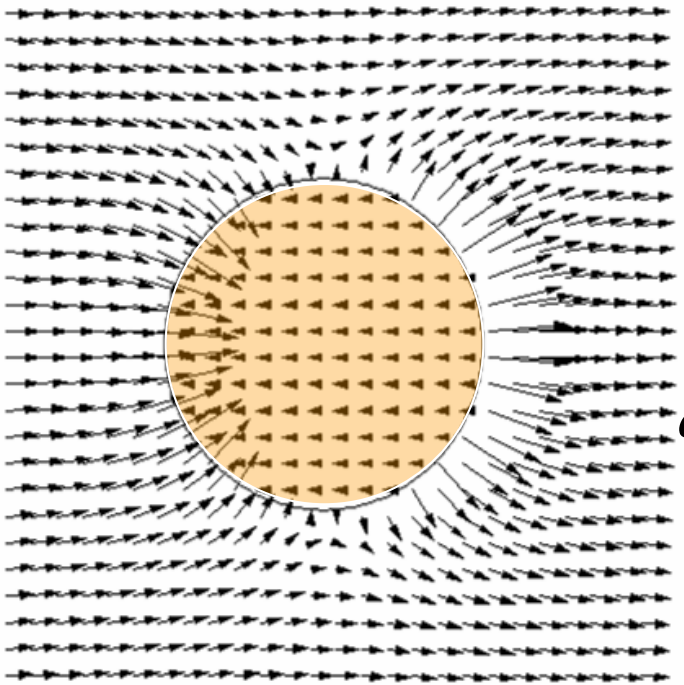

Wavelength, ~1000 nm

Mean free path, ~40 nm

Skin depth, ~25 nm

Nanoplasmonics: ~10 nm

$v_F/\omega$ Spatial dispersion/Nonlocality radius, ~1 nm

Polarizability:

$$\alpha = R^3 \frac{\varepsilon_m - \varepsilon_d}{\varepsilon_m + 2\varepsilon_d}, \quad \varepsilon_m = -2\varepsilon_d$$

Field enhancement or Quality factor:

$$Q = \frac{-\operatorname{Re}\varepsilon_m}{\operatorname{Im}\varepsilon_m} \sim 10-100$$

Localized Surface Plasmon:

Lattice

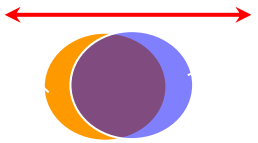

Electrons

Department of Physics and Astronomy
Georgia State University
Atlanta, GA 30303-3083

## Lycurgus Cup (4th Century AD): Roman Nanotechnology

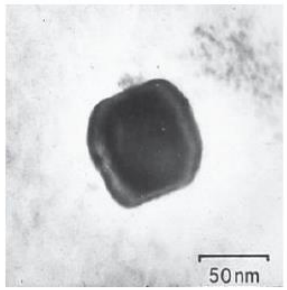


I. Freestone, N. Meeks, M. Sax, and C. Higgitt, *The Lycurgus Cup - a Roman Nanotechnology*, Gold Bull. **40**, 270-277 (2007)



Nanoplasmonic colors are very bright. Scattering and absorption of light by them are very strong. This is due to the fact that all of the millions of electrons move in unison in plasmonic oscillations Nanoplasmonic colors are also eternal: metal nanoparticles are stable in glass: they do not bleach and do not blink. Gold is stable under biological conditions and is not toxic *in vivo*

## Colors of Silver Nanocrystals and Gold Nanoshapes

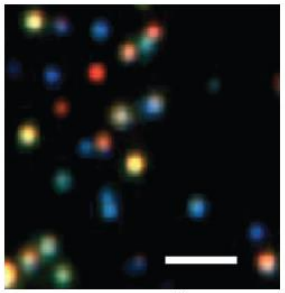


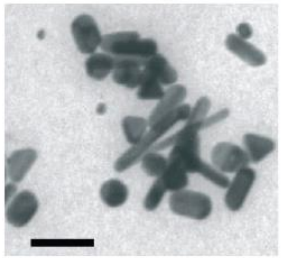


C. Orendorff, T. Sau, and C. Murphy, *Shape-Dependent* ..., Small **2**, 636-639 (2006)

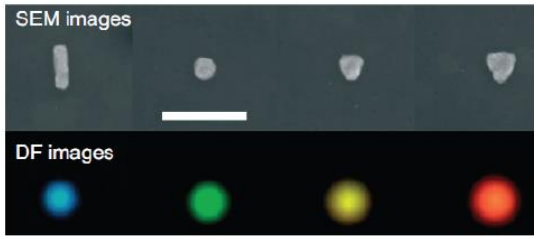


Scanning electron microscopy

Dark field optical microscopy

W. A. Murray and W. L. Barnes, *Plasmonic Materials*, Adv. Mater. **19**, 3771-3782 (2007) [Scale bar: 300 nm]

# Eternal nanoplasmonic colors (Notre Dame de Paris)

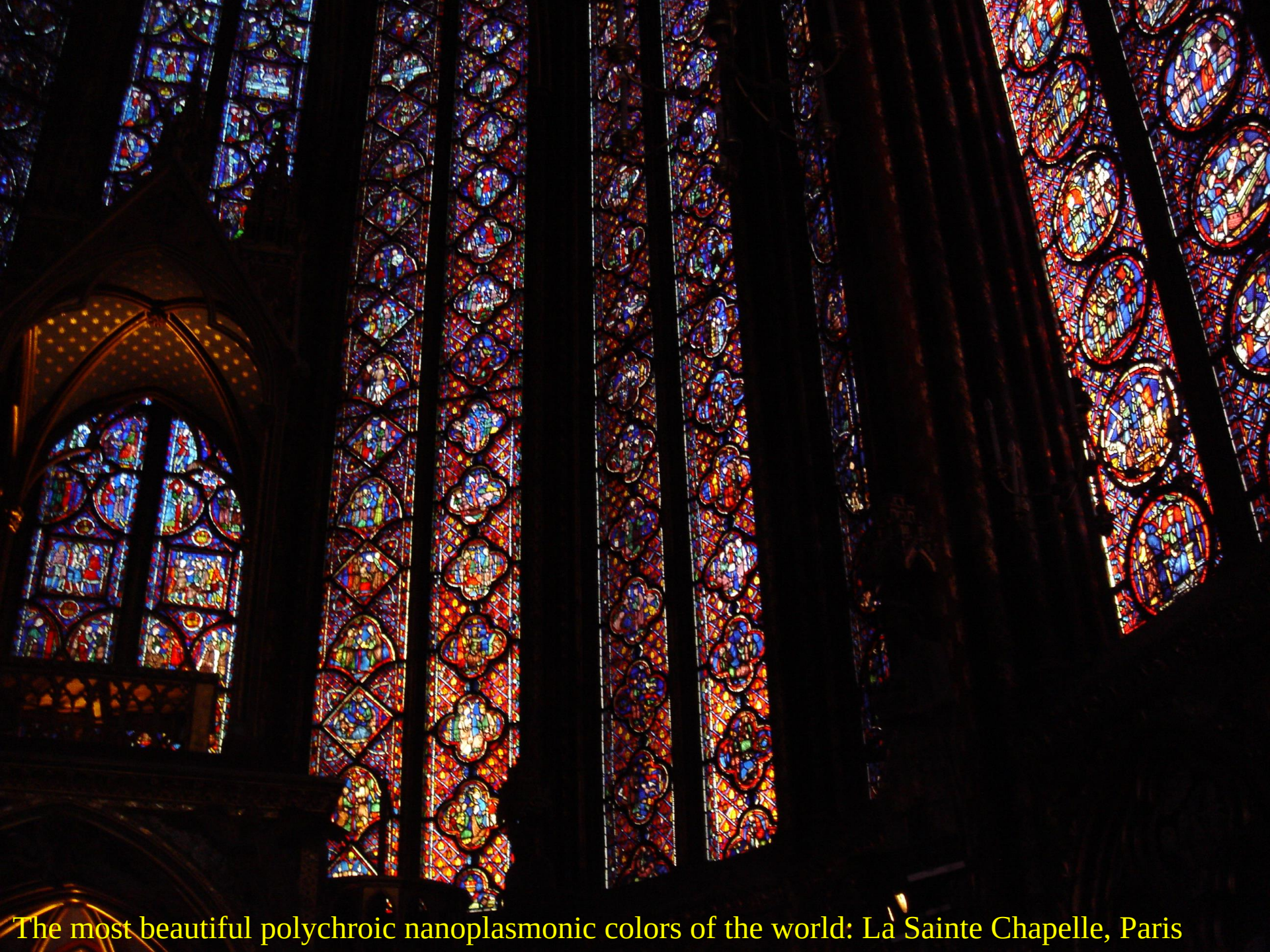

The most beautiful polychroic nanoplasmonic colors of the world: La Sainte Chapelle, Paris

Department of Physics and Astronomy
Georgia State University
Atlanta, GA 30303-3083

# Chagall Windows

Hadassah Hospital Jerusalem

Department of Physics and Astronomy
Georgia State University
Atlanta, GA 30303-3083

# Plasmonic Hot Spots

## Happy 23h Anniversary!

- D. P. Tsai *et al.*, *Phys. Rev. Lett.* **72**, 4149 (1994)
- M. I. Stockman et al., *Phys. Rev. Lett.* **75**, 2450 (1995)
- M. I. Stockman, L. N. Pandey, and T. F. George, Phys. Rev. B **53**, 2183-2186 (1996)

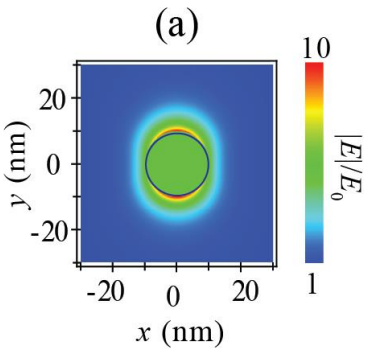


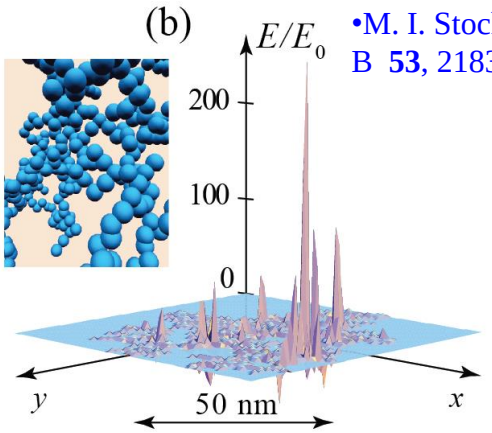


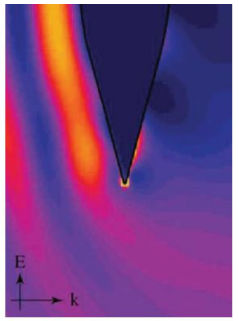


L. Novotny and S. J. Stranick, Annual Rev. Phys. Chem. **57**, 303-331 (2006)

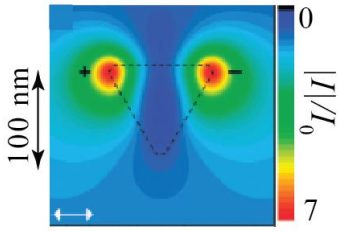


M. Rang et al., Nano Lett. **8**, 3357 (2008)

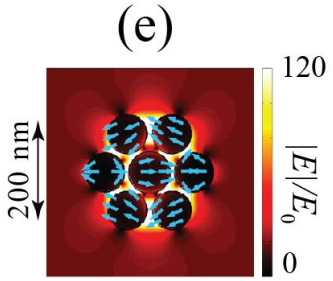


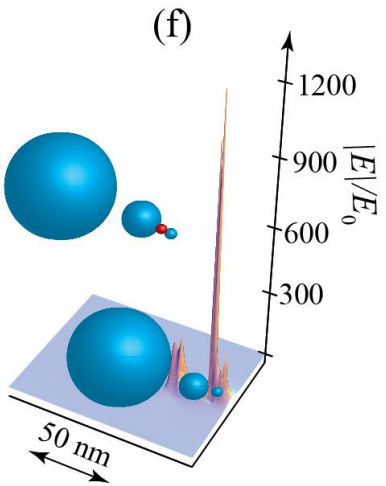


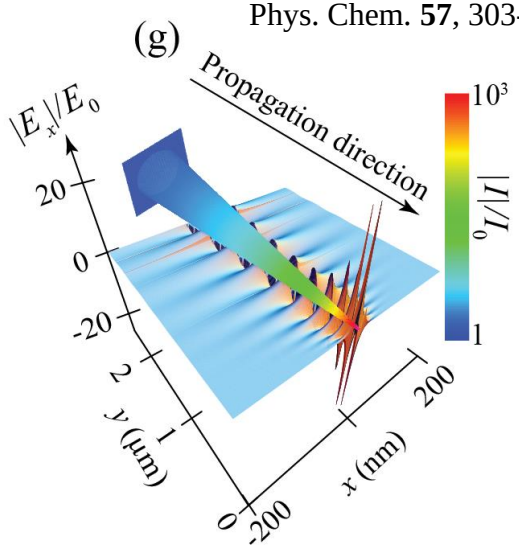


- J. A. Fan et al., Science **328**, 1135 (2010)
- M. Hentschel et al., Nano Lett. **10**, 2721 (2010)

K. Li, M. I. Stockman, and D. J. Bergman, Phys. Rev. Lett. **91**, 227402 (2003)

M. I. Stockman, Phys. Rev. Lett. **93**, 137404 (2004)

Department of Physics and Astronomy
Georgia State University
Atlanta, GA 30303-3083

A. Kubo, K. Onda, H. Petek, Z. Sun, Y. S. Jung, and H. K. Kim, *Femtosecond Imaging of Surface Plasmon Dynamics in a Nanostructured Silver Film*, Nano Lett. 5, 1123 (2005).

**200 nm**

**30 femtoseconds from life of a nanoplasmonic systems**

**Localized SP hot spots are deeply subwavelength as seen in PEEM (photoemission electron microscope)**

Delay

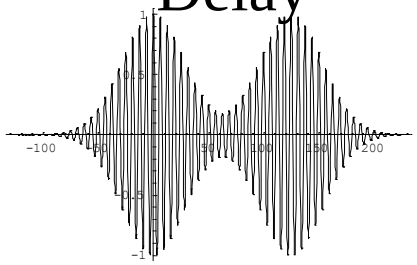


**PEEM Image as a Function of Delay (250 as per frame)**

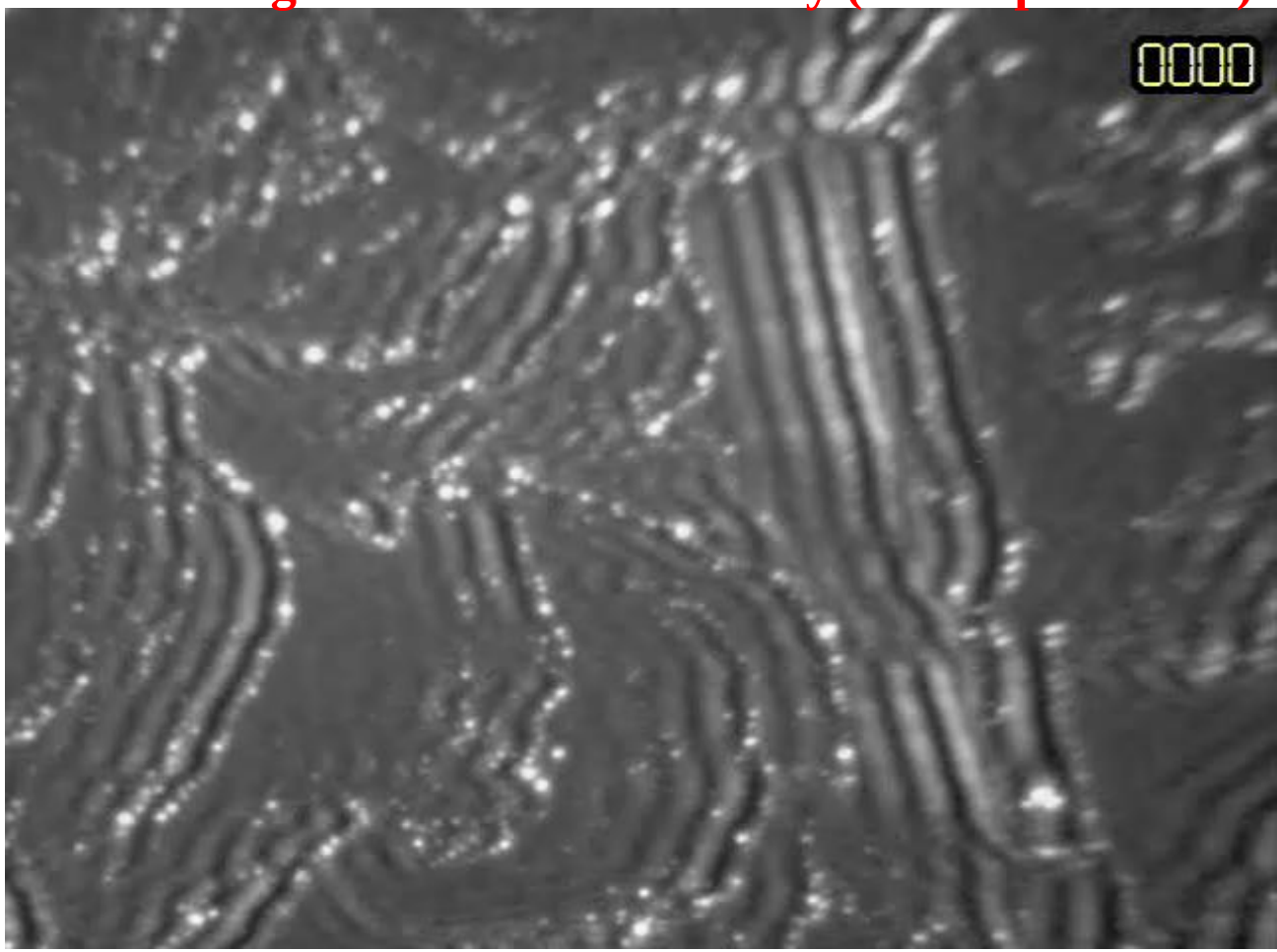

## Applications of Nanoplasmonics:

1. Ultrasensitive and express sensing and detection using both SPPs and SPs (LSPRs): see,e.g., J. N. Anker, W. P. Hall, O. Lyandres, N. C. Shah, J. Zhao, and R. P. Van Duyne, *Biosensing with Plasmonic Nanosensors*, Nature Materials 7, 442-453 (2008);
2. NSOM (SNOM)
3. Nanoantennas: Coupling of light to nanosystems. Extraction of light from LEDs and lasers [N. F. Yu, J. Fan, Q. J. Wang, C. Pflugl, L. Diehl, T. Edamura, M. Yamanishi, H. Kan, and F. Capasso, *Small-Divergence Semiconductor Lasers by Plasmonic Collimation*, Nat. Phot. 2, 564-570 (2008)]; nanostructured antennas for photodetectors and solar cells; heat-assisted magnetic memory [W. A. Challener *et al.*, Nat. Photon. 3, 220 (2009)]
4. Photo- and chemically stable labels and probes for biomedical research and medicine
5. Nanoplasmonic-based immunoassays and tests. Home pregnancy test (dominating the market), PSA test (clinic), troponin heart-attack test, and HIV tests (in trials)
6. Near perspective: Generation of EUV and XUV pulses
7. Thermal cancer therapy: L. R. Hirsch, R. J. Stafford, J. A. Bankson, S. R. Sershen, B. Rivera, R. E. Price, J. D. Hazle, N. J. Halas, and J. L. West, *Nanoshell-Mediated Near-Infrared Thermal Therapy of Tumors under Magnetic Resonance Guidance*, Proc. Natl. Acad. Sci. USA 100, 13549-13554 (2003). C. Loo, A. Lowery, N. Halas, J. West, and R. Drezek, *Immunotargeted Nanoshells for Integrated Cancer Imaging and Therapy*, Nano Lett. 5, 709-711 (2005)

Department of Physics and Astronomy
Georgia State University
Atlanta, GA 30303-3083

# Nanosensors based on enhanced local fields

Surface plasmon frequency shifts to red upon molecules adhesion

$$\omega_p = \frac{\omega_{0p}}{\sqrt{\varepsilon_d}}$$

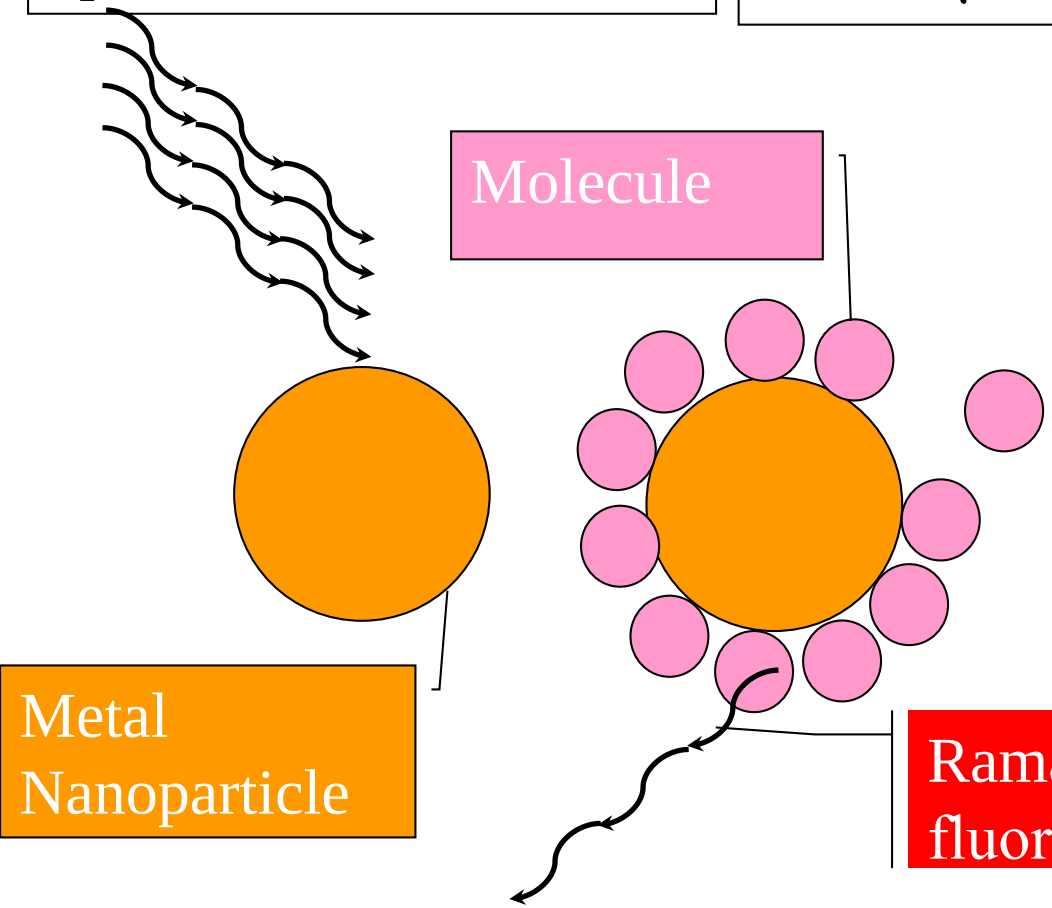


•X. Zhang, M. A. Young, O. Lyandres, and R. P. Van Duyne, *Rapid Detection of an Anthrax Biomarker by Surface-Enhanced Raman Spectroscopy*, Journal of American Chemical Society **127**, 4484 (2005).

•C. R. Yonzon, C. L. Haynes, X. Y. Zhang, J. T. Walsh, and R. P. Van Duyne, *A Glucose Biosensor Based on Surface-Enhanced Raman Scattering*, Anal. Chem. **76**, 78-85 (2004).

Department of Physics and Astronomy
Georgia State University
Atlanta, GA 30303-3083

# Use of Enhanced Local Fields for Nano-Microscopy

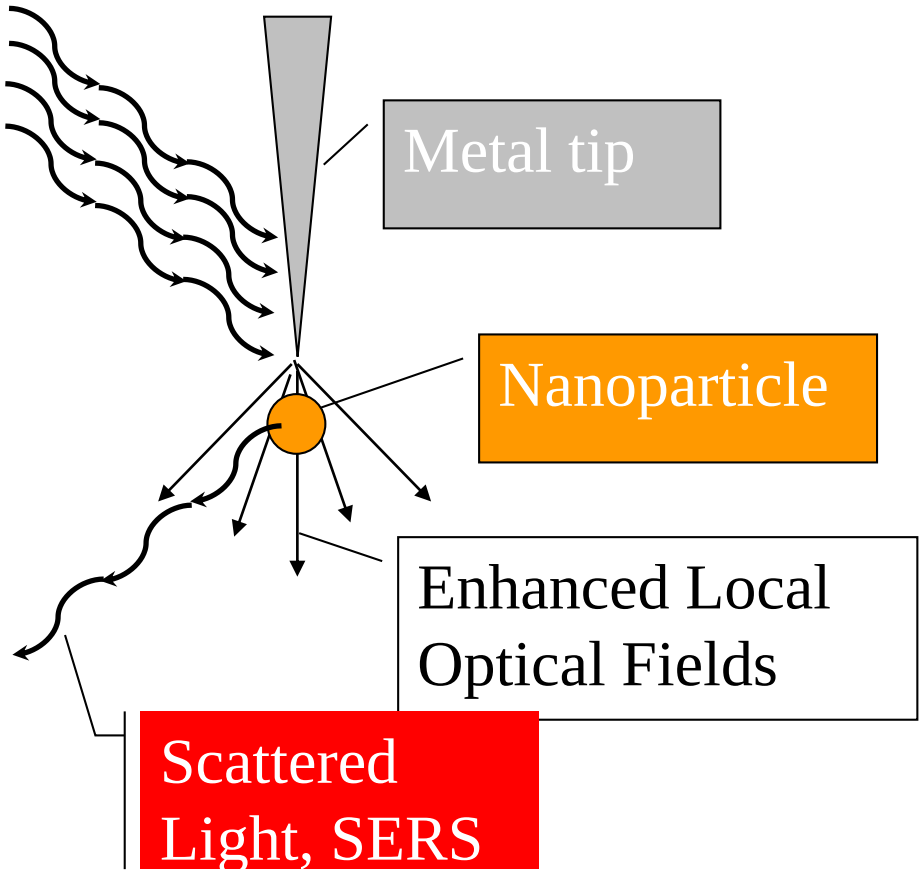


•L. Novotny and S. J. Stranick, *Near-Field Optical Microscopy and Spectroscopy with Pointed Probes*, Annual Rev. Phys. Chem. **57**, 303-331 (2006).

•A. Hartschuh, E. J. Sanchez, X. S. Xie, and L. Novotny, *High-Resolution Near-Field Raman Microscopy of Single-Walled Carbon Nanotubes*, Phys. Rev. Lett. **90**, 095503 -1-4 (2003).

Nanoscale

NANONICS IMAGING Ltd.

NSOM images of healthy human dermal fibroblasts in liquid obtained in transmission mode with a Nanonics cantilevered tip with a gold nanosphere

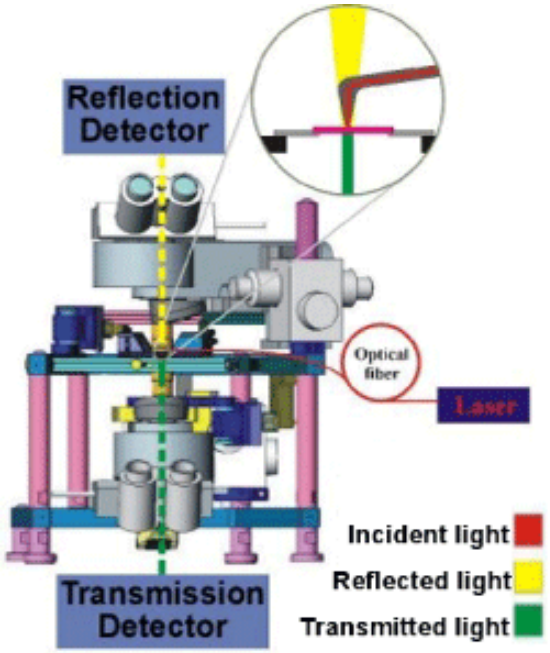


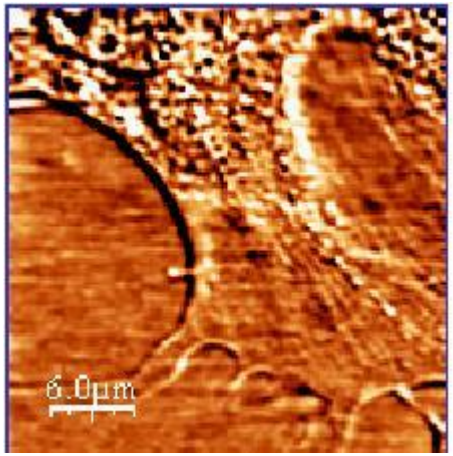


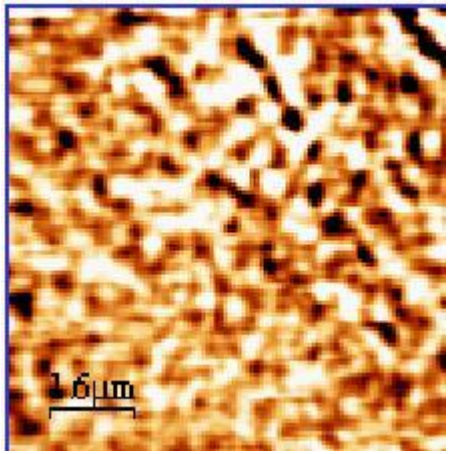

NeuroImage 49 (2010) 517–524

Contents lists available at ScienceDirect

NeuroImage

journal homepage: www.elsevier.com/locate/ynimg

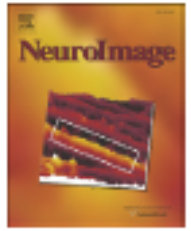


# Novel approaches for scanning near-field optical microscopy imaging of oligodendrocytes in culture

E. Trevisan [a], E. Fabbretti [b,c], N. Medic [d], B. Troian [e], S. Prato [e], F. Vita [f], G. Zabucchi [d], M. Zweyer [a,*]

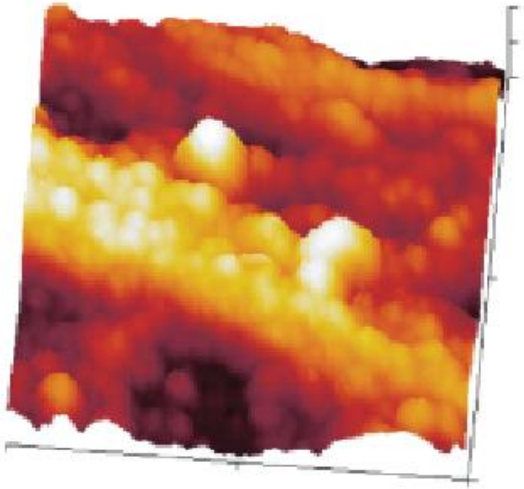

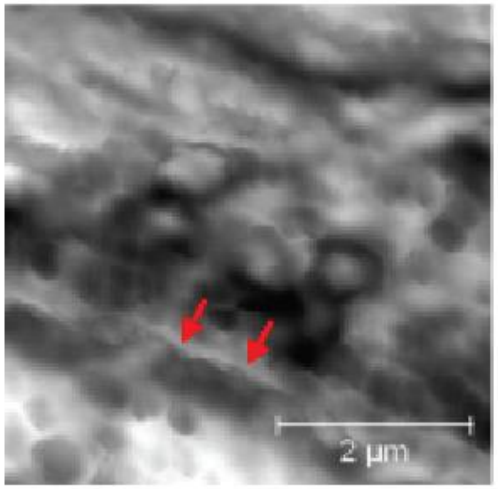


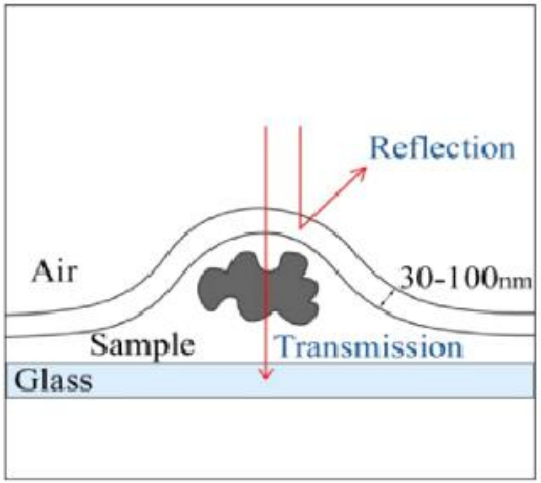

Department of Physics and Astronomy
Georgia State University
Atlanta, GA 30303-3083

# *Chirality Changes in Carbon Nanotubes Studied with Near-Field Raman Spectroscopy*

Neil Anderson, Achim Hartschuh, and Lukas Novotny

Nano Lett. 577 – 582 (2007); DOI: 10.1021/nl0622496

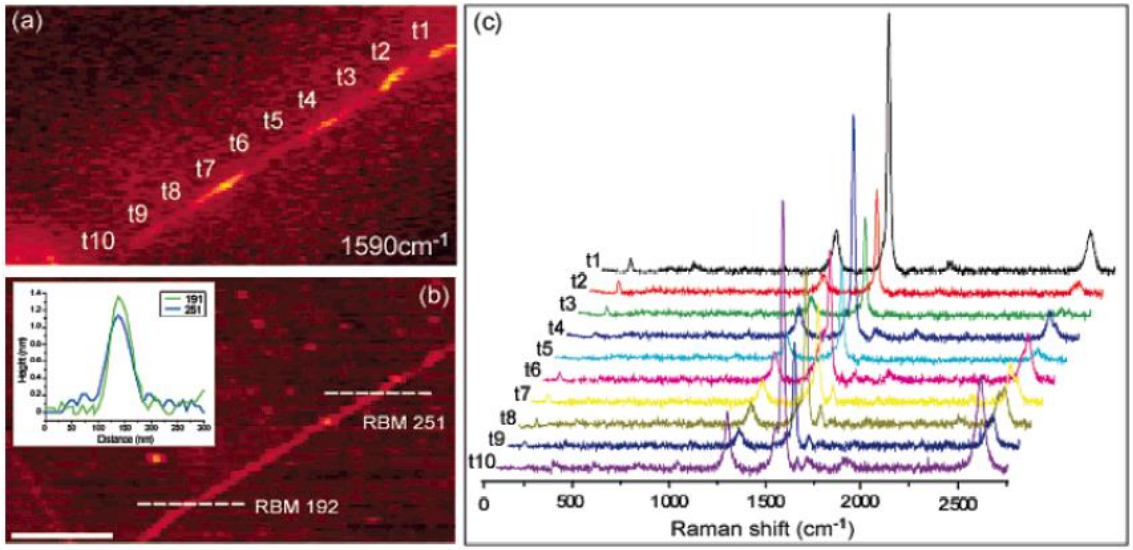


**Figure 1.** Near-field Raman imaging and spectroscopy: near-field Raman image (a) and corresponding topography image (b) of an isolated SWNT, where the optical resolution was determined to be 40 nm (fwhm). Also shown are a series of tip-enhanced Raman spectra (c) acquired along the length of the SWNT. From the recorded spectra, two resonant RBM phonons are detected. One RBM phonon frequency is detected at 251 $cm^{-1}$, from which we assign a semiconducting chirality. The second RBM phonon frequency recorded from the lower section of the SWNT is centered at 192 $cm^{-1}$, from which we assign a metallic chirality. See main text for details. The inset of (b) displays two cross-sectional profiles acquired from both the upper and lower sections, respectively, revealing that the expected diameter change occurs as the SWNT undergoes the transition from a semiconducting to metallic chirality. Scale bar denotes 200 nm and is valid for both (a) and (b).

Next generation of scanning near-field optical microscopy (SNOM) with chemical mapping:

Adiabatic concentration of optical energy and giant surface-enhanced Raman scattering (SERS); resolution 7 nm.s

(to be discussed in the course)

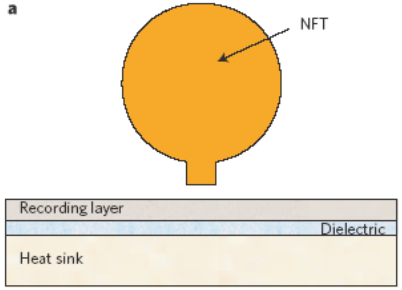


nature photonics
ARTICLES
PUBLISHED ONLINE: 22 MARCH 2009 | DOI: 10.1038/NPHOTON.2009.26

# Heat-assisted magnetic recording by a near-field transducer with efficient optical energy transfer

W. A. Challener*, Chubing Peng, A. V. Itagi, D. Karns, Wei Peng, Yingguo Peng, XiaoMin Yang, Xiaobin Zhu, N. J. Gokemeijer, Y.-T. Hsia, G. Ju, Robert E. Rottmayer, Michael A. Seigler and E. C. Gage

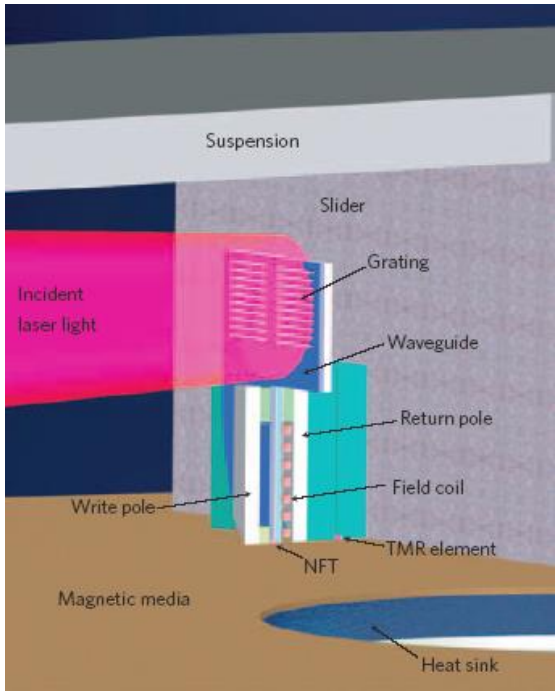


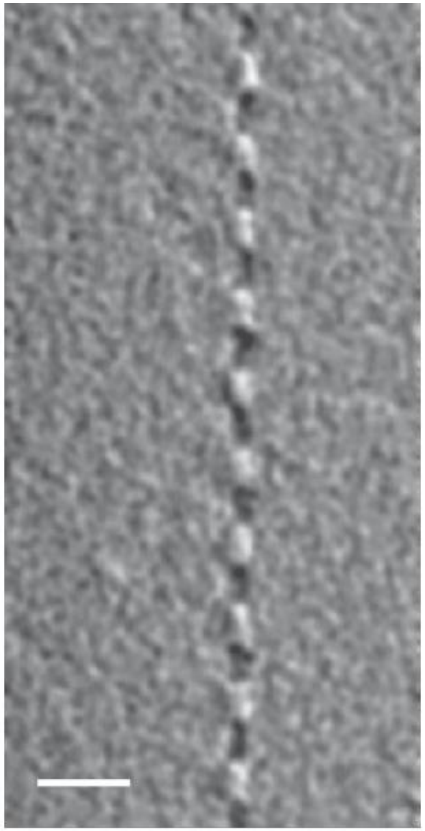

MFM image of a recorded track. The track width is ~70
300 nm.

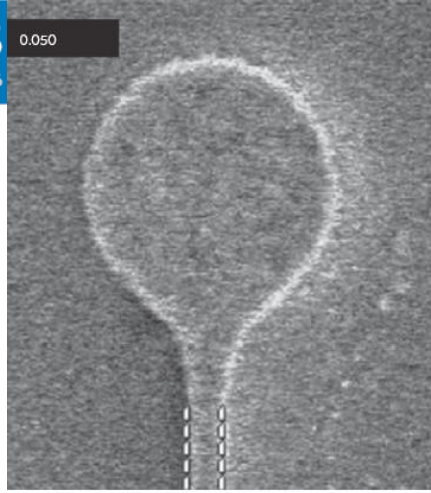


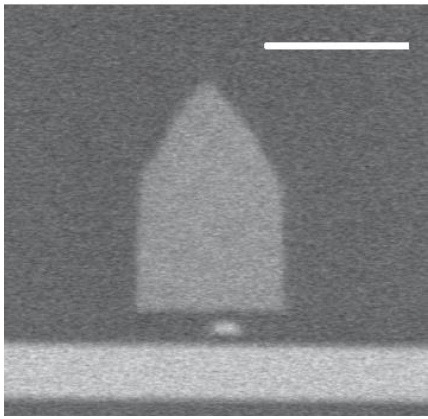

# Nanometre-scale germanium photodetector enhanced by a near-infrared dipole antenna

nature photonics | VOL 2 | APRIL 2008 | www.nature.com/naturephotonics

LIANG TANG[1]*, SUKRU EKIN KOCABAS[1], SALMAN LATIF[1], ALI K. OKYAY[2], DANY-SEBASTIEN LY-GAGNON[1], KRISHNA C. SARASWAT[2] AND DAVID A. B. MILLER[1]

[1]Ginzton Laboratory, Stanford University, Stanford, California 94305, USA

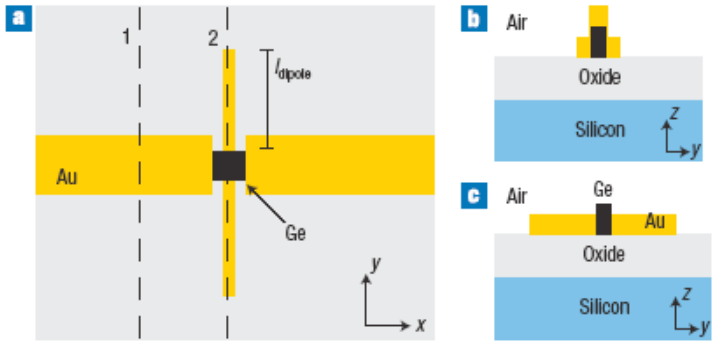


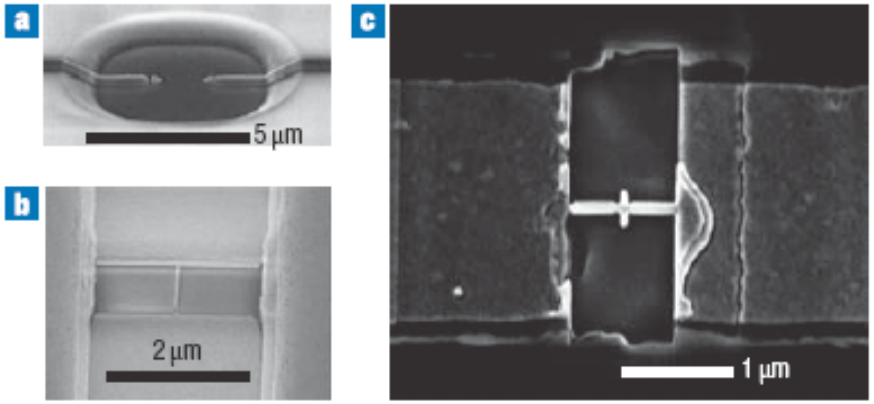


**Figure 3** Scanning electron microscopy (SEM) images of the fabricated devices. **a**, Silicon seeding window with 2-μm-wide germanium crystalline lines. **b**, 60-nm-wide and 2-μm-long germanium nanowire fabricated by the first FIB step. **c**, An open-sleeve dipole antenna detector with $l_{dipole} = 155$ nm (this image is rotated by 90° in relation to that in **b**). (Charging due to a thick oxide layer limits the resolution in this SEM image.)

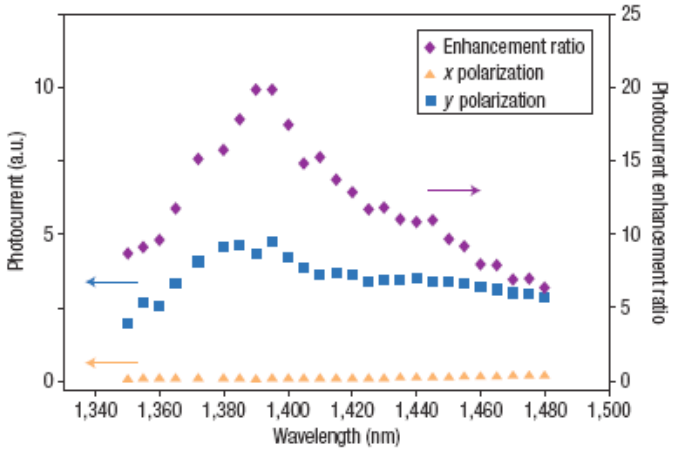


**Figure 5** Measured photocurrent responses for light polarization in the *y* and *x* directions. The wavelengths were 1,350–1,480 nm for the detector with $l_{dipole} = 160$ nm.

# SP Sensing and Detection

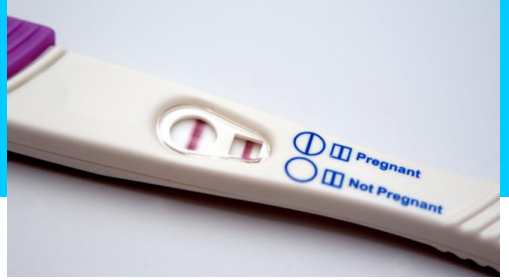


1 – Antigen (hCG)
2 – Primary antibody
3 – Gold nanosphere functionalized with secondary antibody

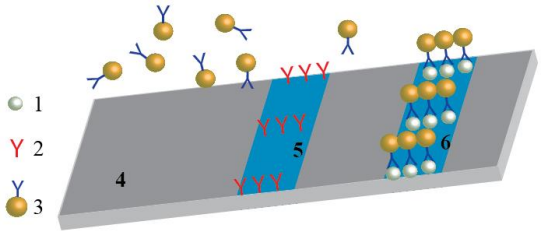


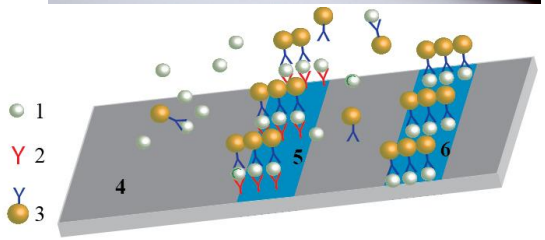


1 – Substrate
2 – Gold nanofilm
3 – Latex nanospheres
4 – Gold nanolayer
5 – Antibodies
6 - Analyte molecules
Adapted from:
T. Endo et al., Anal. Chem. **78**, 6465 (2006).

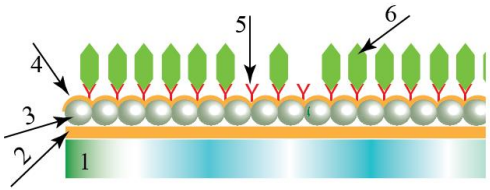


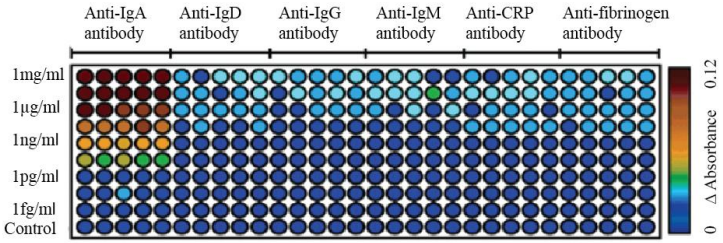


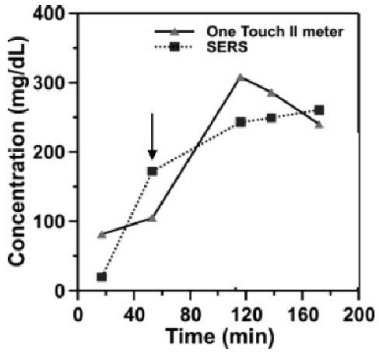


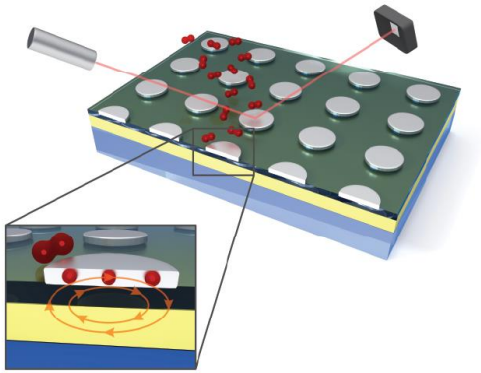

J.N. Anker et al. , Nature Materials **7**, 442 (2008)

N. Liu et al., Nat. Mater. **advance online publication DOI: 10.1038/nmat3029 (2011)**

Department of Physics and Astronomy
Georgia State University
Atlanta, GA 30303-3083

M. I. Stockman, *Nanoplasmonic Sensing and Detection*, Science **348,** 287-288 (2015).

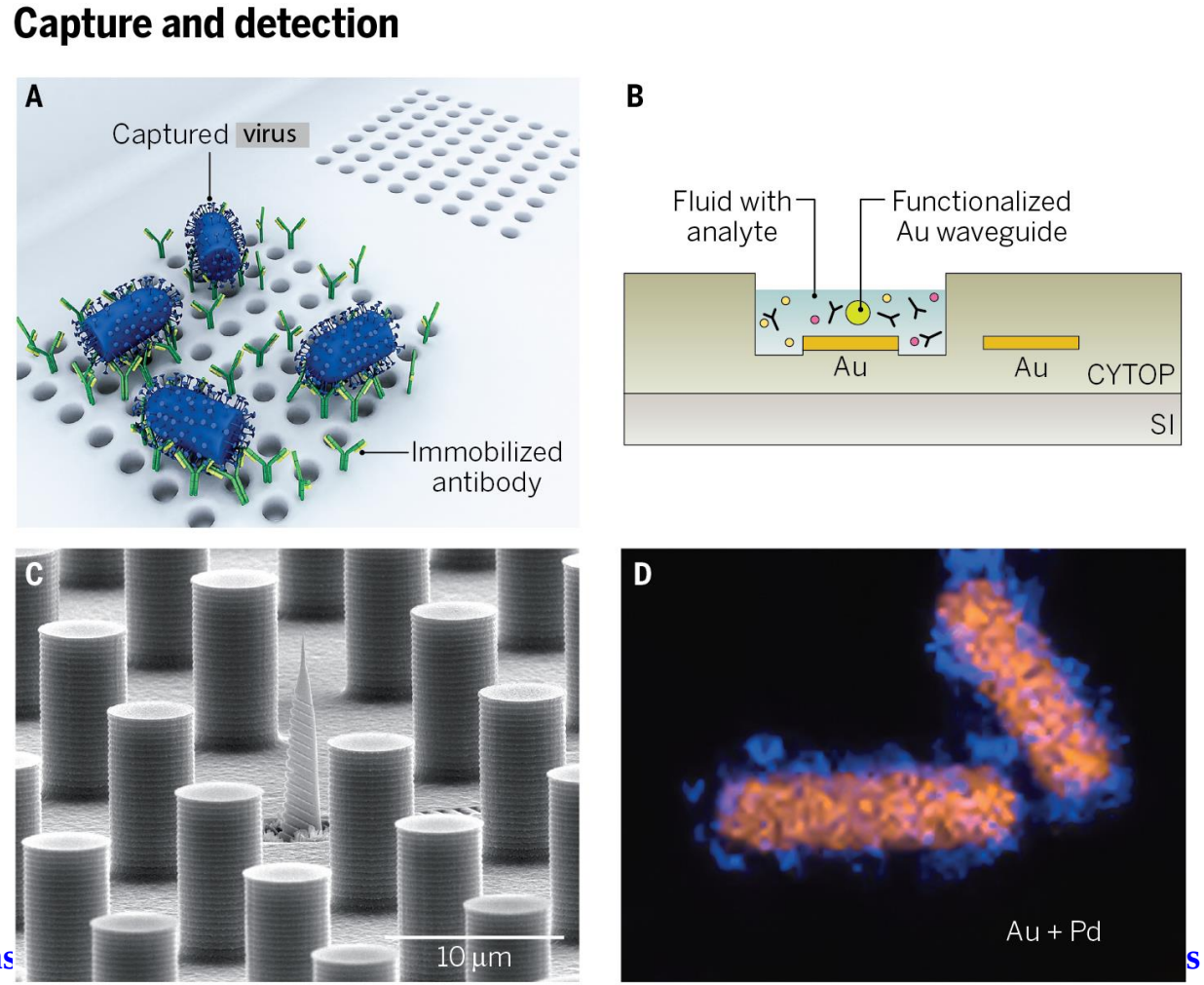

nature nanotechnology

LETTERS

PUBLISHED ONLINE: 20 JULY 2014 | DOI: 10.1038/NNANO.2014.135

# Explosives detection in a lasing plasmon nanocavity

Ren-Min Ma[1†], Sadao Ota[1†], Yimin Li[1], Sui Yang[1] and Xiang Zhang[1,2*]

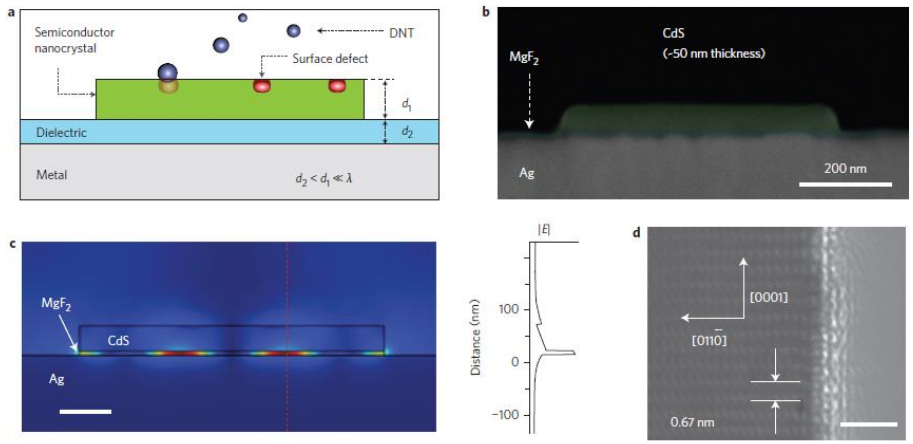


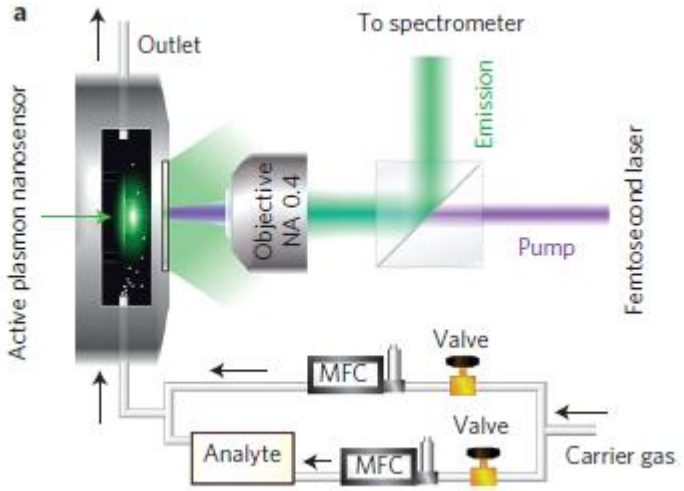


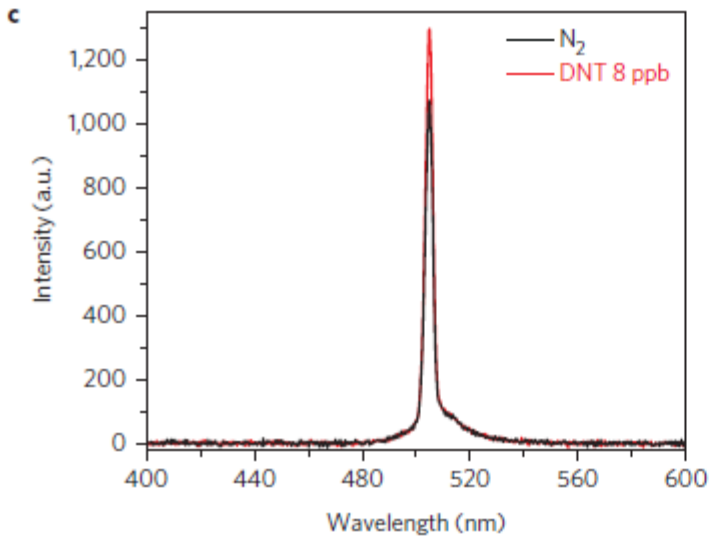


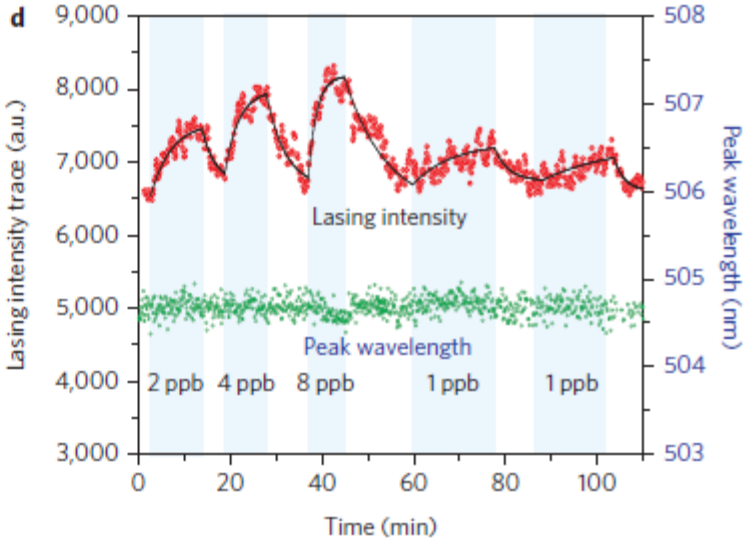

Department of Physics and Astronomy
Georgia State University
Atlanta, GA 30303-3083

# Dawn of the new bold era: seminal first paper on laser (originally "optical maser", then laser)



letters to nature

*Nature* 187, 493 - 494 (06 August 1960); doi:10.1038/187493a0

## Stimulated Optical Radiation in Ruby

T. H. MAIMAN

Hughes Research Laboratories, A Division of Hughes Aircraft Co., Malibu, California.

Schawlow and Townes[1] have proposed a technique for the generation of very monochromatic radiation in the infra-red optical region of the spectrum using an alkali vapour as the active medium. Javan[2] and Sanders[3] have discussed proposals involving electron-excited gaseous systems. In this laboratory an optical pumping technique has been successfully applied to a fluorescent solid resulting in the attainment of negative temperatures and stimulated optical emission at a wave-length of 6943 Å. ; the active material used was ruby (chromium in corundum).

1. Schawlow, A. L. , and Townes, C. H. , *Phys. Rev.*, **112**, 1940 (1958). | Article | ISI | ChemPort |
2. Javan, A. , *Phys. Rev. Letters*, **3**, 87 (1959). | Article | ISI |
3. Sanders, J. H. , *Phys. Rev. Letters*, **3**, 86 (1959). | Article | ISI | ChemPort |
4. Maiman, T. H. , *Phys. Rev. Letters*, **4**, 564 (1960). | Article | ISI |

VOLUME 90, NUMBER 2 PHYSICAL REVIEW LETTERS week ending 17 JANUARY 2003

# Surface Plasmon Amplification by Stimulated Emission of Radiation: Quantum Generation of Coherent Surface Plasmons in Nanosystems

David J. Bergman[1,*] and Mark I. Stockman[2,†]

[1]*School of Physics and Astronomy, Raymond and Beverly Sackler Faculty of Exact Sciences, Tel Aviv University, Tel Aviv, 69978, Israel*

[2]*Department of Physics and Astronomy, Georgia State University, Atlanta, Georgia 30303*

(Received 15 September 2002; published 14 January 2003)

We make a step towards quantum nanoplasmonics: surface plasmon fields of a nanosystem are quantized and their stimulated emission is considered. We introduce a quantum generator for surface plasmon quanta and consider the phenomenon of surface plasmon amplification by stimulated emission of radiation (spaser). Spaser generates temporally coherent high-intensity fields of selected surface plasmon modes that can be strongly localized on the nanoscale, including dark modes that do not couple to far-zone electromagnetic fields. Applications and related phenomena are discussed.

**The original spaser proposal**

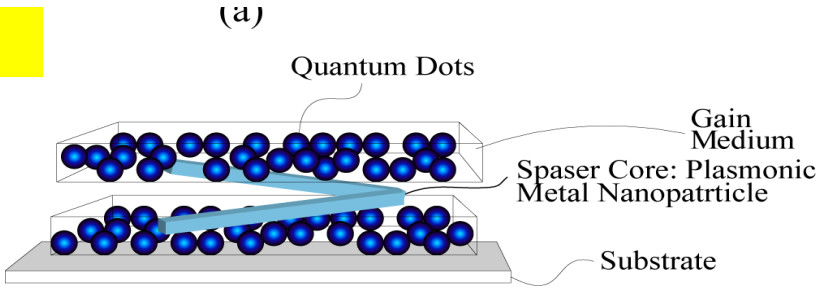


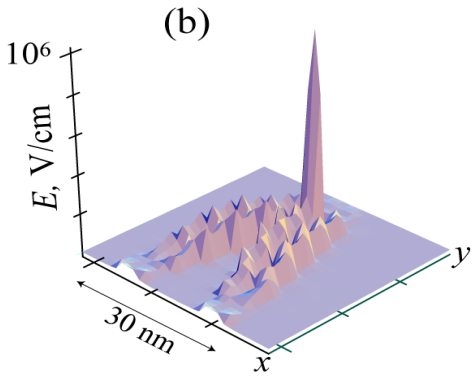


**Spaser field per one plasmon in the core**

Department of Physics and A
Georgia State University
Atlanta, GA 30303-3083

# Spasers explained

nature photonics | VOL 2 | JUNE 2008 |

MARK I. STOCKMAN

is in the Department of Physics and
e-mail: mstockman@gsu.edu

The spaser is a propos ling labo cluding e of

## Spaser is the ultimately smallest quantum nano-generator

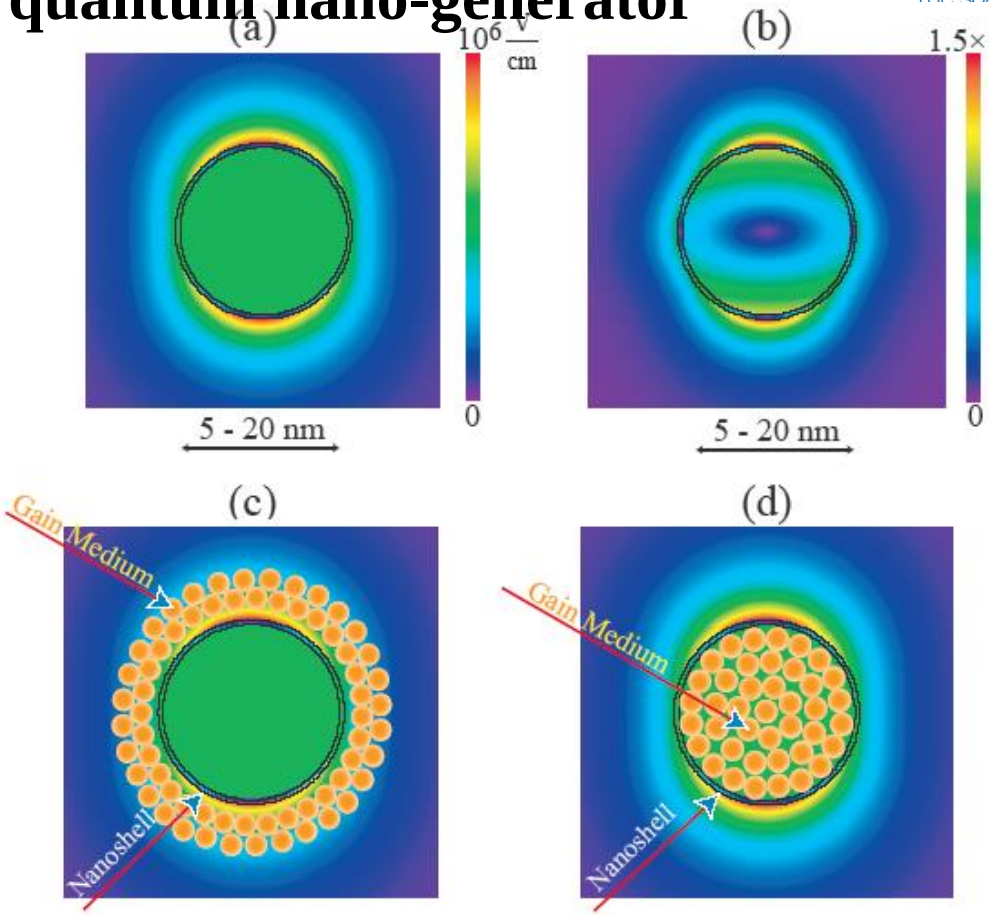


For small nanoparticles, radiative loss is negligible.

**Spaser is fully scalable**

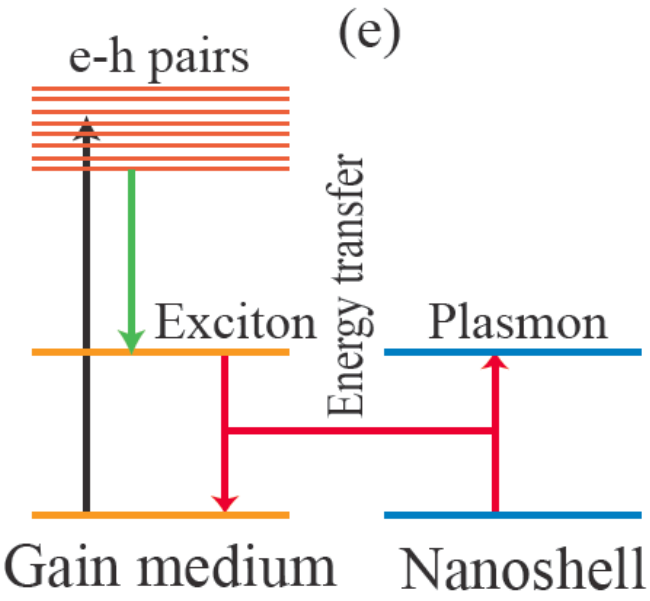


D. J. Bergman and M. I. Stockman, *Surface Plasmon Amplification by Stimulated Emission of Radiation: Quantum Generation of Coherent Surface Plasmons in Nanosystems*, Phys. Rev. Lett. **90**, 027402-1-4 (2003).

Department of Physics and Astronomy
Georgia State University
Atlanta, GA 30303-3083

# Plasmon Lifetimes: Quantization without Quantization

General behavior of polarizability close to a (plasmon) pole in quantum theory [See: V. B. Berestetskii, E. M. Lifshits, and L. P. Pitaevskii, *Quantum Electrodynamics* (Pergamon Press, Oxford and New York, 1982)]:

$$\alpha = \frac{\left|\mathbf{d}_{0p}\right|^2}{\hbar\left(\omega - \omega_p\right)}$$

Compare this to the polarizability of a nanosphere:

$$\alpha = R^3 \frac{\varepsilon_m(\omega) - \varepsilon_d}{\varepsilon_m(\omega) + 2\varepsilon_d} \approx R^3 \frac{-3\varepsilon_d}{\left(\omega - \omega_p\right)\left.\frac{\partial\left(\mathrm{Re}\,\varepsilon_m(\omega)\right)}{\partial\omega}\right|_{\omega=\omega_p}},$$

where $\mathrm{Re}\,\varepsilon_m(\omega_p) = -2\varepsilon_d$

From this, we find the transition dipole of a plasmon:

$$\left|\mathbf{d}_{0p}\right|^2 = \hbar R^3 \frac{3\varepsilon_d}{\left.\frac{\partial\left(\mathrm{Re}\,\varepsilon_m(\omega)\right)}{\partial\omega}\right|_{\omega=\omega_p}}$$

Substituting it into standard formula for radiative decay rate,

$$\gamma_n^{(r)} = \frac{4}{3}\frac{\omega_n^3\sqrt{\varepsilon_d}}{\hbar c^3}\left|(\mathbf{d})_{n0}\right|^2$$

, we obtain:

$$\boxed{\gamma_n^{(r)} = 4\left(\frac{\omega R}{c}\right)^3 \frac{\varepsilon_d}{\left.\frac{\partial\left(\mathrm{Re}\,\varepsilon_m(\omega)\right)}{\partial\omega}\right|_{\omega=\omega_p}}}$$

**Nonradiative decay rate** can be found from the pole of the polarizability

$$\varepsilon_m(\omega_p - i\gamma_{nr}) + 2\varepsilon_d = 0$$

Expanding, we find the non-radiative rate

$$\gamma_n^{(nr)} = \frac{\operatorname{Im}\varepsilon_m(\omega_p)}{\left.\frac{\partial\left(\operatorname{Re}\varepsilon_m(\omega)\right)}{\partial\omega}\right|_{\omega=\omega_p}}$$

Comparing to the radiative rate:

$$\frac{\gamma_n^{(r)}}{\gamma_n^{(nr)}} = 4\left(\frac{R}{\lambda\!\!\!^{-}}\right)^3 \frac{1}{\operatorname{Im}\varepsilon_m(\omega_p)}$$

Department of Physics and Astronomy
Georgia State University
Atlanta, GA 30303-3083

Nonradiative lifetime (fs): $\tau_{nr} = \dfrac{1}{\gamma_n^{(nr)}}$

Radiative lifetime (fs): $\tau_r = \dfrac{1}{\gamma_n^{(r)}}$

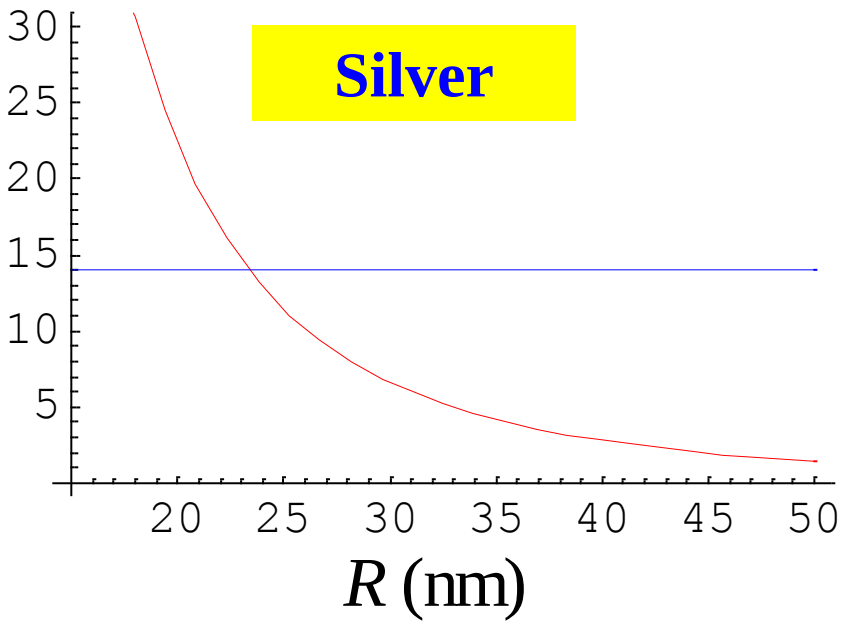


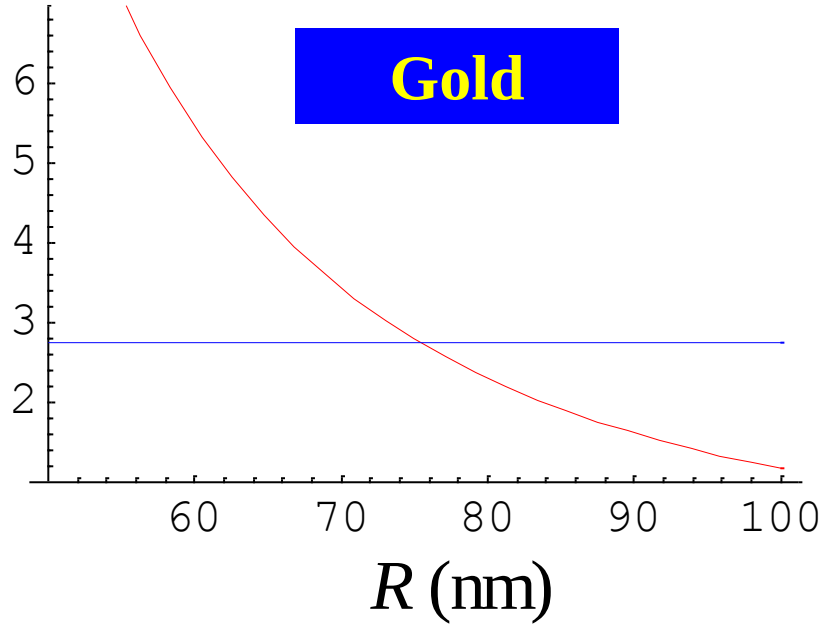

Department of Physics and Astronomy
Georgia State University
Atlanta, GA 30303-3083

# Quantization: Quasistatic Approximation

$$\nabla\varepsilon(\boldsymbol{r})\nabla\varphi(\boldsymbol{r})=0$$

$$\varepsilon(\boldsymbol{r}) = \Theta(\boldsymbol{r})\varepsilon_m + \big(1-\Theta(\boldsymbol{r})\big)\varepsilon_d \text{ , or:}$$

$$\varepsilon(\boldsymbol{r}) = \frac{\varepsilon_d}{s(\omega)}\big(s(\omega)-\Theta(\boldsymbol{r})\big), \text{ where Bergman spectral parameter is}$$

$$s(\omega) = \frac{\varepsilon_d}{\varepsilon_d - \varepsilon_m(\omega)}$$

Substituting into the field equation

$$\nabla\Theta(\boldsymbol{r})\nabla\varphi(\boldsymbol{r}) = s(\omega)\nabla^2\varphi(\boldsymbol{r})$$

This is a linear homogeneous equation that has only trivial solutions except an eigenfunction $\varphi_{\mathrm{n}}(\boldsymbol{r})$ for an eigenvalue $s_n$

$$\nabla\Theta(\boldsymbol{r})\nabla\varphi_{\mathrm{n}}(\boldsymbol{r}) = s_n\nabla^2\varphi(\boldsymbol{r}), \qquad s(\omega_n + i\gamma_n) = s_n$$

A problem: What are limits for $s_n$?

$$? \le s_n \le ?$$

**Solution:**

Multiply both sides by $\varphi_n(\boldsymbol{r})$

$$\varphi_n(\boldsymbol{r})\nabla\Theta(\boldsymbol{r})\nabla\varphi_n(\boldsymbol{r}) = s_n\varphi_n(\boldsymbol{r})\nabla^2\varphi(\boldsymbol{r})$$

And integrate by parts (use Gauss theorem), getting

$$s_n = \frac{\int_V \Theta(\boldsymbol{r})\,(\nabla\varphi_n(\boldsymbol{r}))^2 dV}{\int_V (\nabla\varphi_n(\boldsymbol{r}))^2 dV}$$

Because $1 \le \Theta(\boldsymbol{r}) \le 1$, these re also limits for $s_n$,

$$\boxed{0 \le s_n \le 1}$$

Normalizing $\int_V (\nabla\varphi_n(\boldsymbol{r}))^2 dV = 1$ , we get

$$\int_V \Theta(\boldsymbol{r})\,(\nabla\varphi_n(\boldsymbol{r}))^2 dV = s_n$$

VOLUME 90, NUMBER 2 PHYSICAL REVIEW LETTERS week ending 17 JANUARY 2003

# Surface Plasmon Amplification by Stimulated Emission of Radiation: Quantum Generation of Coherent Surface Plasmons in Nanosystems

David J. Bergman[1,*] and Mark I. Stockman[2,†]

[1]*School of Physics and Astronomy, Raymond and Beverly Sackler Faculty of Exact Sciences, Tel Aviv University, Tel Aviv, 69978, Israel*

[2]*Department of Physics and Astronomy, Georgia State University, Atlanta, Georgia 30303*

(Received 15 September 2002; published 14 January 2003)

We make a step towards quantum nanoplasmonics: surface plasmon fields of a nanosystem are quantized and their stimulated emission is considered. We introduce a quantum generator for surface plasmon quanta and consider the phenomenon of surface plasmon amplification by stimulated emission of radiation (spaser). Spaser generates temporally coherent high-intensity fields of selected surface plasmon modes that can be strongly localized on the nanoscale, including dark modes that do not couple to far-zone electromagnetic fields. Applications and related phenomena are discussed.

DOI: 10.1103/PhysRevLett.90.027402 PACS numbers: 78.67.–n, 42.50.–p, 78.20.Bh, 78.45.+h

Department of Physics and Astronomy
Georgia State University
Atlanta, GA 30303-3083

## Plasmon Quantization: Theoretical Approach

Because the characteristic size of a spaser is much smaller than the wavelength, the quasistatic approximation in field equations is valid.

Surface plasmon field equations and boundary conditions in a material-independent form, where $s_n$ are eigenvalues and $\varphi_n$ are eigenfunctions:

$$\frac{\partial}{\partial \mathbf{r}}\theta(\mathbf{r})\frac{\partial}{\partial \mathbf{r}}\varphi_n(\mathbf{r}) = s_n \frac{\partial^2}{\partial \mathbf{r}^2}\varphi_n(\mathbf{r}),$$

where $\theta(\mathbf{r} \in metal) = 1$ and $\theta(\mathbf{r} \in elsewhere) = 0$ ;

$$\varphi_n(\mathbf{r})\frac{\partial}{\partial \mathbf{r}}\varphi_n(\mathbf{r})\Big|_{Boundary} = 0 \quad \text{(Dirichlet-Neumann)}$$

Normalization: $\int_v \left(\frac{\partial}{\partial \mathbf{r}}\varphi_n(\mathbf{r})\right)^2 = 1$ is arbitrary but common

Spectral parameter: $s(\omega) = \left[1 - \varepsilon_m(\omega)/\varepsilon_d\right]^{-1}$

Frequency $\omega_n$ and decay rate $\gamma_n$ of surface plasmons:

$$\mathrm{Re}\left[s(\omega_n)\right] = s_n\,,\ \gamma_n = \frac{\mathrm{Im}[s(\omega_n)]}{s_n'},\quad \text{where}\quad s_n' \equiv \frac{d\,\mathrm{Re}\left[s(\omega_n)\right]}{d\omega_n}$$

Quasielectrostatic energy (Hamiltonian) of an inhomogeneous dispersive nanosystem (Brillouin formula):

$$H = \frac{1}{4\pi}\int_{-\infty}^{\infty} \frac{d\left[\omega\ \varepsilon(\mathbf{r},\omega)\right]}{d\omega}\,\mathbf{E}(\mathbf{r},\omega)\mathbf{E}^{\dagger}(\mathbf{r},\omega)\frac{d\omega}{2\pi}d^3r$$

where is $\mathbf{E}(\mathbf{r},\omega) = -\nabla\hat{\varphi}(\mathbf{r},\omega)$ the electric field operator.

Problem is to find quantization coefficient $A_n$

$$\hat{\varphi}(\mathbf{r},t) = \sum\nolimits_n A_n\ \varphi_n(\mathbf{r})\left[a_n e^{-i\omega_n t} + a_n^{+} e^{i\omega_n t}\right]$$

Potential operator is (to be obtained later):

$$\hat{\varphi}(\mathbf{r},t)=\sum_n\sqrt{\frac{4\pi\hbar s_n}{\varepsilon_d s_n'}}\;\varphi_n(\mathbf{r})\left[a_n e^{-i\omega_n t}+a_n^{+}e^{i\omega_n t}\right]$$

where $a_n^{+}$ and $a_n$ are the surface plasmon creation and annihilation operators. With this, the Hamiltonian becomes $H=\sum_n\hbar\omega_n\left(a_n^{+}a_n+\frac{1}{2}\right)$

The interaction Hamiltonian of the surface plasmons and two-level systems (quantum dots) of the active medium is:

$$H'=-\sum_a\mathbf{d}^{(a)}\mathbf{E}_n(\mathbf{r}_a,t)$$

Using the perturbation theory, kinetic equation for the population number of surface plasmons in an *n*-th mode is:

$$\frac{dN_n}{dt}=\left(B_n-\gamma_n\right)N_n+A_n$$

The Einstein stimulated emission coefficient is

$$B_n = \frac{4\pi}{3\hbar}\frac{s_n \left|\mathbf{d}_{10}\right|^2 p_n q_n}{\varepsilon_h s_n' \gamma_n} > \gamma_n \quad \Rightarrow \quad \boxed{\frac{\left|\mathbf{d}_{10}\right|^2 NQ}{\hbar \gamma_n V_n} \geq 1}$$

Here $p_n$ is the spatial overlap factor, $q_n$ is the spectral overlap factor between the eigenmode intensity and the population inversion,, $Q=\omega_n/\gamma$ is the plasmon quality factor.

$$p_n = \int \left[\nabla \phi_n(\mathbf{r})\right]^2 \rho(\mathbf{r}) d^3 r \ , \ q_n = \int F(\omega)[1+\left(\omega-\omega_n\right)^2/\gamma_n^2]^{-1} d\omega$$

$\boldsymbol{d}_{10}$ is transition dipole element in gain chromophores, $V_n$ is the modal volume, $\rho(\boldsymbol{r})$ is the density of the gain chromophores, and $N$ is the number of the gain chromophores within this modal volume

Problem: Assume $\boldsymbol{d}_{10} = 0.5\text{e nm}$, $\frac{N}{V} = \frac{1}{\text{nm}^3}$, $Q = 100$, $\gamma_n = \frac{1}{10\text{ fs}}$

Will it spase?

## Solution

$(d^2 \nu Q)/(\text{hbar}\ \gamma)/.\{d->0.5\ e\ nm, \nu->1/nm^3, Q->100., \gamma->1/(10\ fs)\}$

546.923

Yes, it will

Spaser gain $\alpha_n = \dfrac{B - \gamma_n}{\gamma_n}$

shows how many times faster the surface plasmons are born by the stimulated emission than they decay.

The local RMS field produced by spaser: $E(\mathbf{r}) = \left\langle \left[\nabla \phi(\mathbf{r})\right]^2 \right\rangle^{1/2}$ is calculated as:

$$E(\mathbf{r}) = E_n(\mathbf{r})\left(N_n + \frac{1}{2}\right)^{1/2}, \text{ where}$$

$$E_n(\mathbf{r}) = \left\{ \frac{4\pi\hbar s_n}{\varepsilon_h s_n'} \left\langle \left[\nabla \varphi_n(\mathbf{r})\right]^2 \right\rangle \right\}^{1/2}$$

Department of Physics and Astronomy
Georgia State University
Atlanta, GA 30303-3083

# RESULTS

The resonant nanoparticle is an "engineered" V-shape. The material is silver; the spatial scale is 2-5 nm/grid unit.

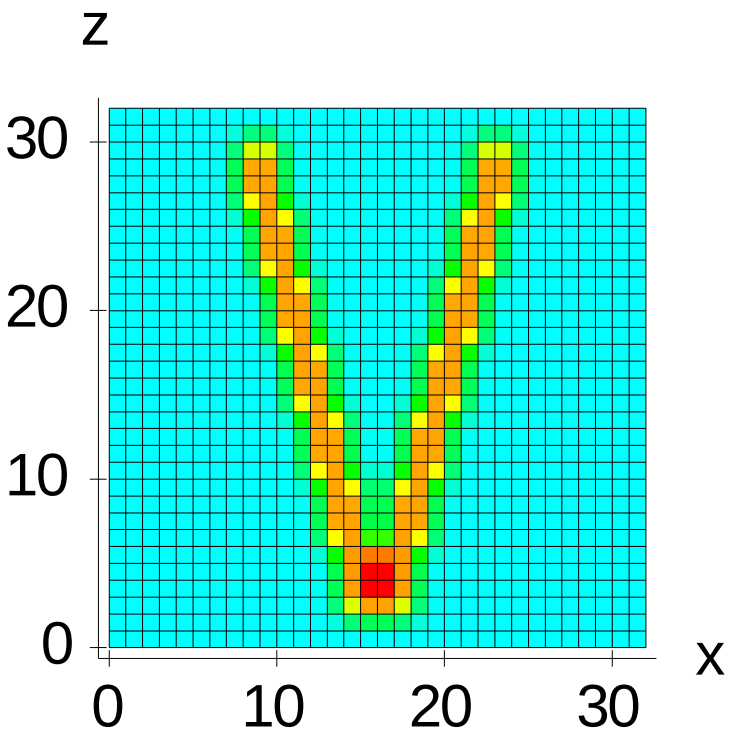

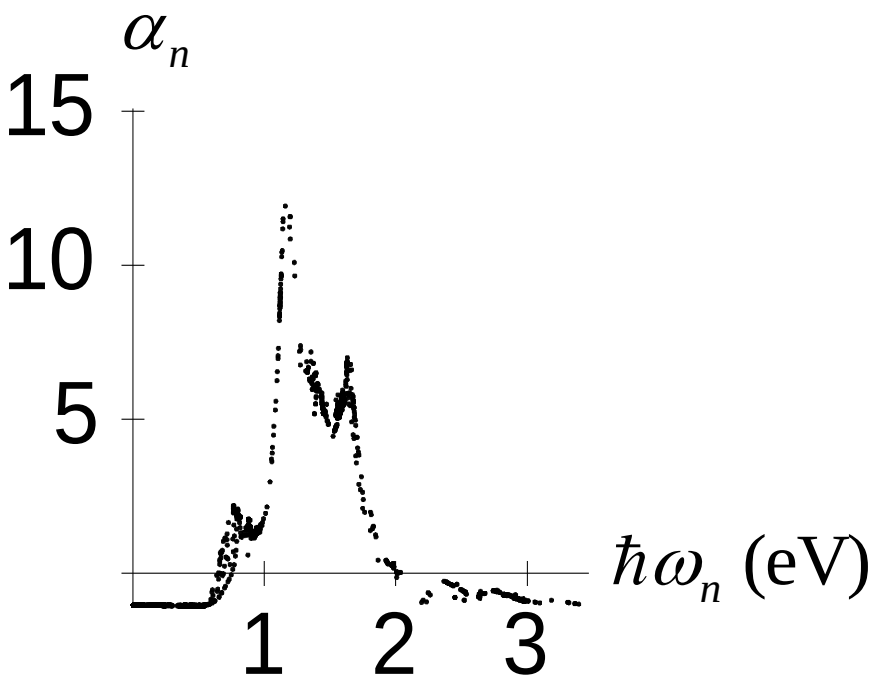


Calculated gain for thin (three monolayers of quantum dots) active medium

Department of Physics and Astronomy
Georgia State University
Atlanta, GA 30303-3083

# Eigenmodes with highest yields for the spectral maximum at 1.2 eV

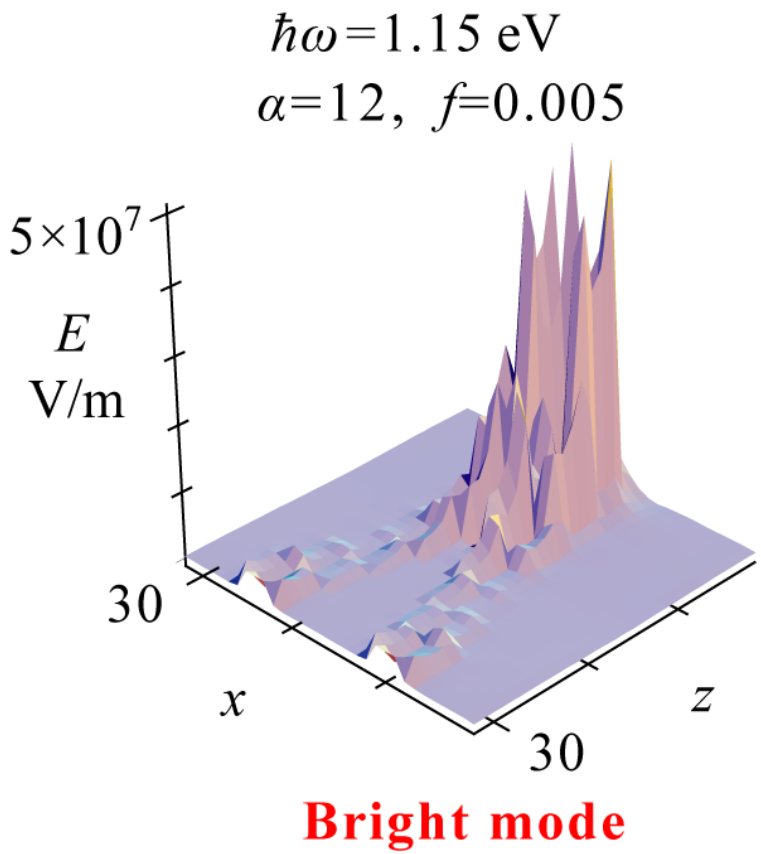


Bright mode

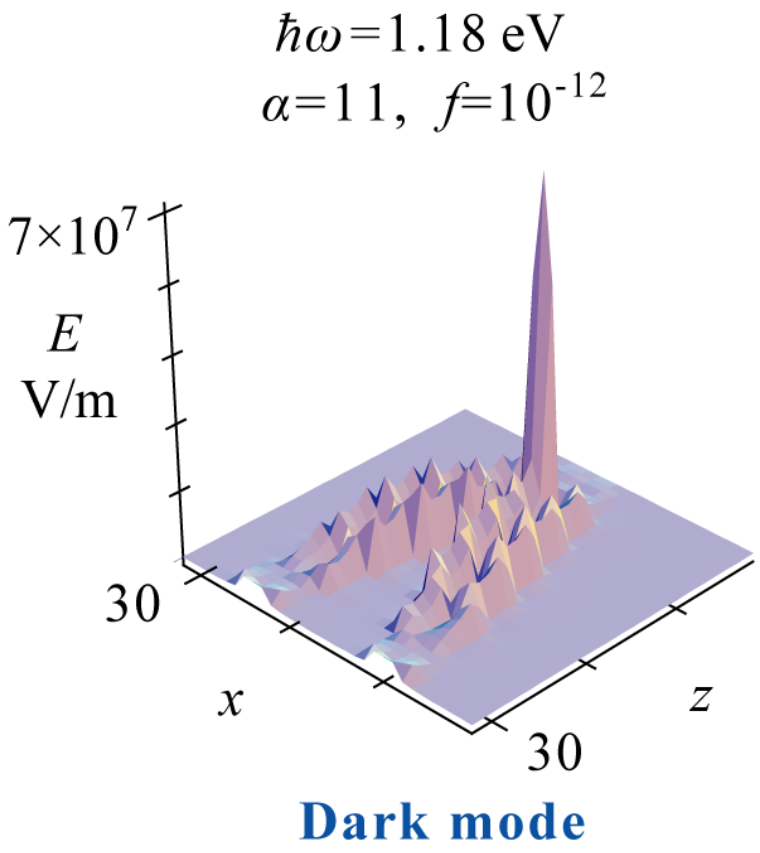


Dark mode

Department of Physics and Astronomy
Georgia State University
Atlanta, GA 30303-3083

# Quantum Theory of Spaser: Quantization of SPs

Brillouin thermodynamic energy:

$$u=\frac{1}{8\pi}\left(\frac{\partial\omega\varepsilon(\omega)}{\partial\omega}\left\langle\mathbf{E}^2(t)\right\rangle+\frac{\partial\omega\mu(\omega)}{\partial\omega}\left\langle\mathbf{H}^2(t)\right\rangle\right)$$

where angle brackets denote averaging over period in $t$ and over a quantum state. In quantum case, the field operator

Classical mode field

$$\hat{\mathbf{E}}(t)=A_n\mathbf{E}_n(\mathbf{r})(a^{\dagger}e^{i\omega t}+ae^{-i\omega t})$$

where $a, a^{+}$ are the annihilation and creation operators.

The averaged value of Hamiltonian is

$$\left\langle H\right\rangle=\frac{1}{8\pi}\int_V\frac{\partial\omega\varepsilon(\mathbf{r},\omega)}{\partial\omega}\left\langle\hat{\mathbf{E}}^2(t)\right\rangle dV=$$

$$\frac{1}{8\pi}\int_V\left[\omega\frac{\partial\varepsilon_m(\omega)}{\partial\omega}\Theta(\mathbf{r})\left\langle\hat{\mathbf{E}}^2(t)\right\rangle+\varepsilon(\mathbf{r},\omega)\left\langle\hat{\mathbf{E}}^2(t)\right\rangle\right]dV$$

Classical modal field

$$\langle H\rangle = \frac{1}{8\pi}\int_V \left[\omega\frac{\partial\varepsilon_m(\omega)}{\partial\omega}\Theta(\mathbf{r})\left|\mathbf{E}_n(\mathbf{r})\right|^2 + \varepsilon(\mathbf{r},\omega)\left|\mathbf{E}_n(\mathbf{r})\right|^2\right] dV A_n^2 2\left\langle a^\dagger a + \frac{1}{2}\right\rangle$$

From the field equation, $\nabla\varepsilon(\boldsymbol{r})\nabla\varphi(\boldsymbol{r}) = 0$, it follows immediately by multiplying by $\varphi(\boldsymbol{r})$, integrating over volume and using the Gauss theorem that $\int_V \varepsilon(\boldsymbol{r})|\boldsymbol{E}_n(\boldsymbol{r})|^2 dV = 0$, and we found earlier that $\int_V \Theta(\boldsymbol{r})\varepsilon(\boldsymbol{r})|\boldsymbol{E}_n(\boldsymbol{r})|^2 dV = s_n$. This leads to (in the vicinity of $\omega \approx \omega_n$) to

$$\langle H\rangle = \frac{1}{4\pi}A_n^2\left\langle a^\dagger a + \frac{1}{2}\right\rangle\omega\frac{\partial\varepsilon_m(\omega)}{\partial\omega}s_n = \hbar\omega\left\langle a^\dagger a + \frac{1}{2}\right\rangle$$

From this, we immediately find the required quantization constant

$$A_n = \sqrt{\frac{4\pi\hbar}{s_n\dfrac{\partial\varepsilon_m(\omega_n)}{\partial\omega_n}}} = \sqrt{\frac{4\pi\hbar s_n}{\varepsilon_d\dfrac{\partial s(\omega_n)}{\partial\omega_n}}}$$

The quantized SP field is

$$\hat{\mathbf{E}}(\mathbf{r}) = A_n \mathbf{E}_n(\mathbf{r})(a_n^\dagger + a_n), \quad A_n = \sqrt{\frac{4\pi\hbar}{s_n \dfrac{\partial \varepsilon_m(\omega_n)}{\partial \omega_n}}}, \quad \mathbf{E}_n(\mathbf{r}) = -\nabla \varphi_n(\mathbf{r})$$

The spaser Hamiltonian is

$$H = H_g + \hbar \sum_n \omega_n a_n^\dagger a_n - \sum_p \hat{\mathbf{E}}(\mathbf{r}_p)\hat{\mathbf{d}}^p$$

where $H_g$ is the Hamiltonian of the gain medium of the spaser, $p$ denotes a chromophore in the gain medium, and $\hat{\mathbf{d}}^p$ is the dipole transition operator of a $p$-th chromophore.

Department of Physics and Astronomy
Georgia State University
Atlanta, GA 30303-3083

# Quantum Kinetics of the Spaser

Quantum Liouville equation for density matrix $\rho$

$$i\hbar\frac{\partial\rho}{\partial t} = [H, \rho]$$

After the commutators are evaluated and equations written, relaxation is added since no relaxation can be described by Hamiltonian in a truncated system. As an example consider

$$i\hbar\dot{\rho}_{21} = \langle 2 | H_g\rho - \rho H_g | 1\rangle - \langle 2 | \mathbf{d}\rho - \rho\mathbf{d} | 1\rangle \left(\mathbf{E}_n a_n e^{-i\omega t} + \mathbf{E}_n^* a_n{}^\dagger e^{i\omega t}\right)$$

For a resonant ("working") transition in a gain chromophore

$$i\hbar\dot{\rho}_{21} = (\varepsilon_2 - \varepsilon_1)\rho - d_{21}(\rho_{11} - \rho_{22})\left(\mathbf{E}_n a_n e^{-i\omega t} + \mathbf{E}_n^* a_n{}^\dagger e^{i\omega t}\right)$$

We set resonant approximation ("Rotating Wave Approximation", RWA) as

$$\rho_{21} = \bar{\rho}_{21} e^{-i\omega t} + \bar{\rho}_{12}^* e^{i\omega t}$$

Substituting leads to an equation

$$i\left[\dot{\bar{\rho}}_{21}e^{-i\omega t}-i\omega\bar{\rho}_{21}e^{-i\omega t}+\dot{\bar{\rho}}_{12}^{*}e^{i\omega t}+i\omega\bar{\rho}_{12}^{*}e^{i\omega t}\right]=$$

$$\omega_{21}\left(\bar{\rho}_{21}e^{-i\omega t}+\bar{\rho}_{12}^{*}e^{i\omega t}\right)-\frac{\mathbf{d}_{21}}{\hbar}\left(\mathbf{E}_n a_n e^{-i\omega t}+\mathbf{E}_n^{*}a_n^{\dagger}e^{i\omega t}\right)\left(\rho_{11}-\rho_{22}\right)$$

Separating positive- and negative-frequency parts, we get

$$i\dot{\bar{\rho}}_{21}=(\omega_{21}-\omega)\bar{\rho}_{21}-\frac{\mathbf{d}_{21}\mathbf{E}_n}{\hbar}a_n\left(\rho_{11}-\rho_{22}\right)$$

Finally, introducing polarization relaxation rate $\Gamma_{12}$, the final form is

$$i\dot{\bar{\rho}}_{21}=(\omega_{21}-\omega-i\Gamma_{12})\bar{\rho}_{21}+\Omega_{12}^{(n)}a_n n_{21},\quad \Omega_{12}^{(n)}=-\frac{\mathbf{d}_{21}\mathbf{E}_n}{\hbar}$$

This is an equation describing polarization of a gain chromophore
Similarly, for population inversion $n_{21}=n_2-n_1$, we have

$$\dot{\bar{n}}_{21}=4\,\mathrm{Im}\left(\bar{\rho}_{21}\Omega_{12}^{(n)*}a_n^{\dagger}\right)+g\left(1-n_{21}\right)-\gamma_2\left(1+n_{21}\right)$$

Finally, the equations for motion for plasmonic amplitude are

$$\dot{a}_n = \left[ i\left(\omega - \omega_n\right) - \gamma_n \right] a_n + i \sum_p \rho_{12}^{(p)*} \Omega_{12}^{(p)}$$

Similarly to Schawlow-Townes theory of laser linewidth, the spontaneous emission of SPs into the spasing mode leads to the diffusion of the phase of the spasing state. This mechanism defines the spectral width of the spasing line as

$$\gamma_s = \frac{\sum_p \left(1 + n_{21}^p\right) \gamma_2^p}{2\left(2N_n + 1\right)}$$

Department of Physics and Astronomy
Georgia State University
Atlanta, GA 30303-3083

arXiv:0908.3559
Journal of Optics, 024004-1-13 (2010).

## Theory of Spaser in Stationary Regime

Physically, the spaser action is a result of spontaneous symmetry breaking when the phase of the coherent SP field is established from the spontaneous noise. Mathematically, the spaser is described by homogeneous differential Eqs. (4)-(6) derived and solved in Sec. II B. These equations become homogeneous algebraic equations for the stationary (CW) case. These equations always have a trivial, zero solution. However, when their determinant vanishes, they also possess a nontrivial solution describing spasing, whose condition is

$$\left(\omega_s-\omega_n+i\gamma_n\right)^{-1}\times \qquad (9)$$
$$\left(\omega_s-\omega_{21}+i\Gamma_{12}\right)^{-1}\sum_p\left|\tilde{\Omega}_{12}^{(p)}\right|^2 n_{21}^{(p)}=-1\ ,$$

where $\omega_s$ is the spasing frequency, $\tilde{\Omega}_{12}^{(p)}=-A_n\mathbf{d}_{12}^{(p)}\nabla\varphi_n(\mathbf{r}_p)/\hbar$ is the single-plasmon Rabi frequency, $\mathbf{d}_{12}^{(p)}$ is the transition dipole moment of a $p$th chromophore, $\varphi_n(\mathbf{r}_p)$ is the electric potential of the spasing mode at the position this chromophore, $\gamma_n$

$$n_{21}^{(p)}=\left(g-\gamma_2\right)\times \qquad (10)$$
$$\left\{g+\gamma_2+4\left|\Omega_{12}^{(p)}\right|^2\Big/\left[\left(\omega_s-\omega_{21}\right)^2+\Gamma_{12}^2\right]\right\}^{-1}\ ,$$

From the imaginary part of Eq. (10) we immediately find the spasing frequency

$$\omega_s=\left(\gamma_n\omega_{21}+\Gamma_{12}\omega_n\right)/\left(\gamma_n+\Gamma_{12}\right)\ , \qquad (11)$$

which generally does not coincide with either the gain transition frequency $\omega_{21}$ or the SP frequency $\omega_n$, but is between them (this is a frequency walk-off phenomenon similar to that of laser physics). Substituting Eq. (11) back to Eqs. (10)-(11), we obtain a system of equations

$$\frac{\left(\gamma_n+\Gamma_{12}\right)^2}{\gamma_n\Gamma_{12}\left[\left(\omega_{21}-\omega_n\right)^2+\left(\Gamma_{12}+\gamma_n\right)^2\right]}\times$$
$$\sum_p\left|\tilde{\Omega}_{12}^{(p)}\right|^2 n_{21}^{(p)}=1\ , \qquad (12)$$
$$n_{21}^{(p)}=\left(g-\gamma_2\right)\times$$
$$\left[g+\gamma_2+\frac{4N_n\left|\tilde{\Omega}_{12}^{(p)}\right|^2\left(\Gamma_{12}+\gamma_n\right)}{\left(\omega_{12}-\omega_n\right)^2+\left(\Gamma_{12}+\gamma_n\right)^2}\right]^{-1}\ . \qquad (13)$$

This system defines the stationary (CW) number of SPs per spasing mode $N_n$.

Number of plasmons per spasing mode:

$$N_n = N_c \frac{g-\gamma_2}{4\gamma_n} - \frac{g+\gamma_2}{4C}, \quad C = \frac{1}{\Gamma_{12}} \frac{|\Omega_{21}|^2}{\left(\frac{\omega_n - \omega_{21}}{\gamma_n + \Gamma_{12}}\right)^2 + 1}$$

Inversion between the spasing transition levels:

$$n_{21} = \frac{g-\gamma_2}{g+\gamma_2+4N_nC} \xrightarrow{g \gg \gamma_2} \frac{g}{g+4N_nC} \quad \text{clipping}$$

Department of Physics and Astronomy
Georgia State University
Atlanta, GA 30303-3083

## SPASER Threshold Condition [Consistent with PRL **90**, 027402-1-4 (2003)]:

Since $n_{21}^{(p)} \leq 1$, from Eqs. (12), (13) we immediately obtain a necessary condition of the existence of spasing,

$$\frac{(\gamma_n + \Gamma_{12})^2}{\gamma_n \Gamma_{12}\left[(\omega_{21} - \omega_n)^2 + (\Gamma_{12} + \gamma_n)^2\right]} \sum_p \left|\tilde{\Omega}_{12}^{(p)}\right|^2 \geq 1 \,. \tag{14}$$

This expression is fully consistent with [4]. The following order of magnitude estimate of this spasing condition has a transparent physical meaning and is of heuristic value:

$$\boxed{\frac{d_{12}^2 Q N_c}{\hbar \Gamma_{12} V_n} \gtrsim 1,} \tag{15}$$

where $Q = \omega/\gamma_n$ is the quality factor of SPs, $V_n$ is the volume of the spasing SP mode, and $N_c$ is the number of gain medium chromophores within this volume. Deriving this estimate, we have neglected the detuning, i.e., set $\omega_{21} - \omega_n = 0$.

arXiv:0908.3559
Journal of Optics, 024004-1-13 (2010).

The spasing is essentially a quantum effect.

It is non-relativistic: does not depend on *c*

Department of Physics and Astronomy
Georgia State University
Atlanta, GA 30303-3083

# Stationary (CW) spaser regime

This quasilinear dependence of the number of plasmons per mode $N_n(g)$ is a result of the very strong feedback in spaser due to the small modal volume

$$\Gamma_s \propto g^{-1}$$

arXiv:0908.3559
Journal of Optics, **12**, 024004-1-13 (2010).

Plasmon number vs. pumping rate

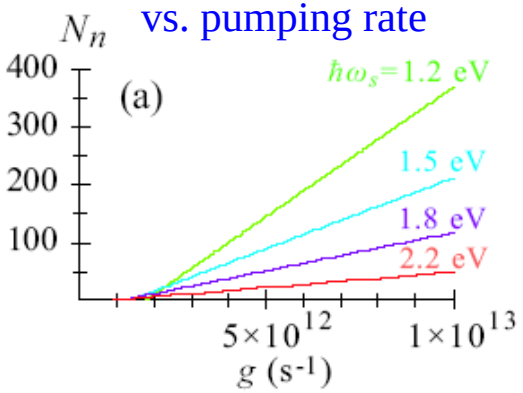


Inversion vs. pumping rate

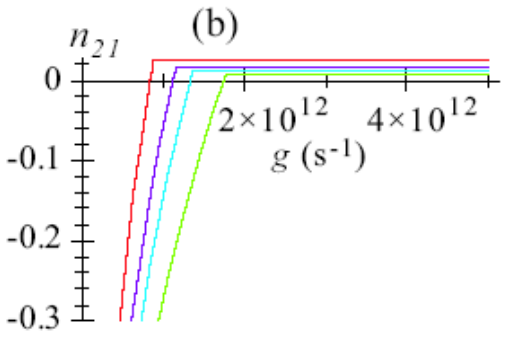


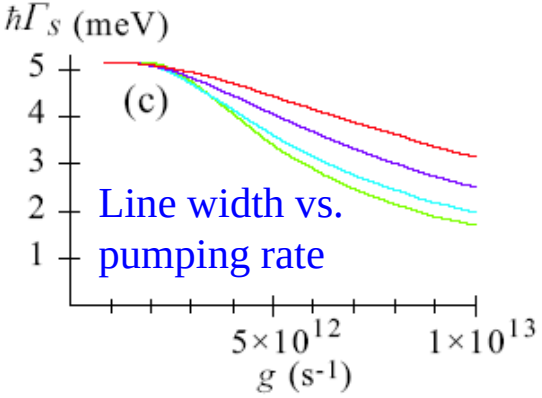


Line width vs. pumping rate

Spectral shape of spaser line

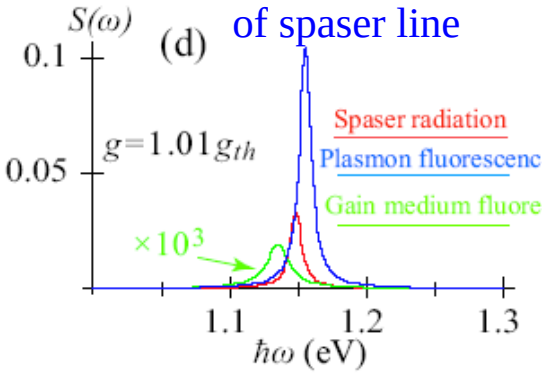


Spectral shape of spaser line

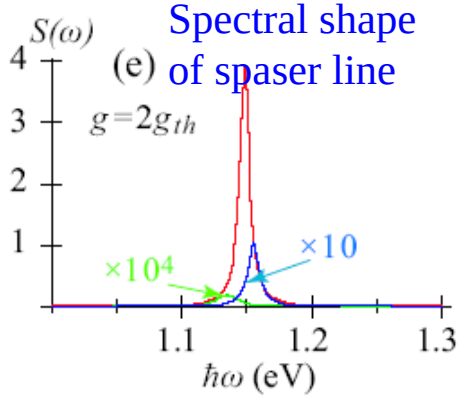


Spectral shape of spaser line

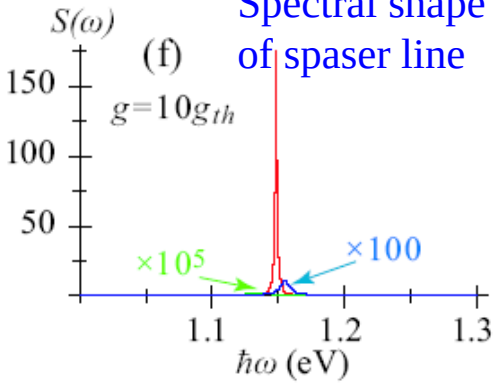

**Gain of bulk medium required for spasing and for loss compensation by gain:** M. I. Stockman, *Spaser Action, Loss Compensation, and Stability in Plasmonic Systems with Gain*, Phys. Rev. Lett. **106**, 156802-1-4 (2011); Phil. Trans. R. Soc. A **369**, 3510 (2011).

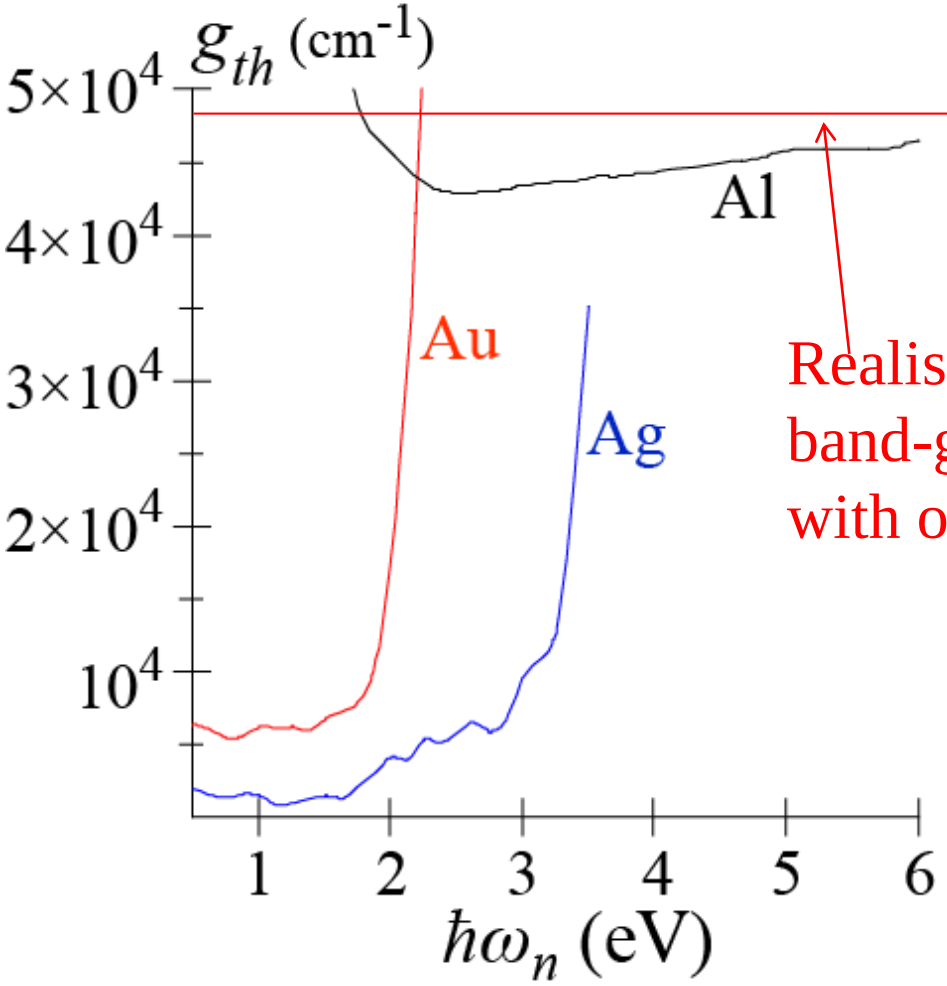


$$g \geq g_{th},\ g_{th} = \frac{\omega}{c\sqrt{\varepsilon_d}} \frac{\mathrm{Re}\, s(\omega)\, \mathrm{Im}\, \varepsilon_m(\omega)}{1 - \mathrm{Re}\, s(\omega)}$$

$$s(\omega) = \frac{\varepsilon_d}{\varepsilon_d - \varepsilon_m(\omega)};\quad 1 > \mathrm{Re}\, s(\omega) > 0$$

Realistic gain for direct band-gap semiconductors with optical pumpimg

Department of Physics and Astronomy
Georgia State University
Atlanta, GA 30303-3083

# Amplification in Spaser without a Saturable Absorber

Stationary pumping

SP coherent population

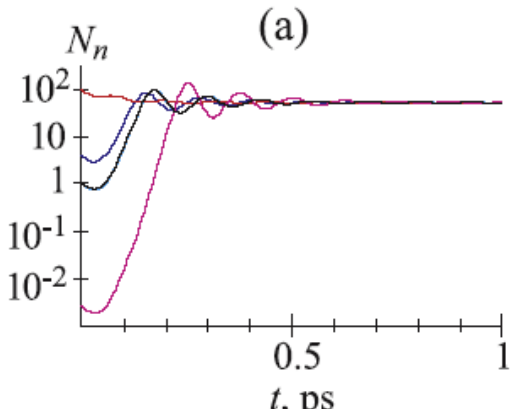


Population inversion

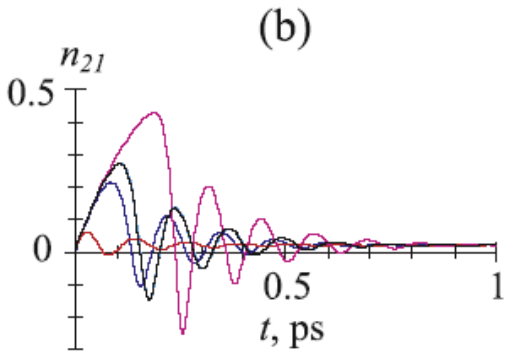


Pulse pumping

SP coherent population

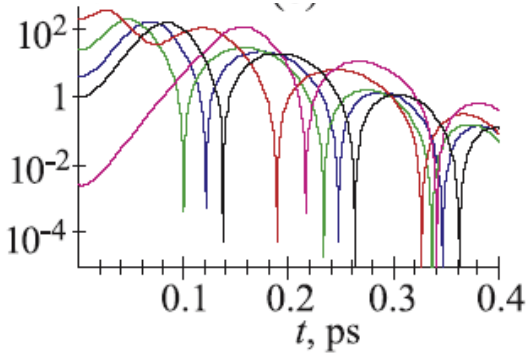


$n$ Population inversion

Department of Phys
Georgia State Unive
Atlanta, GA 30303-3

Bandwidth ~ 10-100 THz

Very high resistance to ionizing radiation

# Amplification in Spaser with a Saturable Absorber (1/3 of the gain chromophores)

Stationary pumping

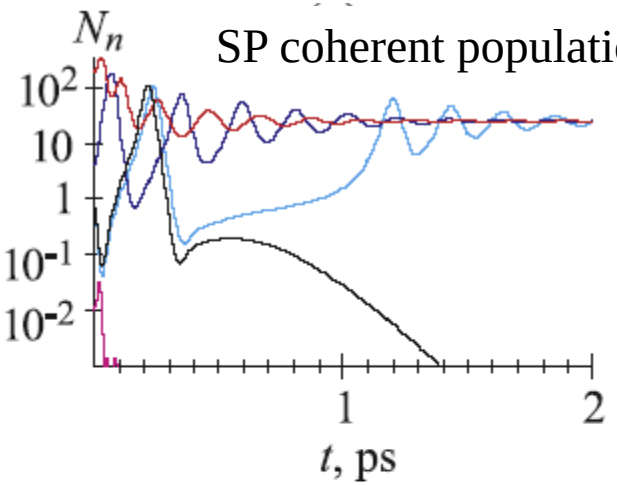


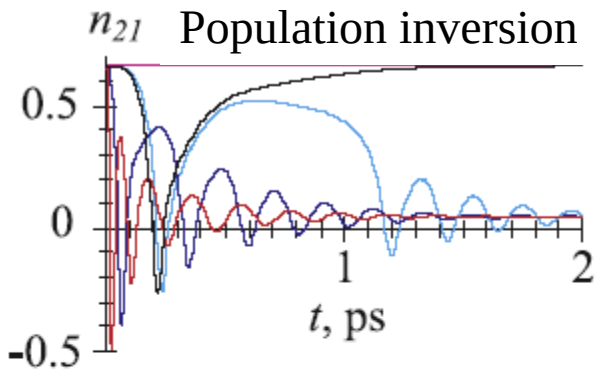


Pulse pumping

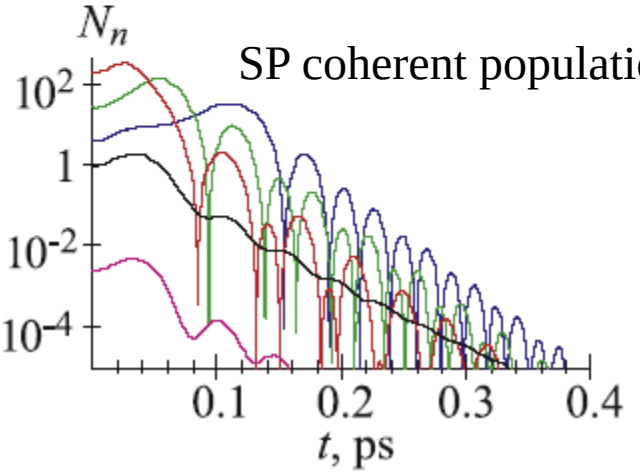


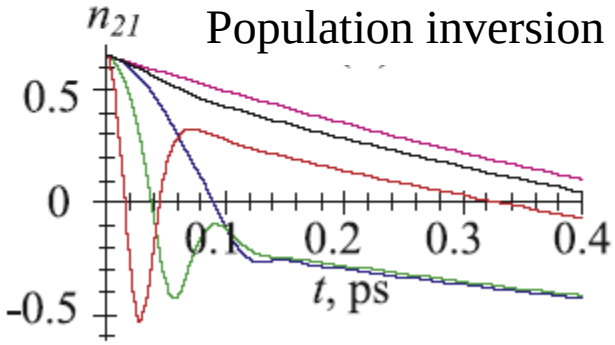

# Experimental Observations of Spaser

doi:10.1038/nature08318 nature

LETTERS

## Demonstration of a spaser-based nanolaser

M. A. Noginov[1], G. Zhu[1], A. M. Belgrave[1], R. Bakker[2], V. M. Shalaev[2], E. E. Narimanov[2], S. Stout[1,3], E. Herz[3], T. Suteewong[3] & U. Wiesner[3]

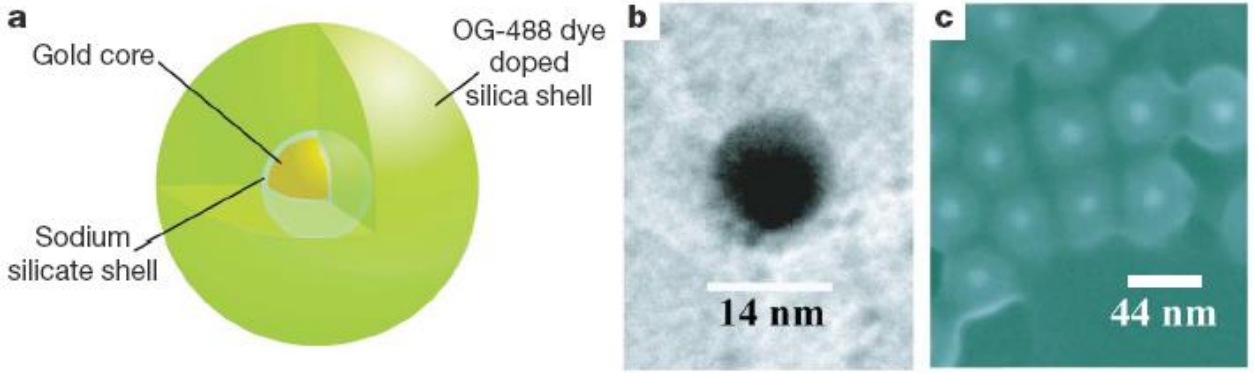


**Figure 1 | Spaser design.** **a**, Diagram of the hybrid nanoparticle architecture (not to scale), indicating dye molecules throughout the silica shell. **b**, Transmission electron microscope image of Au core. **c**, Scanning electron microscope image of Au/silica/dye core–shell nanoparticles. **d**, Spaser mode (in false colour), with $\lambda = 5$ circles represent the 14-nm strength colour scheme is sl

[1]Center for Materials Research, Norfolk State University, Norfolk, Virginia 23504, USA. [2]School of Electrical & Computer Eng University, West Lafayette, Indiana 47907, USA. [3]Materials Science and Engineering Department, Cornell University, Ithaca

Department of Physics and Astronom
Georgia State University
Atlanta, GA 30303-3083

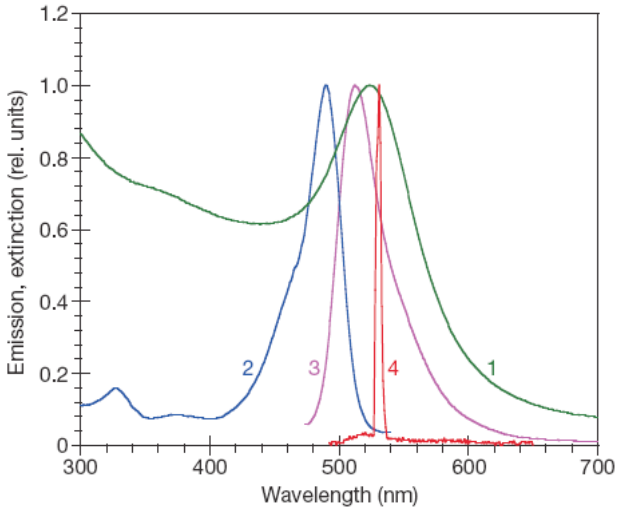


**Figure 2 | Spectroscopic results.** Normalized extinction (1), excitation (2), spontaneous emission (3), and stimulated emission (4) spectra of Au/silica/dye nanoparticles. The peak extinction cross-section of the nanoparticles is $1.1 \times 10^{-12}$ cm$^2$. The emission and excitation spectra were measured in a spectrofluorometer at low fluence.

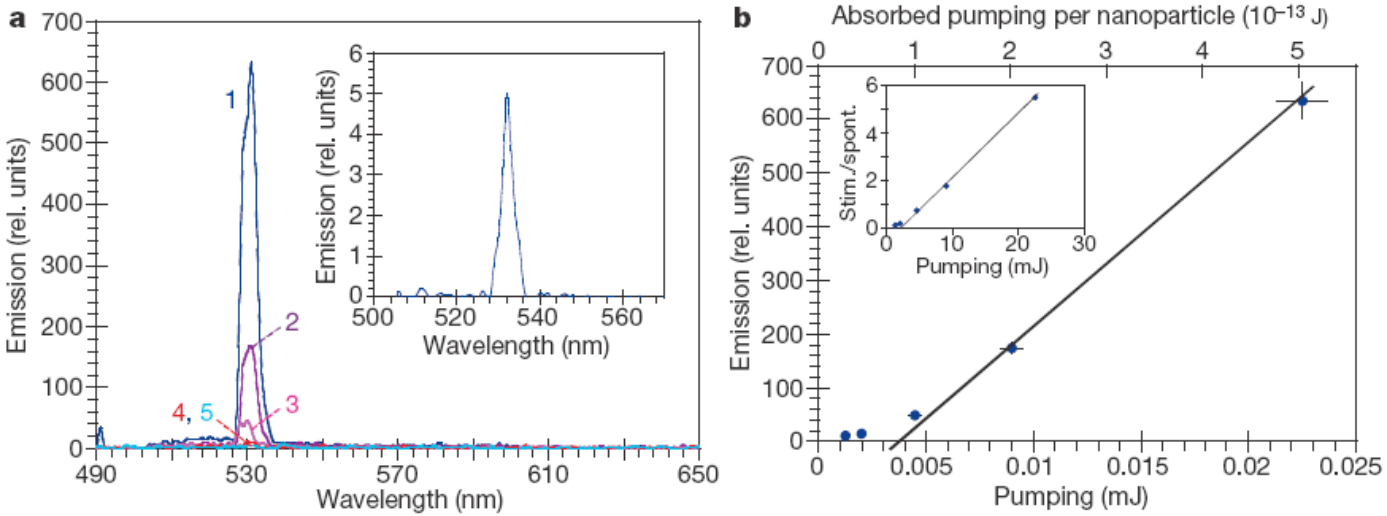


**Figure 4 | Stimulated emission.** **a**, Main panel, stimulated emission spectra of the nanoparticle sample pumped with 22.5 mJ (1), 9 mJ (2), 4.5 mJ (3), 2 mJ (4) and 1.25 mJ (5) 5-ns optical parametric oscillator pulses at $\lambda = 488$ nm. **b**, Main panel, corresponding input–output curve (lower axis, total launched pumping energy; upper axis, absorbed pumping energy per

by the noise of the photodetector and the instability of the pumping laser) do not exceed the size of the symbol. Inset of **a**, stimulated emission spectrum at more than 100-fold dilution of the sample. Inset of **b**, the ratio of the stimulated emission intensity (integrated between 526 nm and 537 nm) to the spontaneous emission background (integrated at <526 nm and

# Lasing in metal-insulator-metal sub-wavelength plasmonic waveguides

**Martin T. Hill[1*], Milan Marell[1], Eunice S. P. Leong[2], Barry Smalbrugge[1], Youcai Zhu[1], Minghua Sun[2], Peter J. van Veldhoven[1], Erik Jan Geluk[1], Fouad Karouta[1], Yok-Siang Oei[1], Richard Nötzel[1], Cun-Zheng Ning[2], and Meint K. Smit[1]**

*[1]COBRA Research Institute, Technische Universiteit Eindhoven, Postbus 513, 5600 MB Eindhoven, The Netherlands*
*[2] Department of Electrical Engineering, Arizona State University, Tempe AZ 85287, USA*
**m.t.hill@ieee.org*

Received 14 Apr 2009; revised 8 Jun 2009; accepted 9 Jun 2009; published 18 Jun 2009
22 June 2009 / Vol. 17, No. 13 / OPTICS EXPRESS 11107

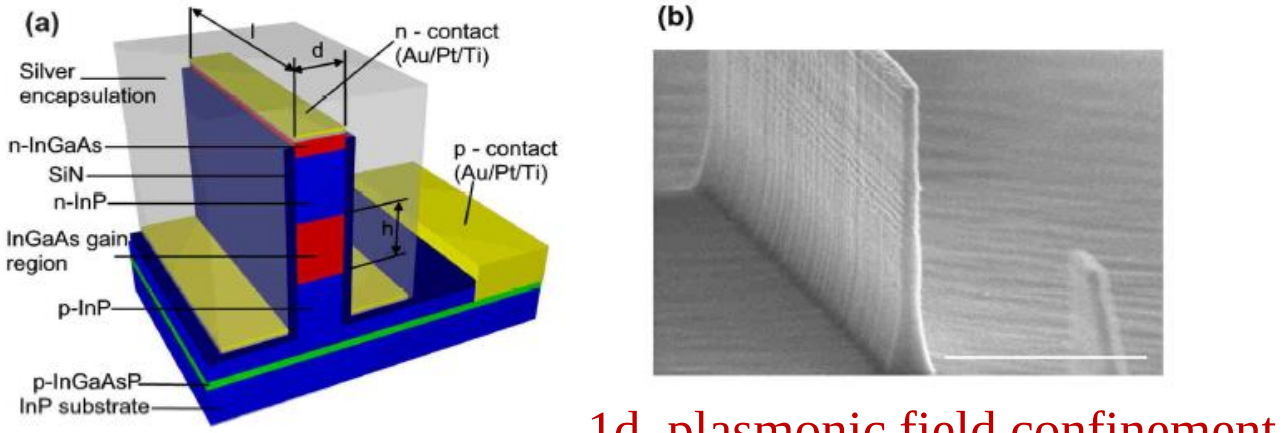


1d plasmonic field confinement

Fig. 1. Structure of cavity formed by a rectangular semiconductor pillar encapsulated in Silver. (a) Schematic showing the device layer structure. (b) Scanning electron microscope image showing the semiconductor core of one of the devices. The scale bar is 1 micron.

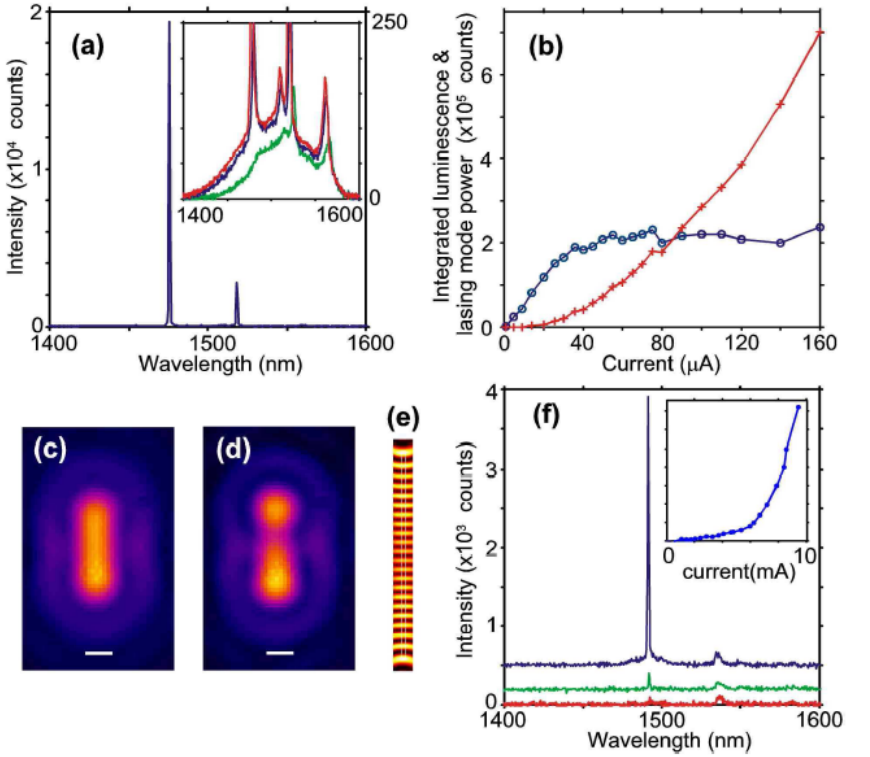


Fig. 2. Spectra and near field patterns showing lasing in devices. (a) Above threshold emission spectrum for 3 micron long device with semiconductor core width d~130nm ( ± 20nm), with pump current 180 μA at 78K. Inset: emission spectra for 20 (green), 40 (blue) and 60 (red) μA, all at 78K. (b) Lasing mode light output (red crosses), integrated luminescence (blue circles), versus pump current for 78K. (c) Actual near field pattern (in x-y plane) for 6 micron ($d$ = 130nm) device captured with 100x, 0.7 NA long working distance microscope objective and infrared camera, the scale bar is 2 micron, for below threshold 30 μA, and (d) above threshold 320 μA. (e) Simulated vertical (z) component of the Poynting vector taken at 0.7 microns below the pillar base, shows most emitted light at ends of device. (f) Spectra for a 6 micron long device with d~310nm at 298K, pulsed operation (28 ns wide pulses, 1MHz repetition). Spectra for peak currents of 5.2mA (red), 5.9mA (green) and 7.4mA (blue), (currents were estimated from the applied voltage pulse amplitude). The spectra for 5.9 and 7.4 mA are offset from 0 for clarity. Inset shows the total light collected by the spectrometer from the device for currents ranging from 0 to 10mA.

doi:10.1038/nature08364 nature

LETTERS

# Plasmon lasers at deep subwavelength scale

Rupert F. Oulton[1]*, Volker J. Sorger[1]*, Thomas Zentgraf[1]*, Ren-Min Ma[3], Christopher Gladden[1], Lun Dai[3], Guy Bartal[1] & Xiang Zhang[1,2]

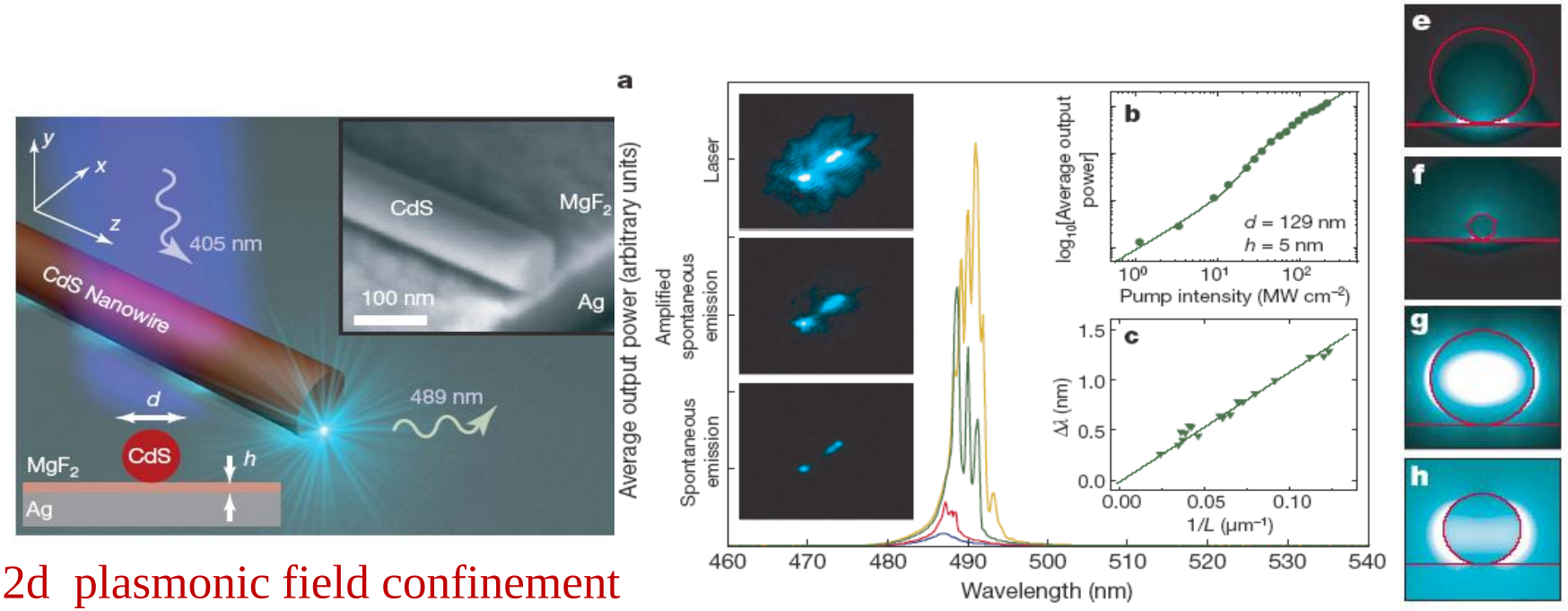


2d plasmonic field confinement

Department of Physics and Astronomy
Georgia State University
Atlanta, GA 30303-3083

# A room-temperature semiconductor spaser operating near 1.5 μm

R. A. Flynn,[1] C. S. Kim,[1] I. Vurgaftman,[1] M. Kim,[1] J. R. Meyer,[1] A. J. Mäkinen,[1]
K. Bussmann,[2] L. Cheng,[3] F.-S. Choa,[3] and J. P. Long[4,*]

25 April 2011 / Vol. 19, No. 9 / OPTICS EXPRESS 8954

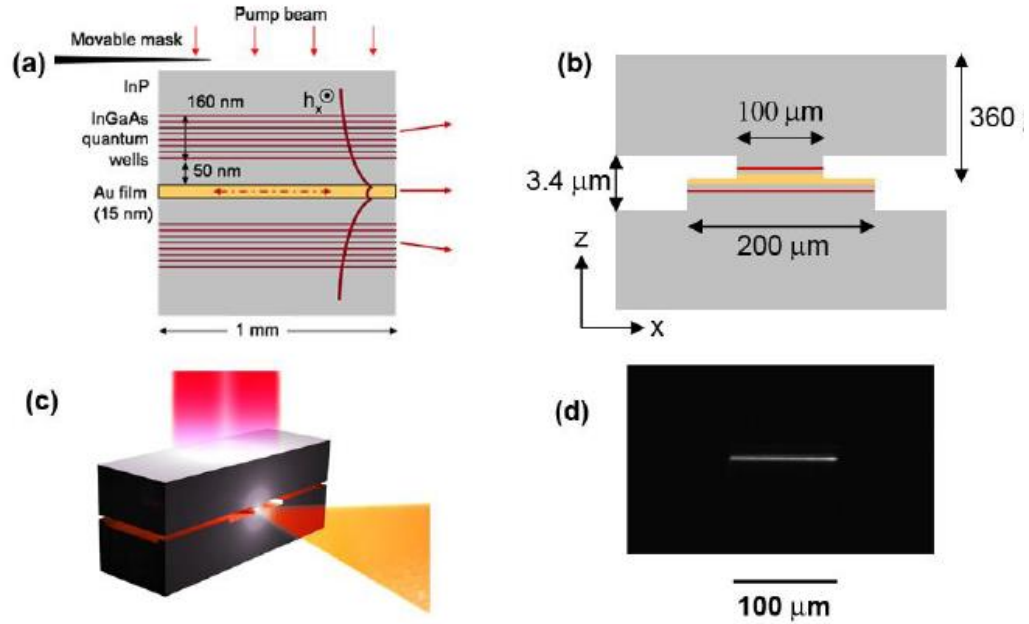


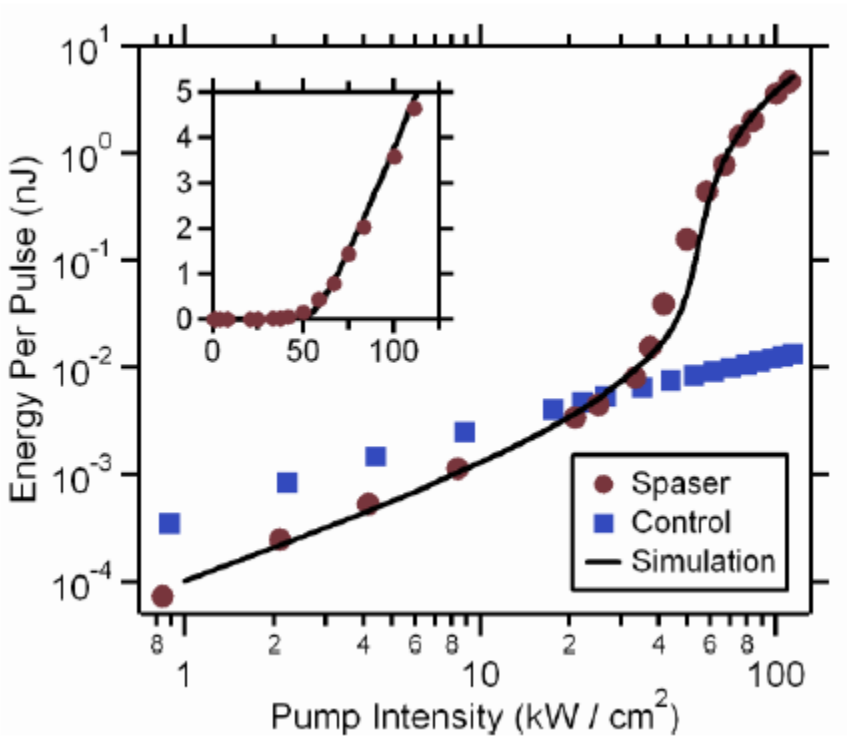

Department o
Georgia State
Atlanta, GA 3

# Plasmonic Nanolaser Using Epitaxially Grown Silver Film

Yu-Jung Lu,[1]* Jisun Kim,[2]* Hung-Ying Chen,[1] Chihhui Wu,[2] Nima Dabidian,[2] Charlotte E. Sanders,[2] Chun-Yuan Wang,[1] Ming-Yen Lu,[3] Bo-Hong Li,[4] Xianggang Qiu,[4] Wen-Hao Chang,[5] Lih-Juann Chen,[3] Gennady Shvets,[2] Chih-Kang Shih,[2]† Shangjr Gwo[1]†

Science
AAAS

Having developed epitaxially grown, atomically smooth Ag films as a scalable plasmonic platform, we report a SPASER under CW operation with an ultralow lasing threshold at liquid nitrogen temperature and a mode volume well below the 3D diffraction limit. The device has

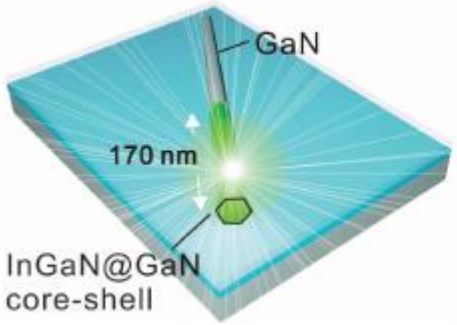


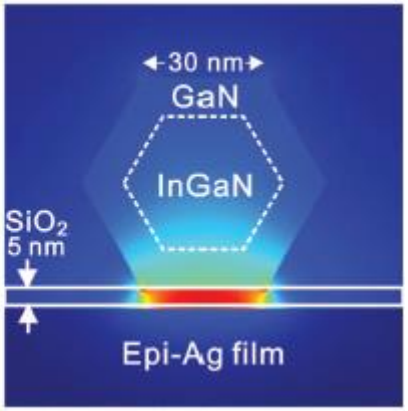


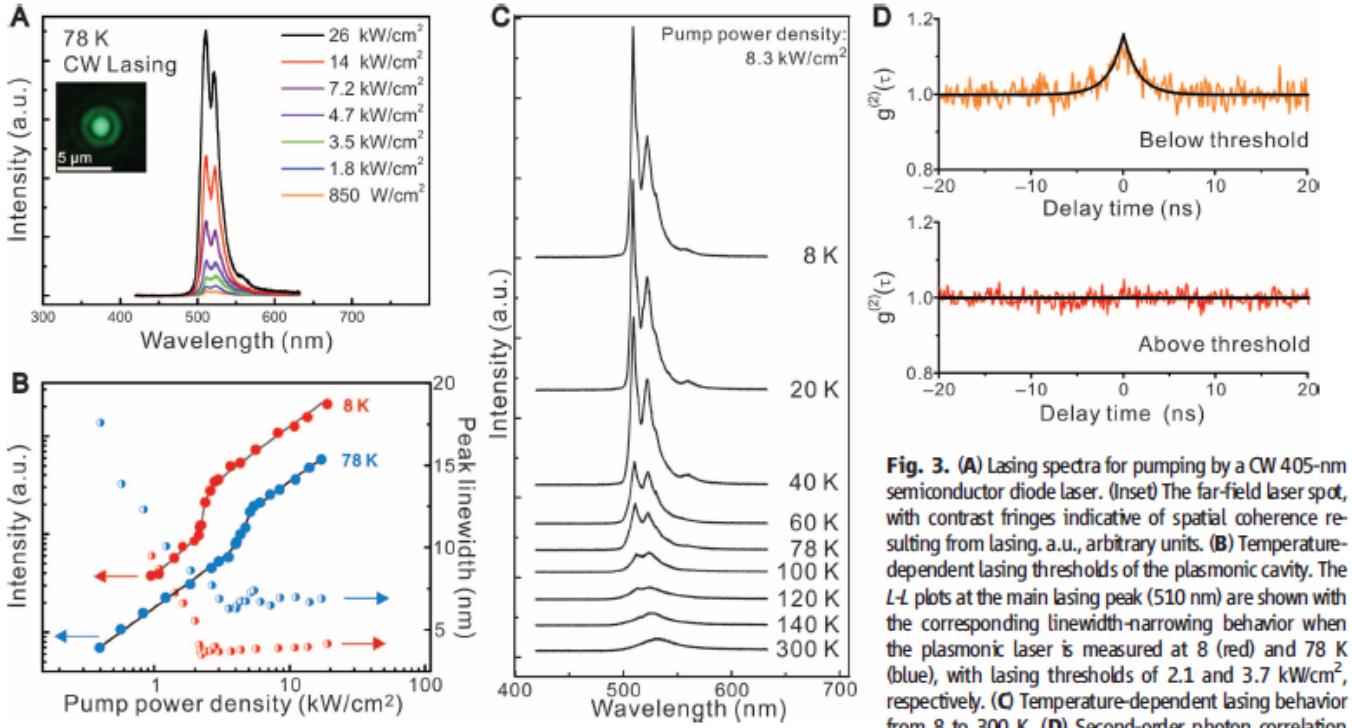


**Fig. 3.** (**A**) Lasing spectra for pumping by a CW 405-nm semiconductor diode laser. (Inset) The far-field laser spot, with contrast fringes indicative of spatial coherence resulting from lasing. a.u., arbitrary units. (**B**) Temperature-dependent lasing thresholds of the plasmonic cavity. The *L-L* plots at the main lasing peak (510 nm) are shown with the corresponding linewidth-narrowing behavior when the plasmonic laser is measured at 8 (red) and 78 K (blue), with lasing thresholds of 2.1 and 3.7 kW/cm$^2$, respectively. (**C**) Temperature-dependent lasing behavior from 8 to 300 K. (**D**) Second-order photon correlation function measurements at 8 K.

Georgia State University
NANO LETTERS
Letter
dx.doi.org/10.1021/nl501273u
pubs.acs.org/NanoLett
Y.-J. Lu *et al.*, Nano Lett. **14**, 4381 (2014)

# All-Color Plasmonic Nanolasers with Ultralow Thresholds: Autotuning Mechanism for Single-Mode Lasing

Yu-Jung Lu,[†] Chun-Yuan Wang,[†] Jisun Kim,[‡] Hung-Ying Chen,[†] Ming-Yen Lu,[∥] Yen-Chun Chen,[⊥] Wen-Hao Chang,[⊥] Lih-Juann Chen,[∥] Mark I. Stockman,[§,#,¶] Chih-Kang Shih,[*,‡] and Shangjr Gwo[*,†]

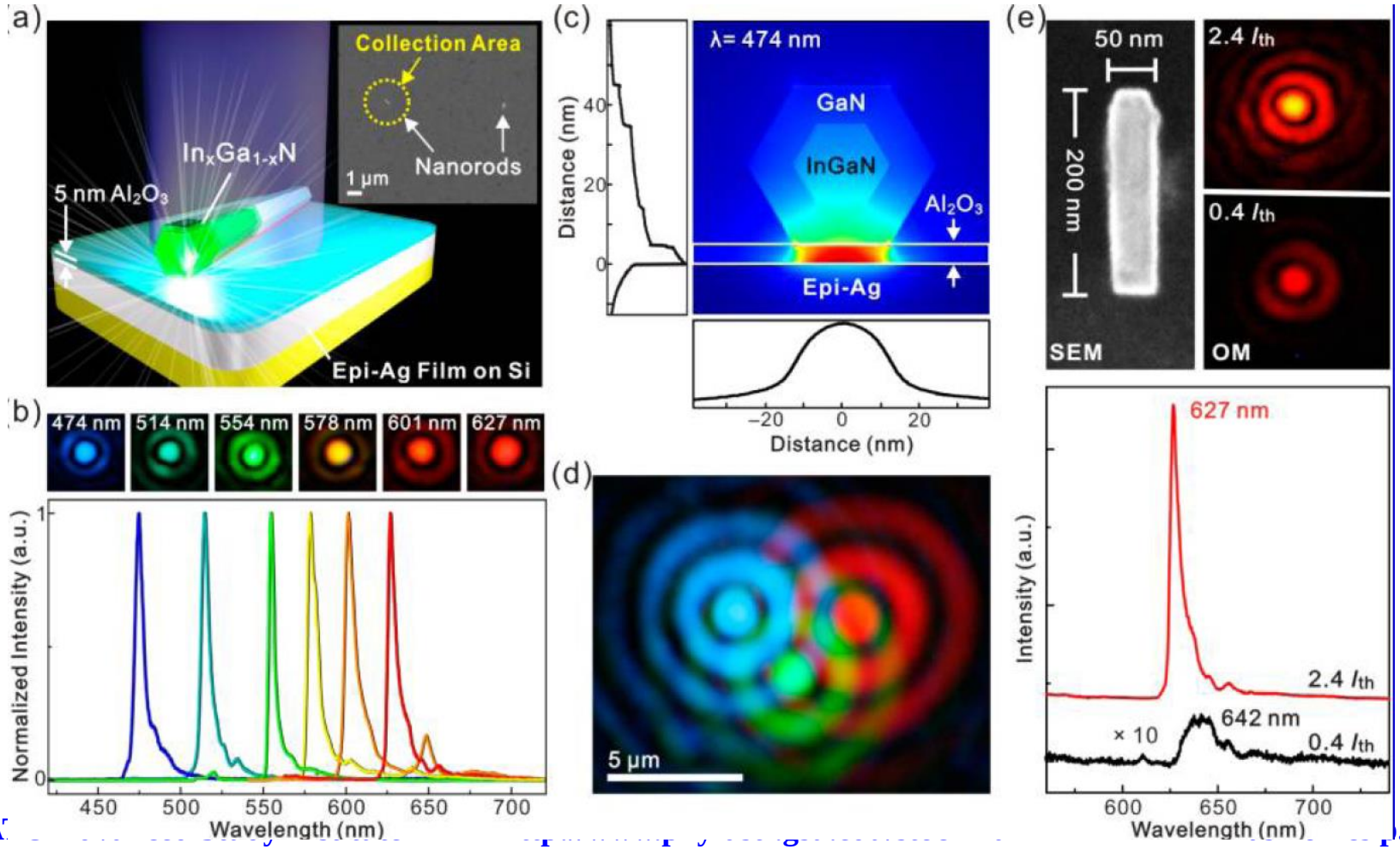

nature COMMUNICATIONS

ARTICLE

Received 28 Dec 2013 | Accepted 11 Aug 2014 | Published 23 Sep 2014

DOI: 10.1038/ncomms5953

# A room temperature low-threshold ultraviolet plasmonic nanolaser

Qing Zhang[1], Guangyuan Li[1], Xinfeng Liu[1], Fang Qian[2], Yat Li[3], Tze Chien Sum[1,4], Charles M. Lieber[5] & Qihua Xiong[1,6]

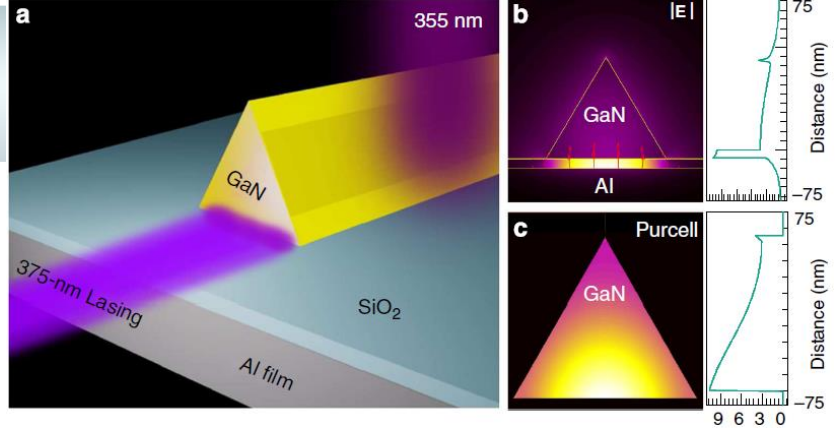


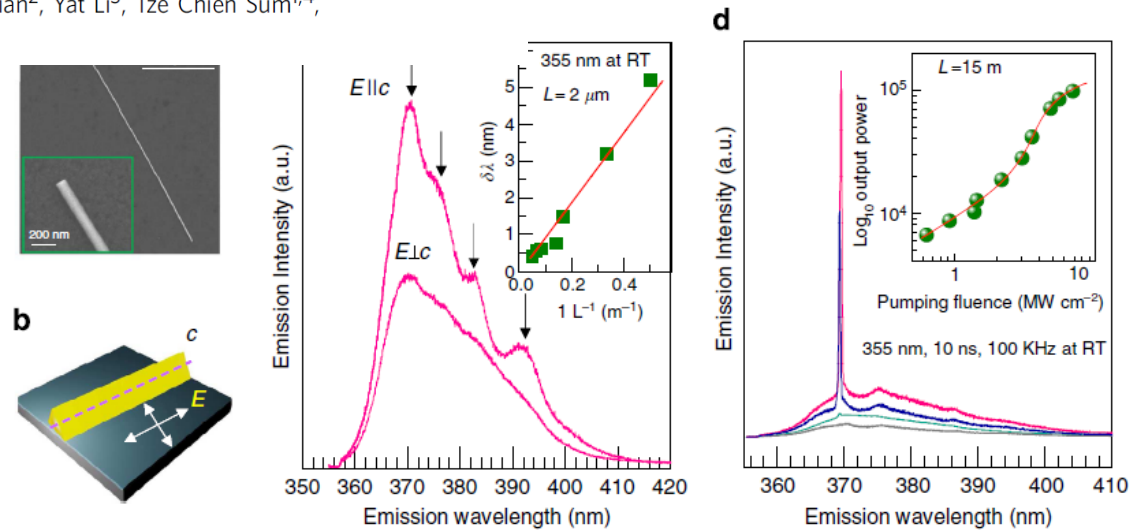


**Figure 2 | Room temperature ultraviolet plasmonic lasing characterization.** (**a**) Scanning electron microscopy (SEM) image of a GaN nanowire sitting on $SiO_2$/Al film. Inset: magnified scanning electron microscopy image of one end of the GaN nanowire. The nanowire length and diameter is 15 μm and 100 nm, respectively. (**b**) Schematic of optical measurement and polarization detection setup. *c* is defined as the orientation of nanowire. The incidence excitation laser is circular polarized and the focused laser beam can cover the whole nanowire. The emission scattered out from two ends is collected and the polarization property along and perpendicular to nanowire axis *c* is analysed. (**c**) Spontaneous emission of as-fabricated plasmonic device below lasing threshold at room temperature under a power fluence of 0.5 MW cm$^{-2}$. Arrows highlight the Fabry–Pérot peaks. The nanowire length is 2 μm. Inset: cavity mode spacing $\delta\lambda$ variation with nanowire length $L$ (green dots). $\delta\lambda$ versus $1/L$ can be well fitted with a linear function (red curve), suggesting a high group index $n_g$ ($n_g = \lambda^2/2L$) of 7.61 due to the high gain requirement of the plasmonic laser device. (**d**) Power-dependent emission spectra of the plasmonic devices. One sharp peak with a maximum full width at half maximum (FWHM) ~0.8 nm appears above the spontaneous emission background. The nanowire length is 15 μm. Inset: integrated emission versus pumping intensity. The *S*-shaped plot suggests the evolution from a spontaneous emission, amplified spontaneous emission to lasing process.

# Graphene spaser

Vadym Apalkov[1] and Mark I. Stockman[1,2,3]
[1] *Department of Physics and Astronomy, Georgia State University, Atlanta, Georgia 30303, USA*
[2] *Fakultät für Physik, Ludwig-Maximilians-Universität, Geschwister-Scholl-Platz 1, D-80539 München, Germany*
[3] *Max-Planck-Institut für Quantenoptik, Hans-Kopfermann-Strasse 1, D-85748 Garching, Germany*
(Dated: May 10, 2013)

We propose a graphene spaser, which is a coherent quantum generator of surface plasmons in nanostructured graphene. The plasmonic core of this spaser is a graphene monolayer nanopatch and its active (gain) element is a multi-quantum well system with a design similar to the design of an active element of quantum cascade laser. For realistic parameters of the multi-quantum well system, the spasing in graphene monolayer can be achieved at a finite doping of graphene and at a plasmon frequency, $\approx 0.15$ eV, close to the typical frequency of intersubband transitions in multi-quantum well systems. The proposed graphene spaser will be an efficient source of intense and coherent nanolocalized fields in the mid-infrared spectral region with wide perspective applications in mid-infrared nanoscopy, nano-spectroscopy, and nano-lithography.

V. Apalkov and M. I. Stockman, *Proposed Graphene Nanospaser,* NPG: Light Sci. Appl. **3,** e191 (2014).

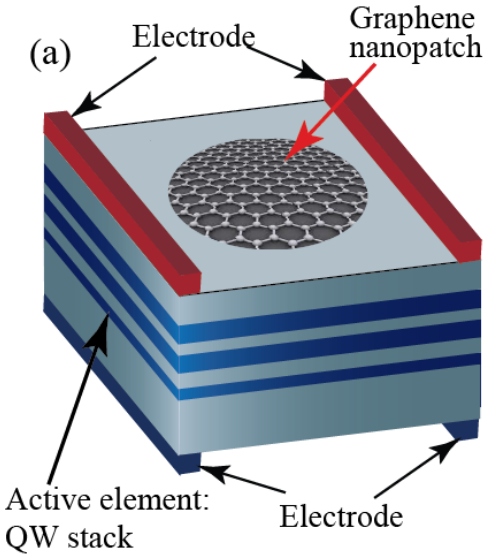


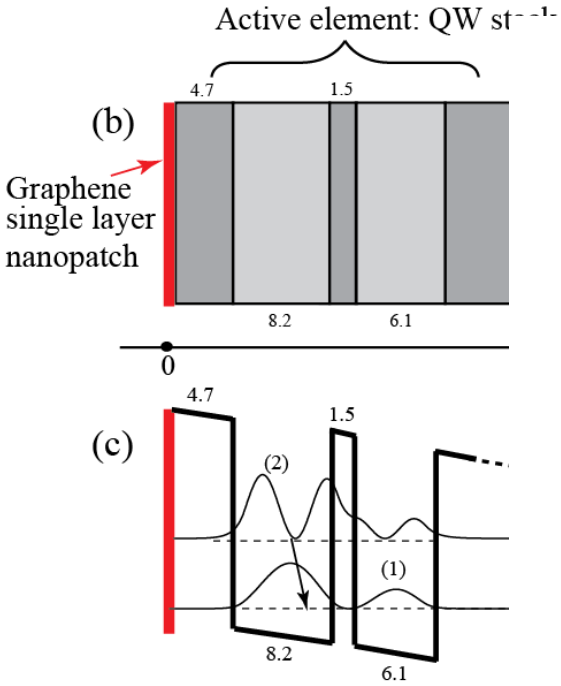


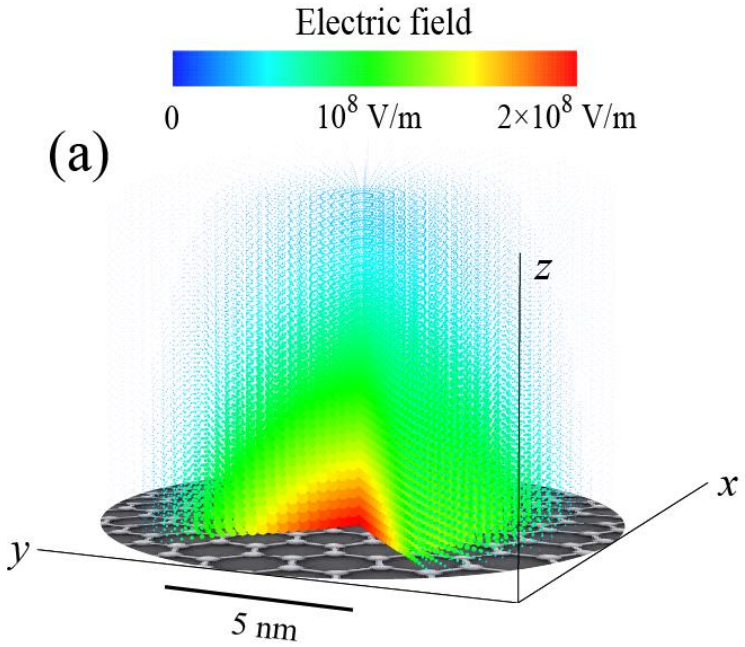

IOP Publishing Journal of Optics
J. Opt. 14 (2012) 114015 (7pp) doi:10.1088/2040-8978/14/11/114015

# Stimulated emission of surface plasmon polaritons on smooth and corrugated silver surfaces

J K Kitur, G Zhu, Yu A Barnakov and M A Noginov

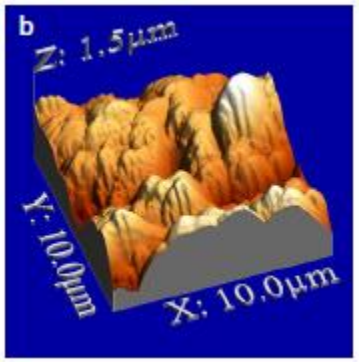


Smooth surface

**Random Spaser**

Rough surface

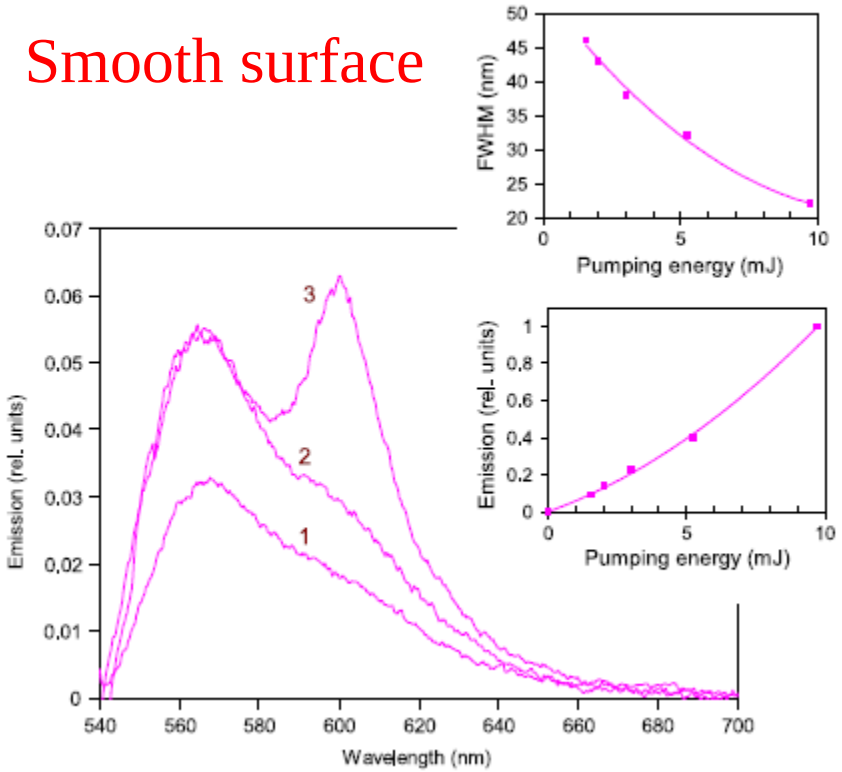


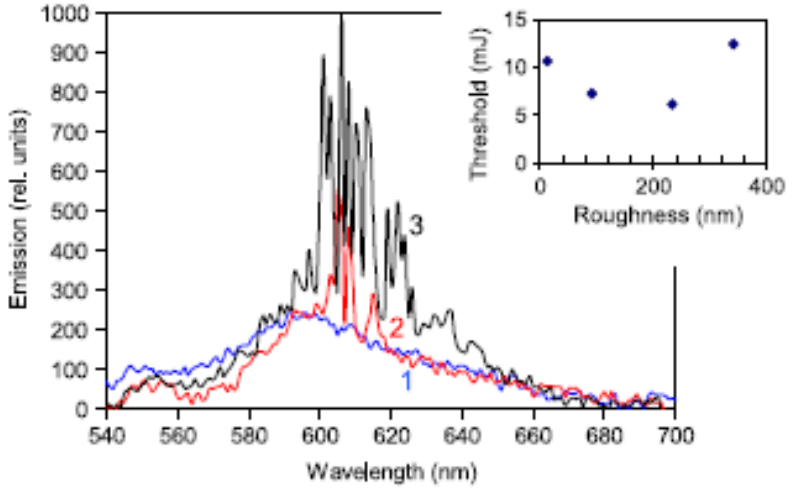


**Figure 5.** Emission spectra in the RB:PMMA film deposited on a roughened silver with surface roughness equal to 234 nm, pumped with 7 mJ (1), 13 mJ (2) and 20 mJ (3) laser pulses. Inset: stimulated emission threshold as a function of the surface roughness.

# Surface plasmon lasing observed in metal hole arrays

Frerik van Beijnum,[1] Peter J. van Veldhoven,[2] Erik Jan Geluk,[2]
Michiel J.A. de Dood,[1] Gert W. 't Hooft,[1,3] and Martin P. van Exter[1]

[1] *Leiden University, Huygens Laboratory, P.O. Box 9504, 2300 RA Leiden, The Netherlands*
[2] *COBRA Research Institute, Technische Universiteit Eindhoven, Postbus 513, 5600 MB Eindhoven, The Netherlands*
[3] *Philips Research Laboratories, Prof. Holstlaan 4, 5656 AA Eindhoven, Netherlands*

Phys. Rev. Lett. **110, 206802-1-5 (2013)**

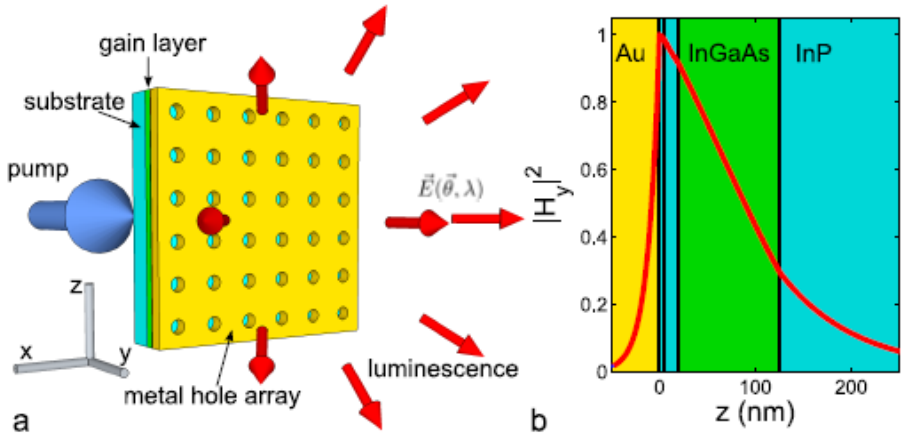


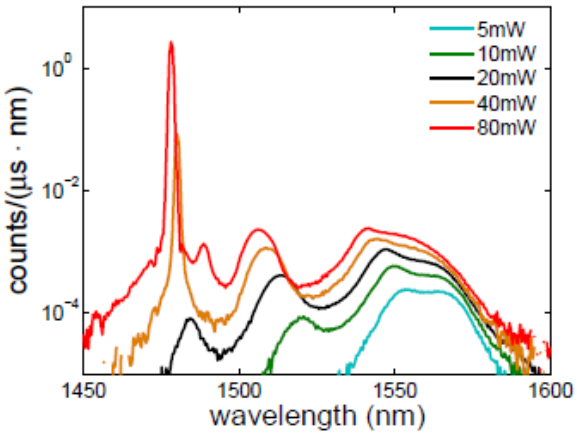


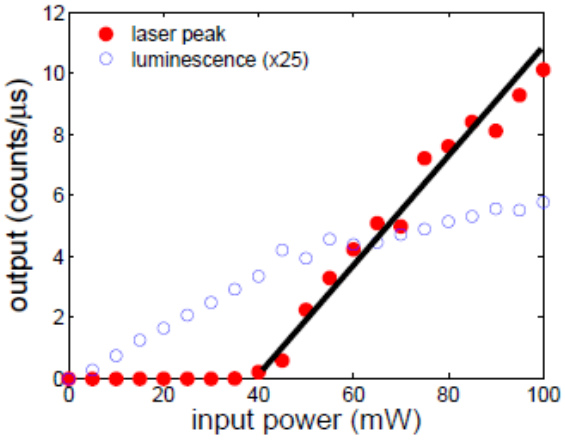


FIG. 2. (a) Luminescence spectra as a function of pump power, plotted on a semilog scale. For increasing pump power the bandwidth of the luminescence increases until the device starts lasing. Above threshold, the emission of the non-lasing resonances starts to saturate at a maximum intensity. 80 mW corresponds to $\sim$ 11 kW/cm$^2$ (b) The output in the lasing peak and in the luminescence in the range of 1485 – 1600 nm. The power in the lasing peak shows a clear threshold (red). The black line is a guide to the eye. The luminescence outside the lasing peak starts to level off, as expected for lasing in semiconductor devices (blue).

LETTERS
PUBLISHED ONLINE: 16 JUNE 2013 | DOI: 10.1038/NNANO.2013.99
nature nanotechn

# Lasing action in strongly coupled plasmonic nanocavity arrays

Wei Zhou[1†], Montacer Dridi[2], Jae Yong Suh[2], Chul Hoon Kim[2,3†], Dick T. Co[2,3], Michael R. Wasielewski[2,3], George C. Schatz[2] and Teri W. Odom[1,2,3*]

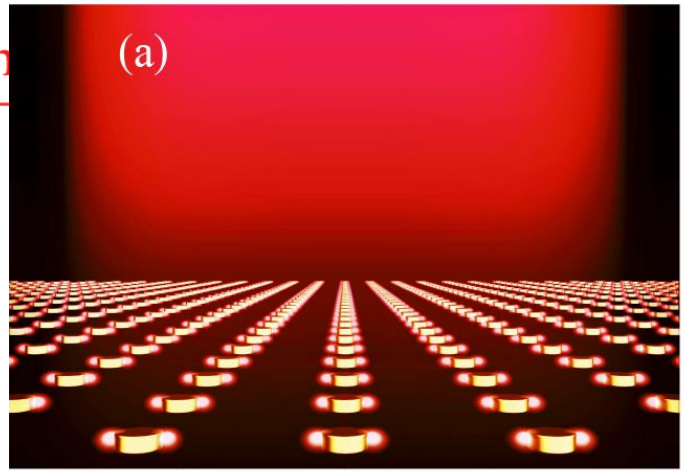


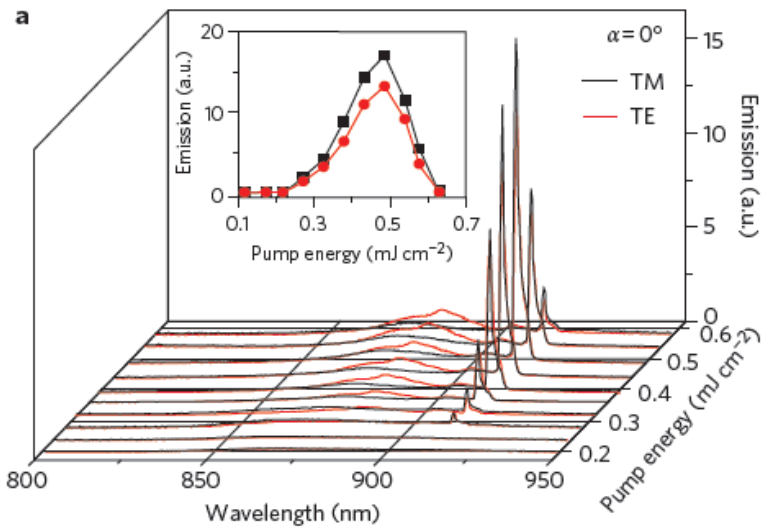


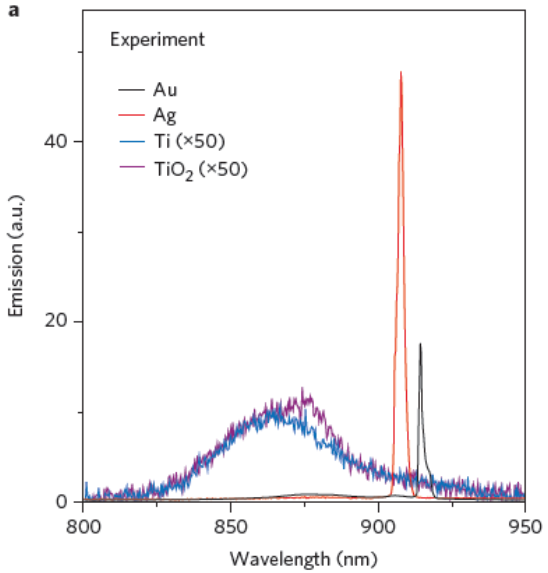


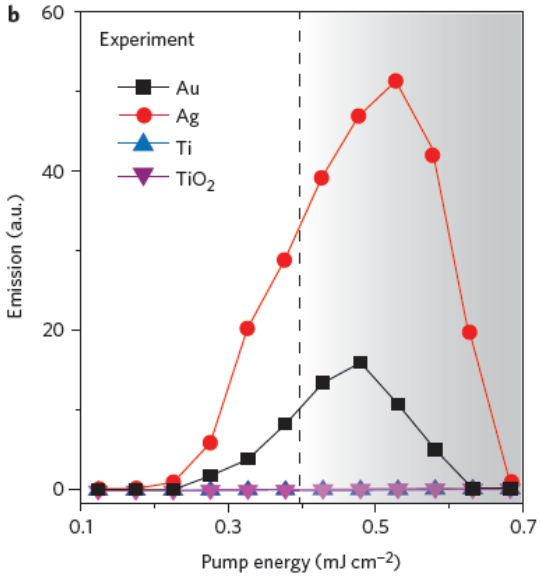

ARTICLES
PUBLISHED ONLINE: 28 SEPTEMBER 2014 | DOI: 10.1038/NPHYS3103
nature physics

# Ultrafast plasmonic nanowire lasers near the surface plasmon frequency

Themistoklis P. H. Sidiropoulos[1]*, Robert Röder[2], Sebastian Geburt[2], Ortwin Hess[1], Stefan A. Maier[1], Carsten Ronning[2] and Rupert F. Oulton[1]*

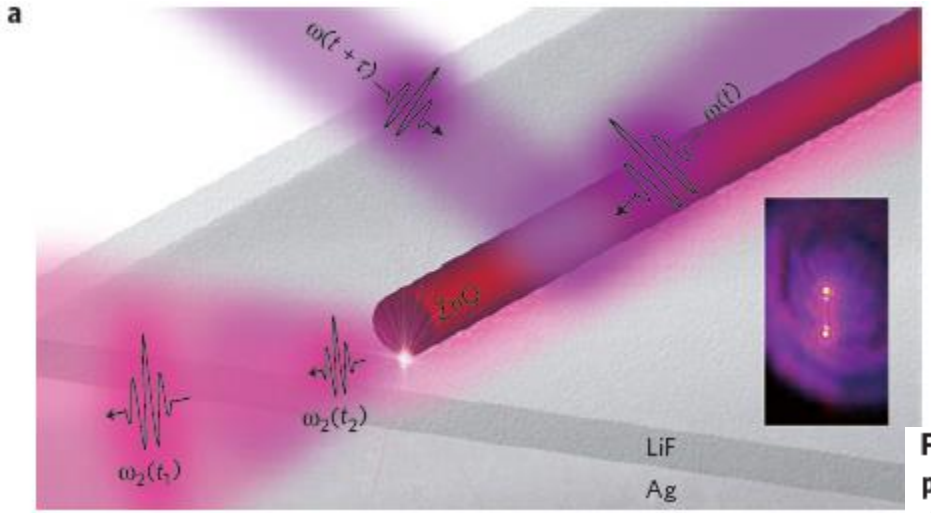


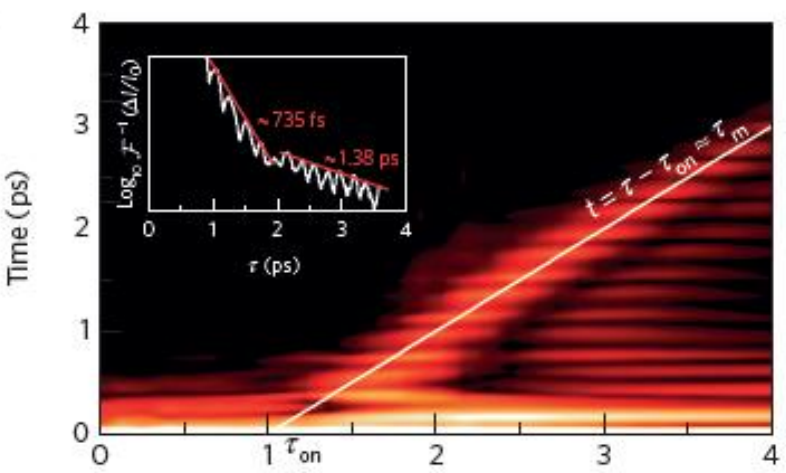


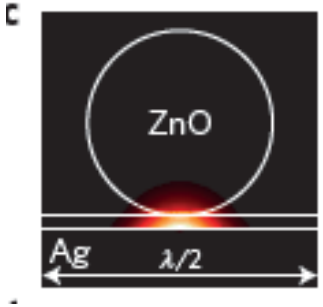


**Figure 5 | Measured spectra versus double-pump pulse delay for the plasmonic nanowire laser and its Fourier transform. a**, Normalized difference spectrum, $\Delta I(\lambda,\tau)/I_0(\lambda) - I(\lambda,\tau)/I_0(\lambda) - 1$, of the plasmonic nanowire laser for $\tau \geq 0$, where $I(\lambda,\tau)$ is the spectrum under double-pump excitation and $I_0(\lambda)$ is the single strong pump pulse spectrum. The two upper panels show the $\Delta I/I_0$ spectra for the pulse delays, $\tau = 2.0$ ps and $\tau = 3.1$ ps, indicating the increasing spectral modulation frequency with pulse delay. **b**, Fourier transform of each spectrum shown in **a** versus pulse delay. The white trend line follows $t = \tau - \tau_{on} \approx \tau_m$, indicating a turn-on time of $\tau_{on} = 1.1$ ps. The inset shows the amplitude decay of the Fourier transform along the white trend line, with linear fits (red lines) to the modulation peaks. The presented data in this figure correspond to measurements at the highest pump power (situation i) shown in Fig. 4a.

nature nanotechnology
LETTERS
PUBLISHED ONLINE: 20 JULY 2014 | DOI: 10.1038/NNANO.2014.135

# Explosives detection in a lasing plasmon nanocavity

Ren-Min Ma[1†], Sadao Ota[1†], Yimin Li[1], Sui Yang[1] and Xiang Zhang[1,2*]

[1]NSF Nanoscale Science and Engineering Centre, 3112 Etcheverry Hall, University of California, Berkeley, California 94720, USA, [2]Materials Sciences Division, Lawrence Berkeley National Laboratory, 1 Cyclotron Road, Berkeley, California 94720, USA,

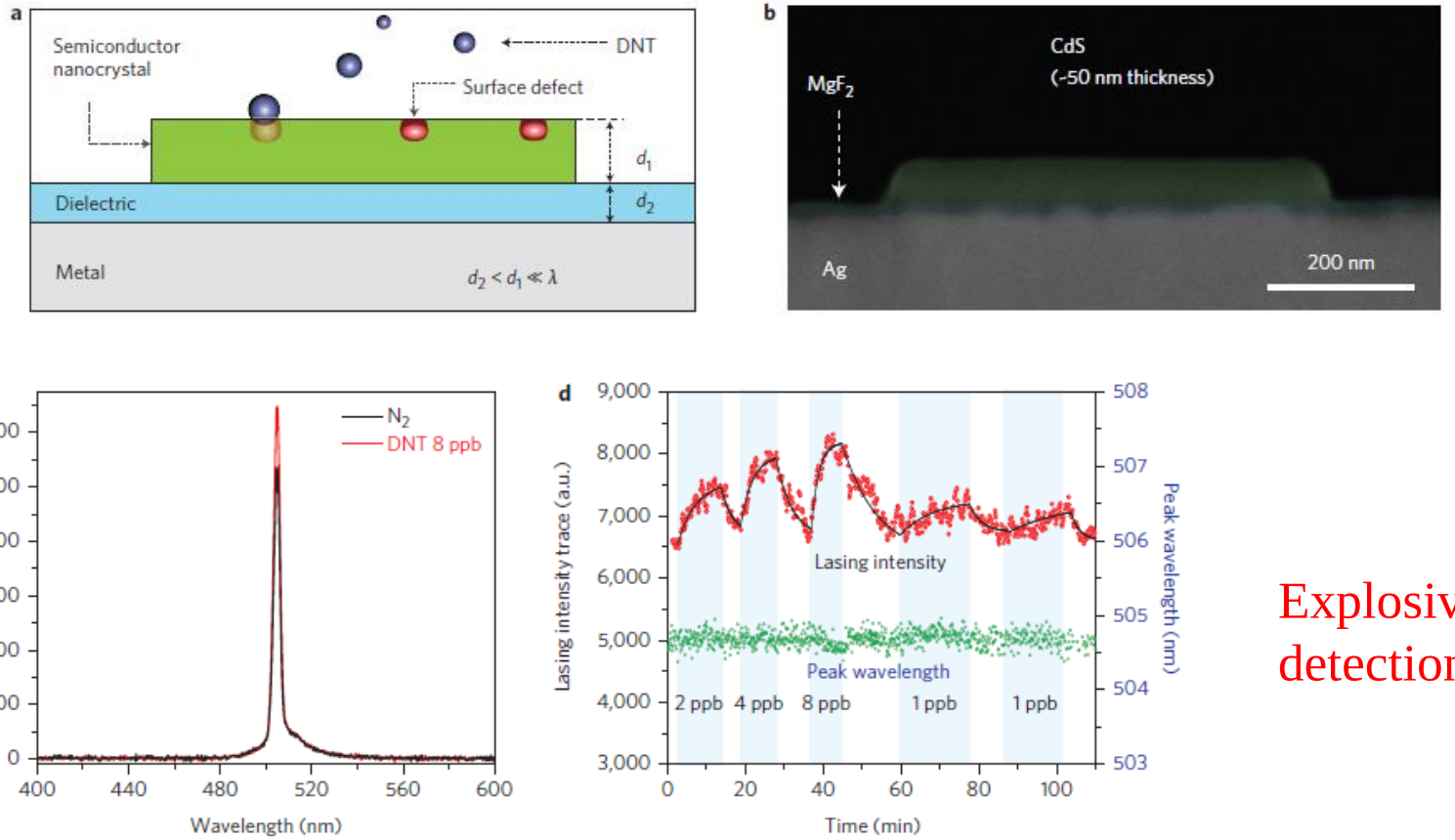


Explosive (DNT) detection

Georgia State University
nature photonics
LETTERS
PUBLISHED ONLINE: 12 JUNE 2011 | DOI: 10.1038/NPHOTON.2011.99

# Single-cell biological lasers

Malte C. Gather[1,2] and Seok Hyun Yun[1,2,3,4]*

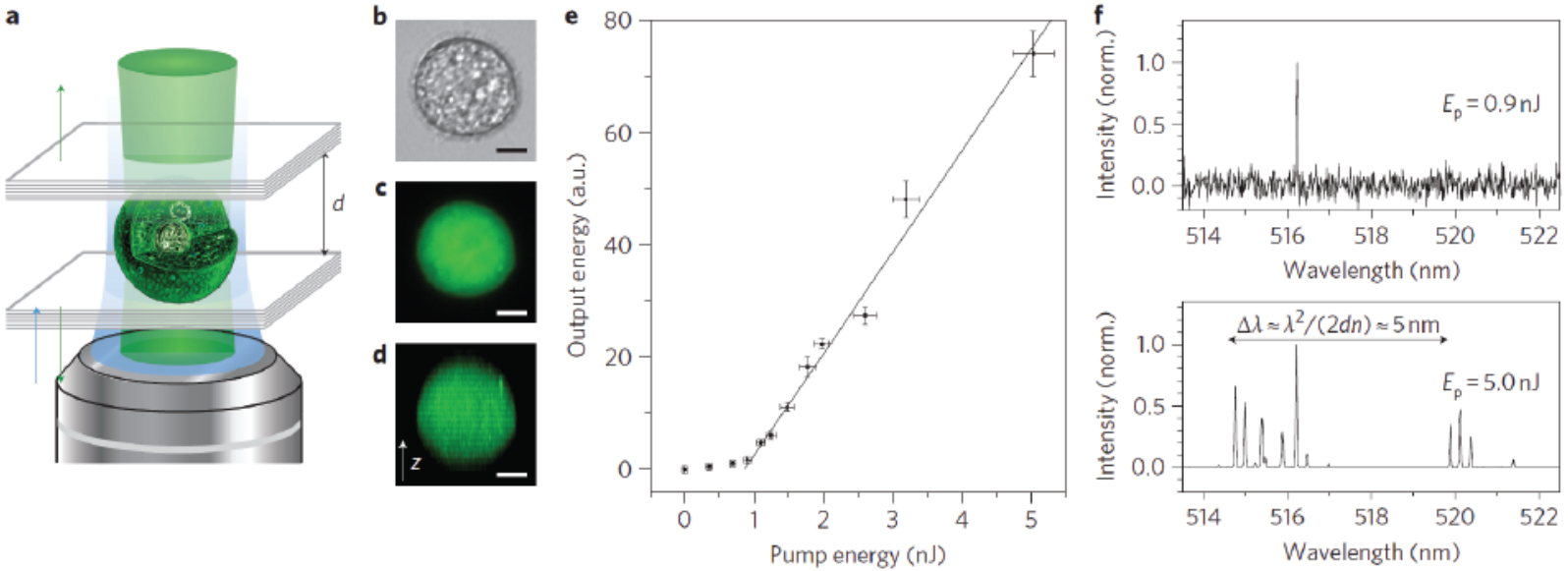


**Figure 2 | Laser formed by a single eukaryotic cell. a**, Illustration of the single-cell laser. A live eGFP-expressing 293ETN cell is placed inside a high-*Q* resonator consisting of two DBRs ($d = 20\,\mu$m). **b–d**, Microscope images of a single 293ETN cell outside the resonator (scale bars, 5 μm): DIC image (**b**); confocal fluorescence microscope image showing the eGFP distribution in the cell (**c**); side-view projection of a *z*-stack of confocal fluorescence images (**d**). **e**, Laser output energy of a cell laser as a function of the pump energy. Line, linear fit to data above 1 nJ. Error bars represent detector noise and pulse-to-pulse variation of output (*y*), and pulse-to-pulse variation of pump (*x*), respectively. **f**, Normalized output spectra of the same laser for pump energies of 0.9 and 5 nJ, respectively. The arrow denotes the expected wavelength spacing of consecutive longitudinal modes.

Department of Physics and Astronomy
Georgia State University
Atlanta, GA 30303-3083

**Applications in Biomedicine: Why spaser is efficient as fluorescent, photothermal and photoacoustic agent? It does not saturate!**

Absorption cross section as a function of the pumping rate for different loads *r* of spaser

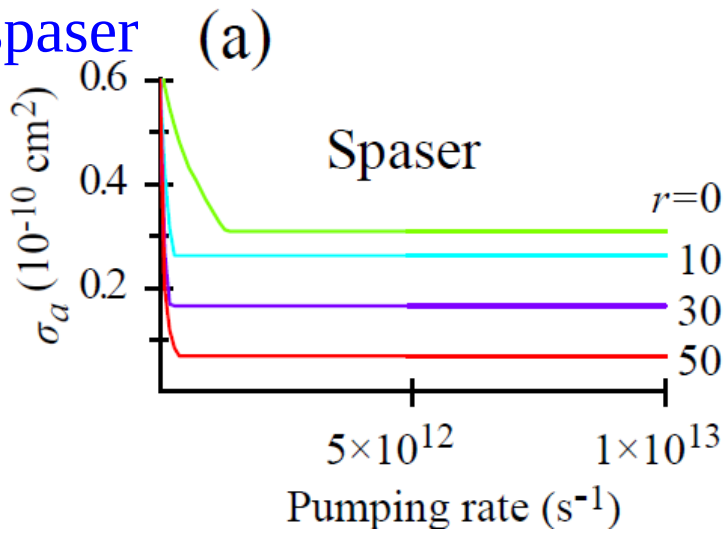


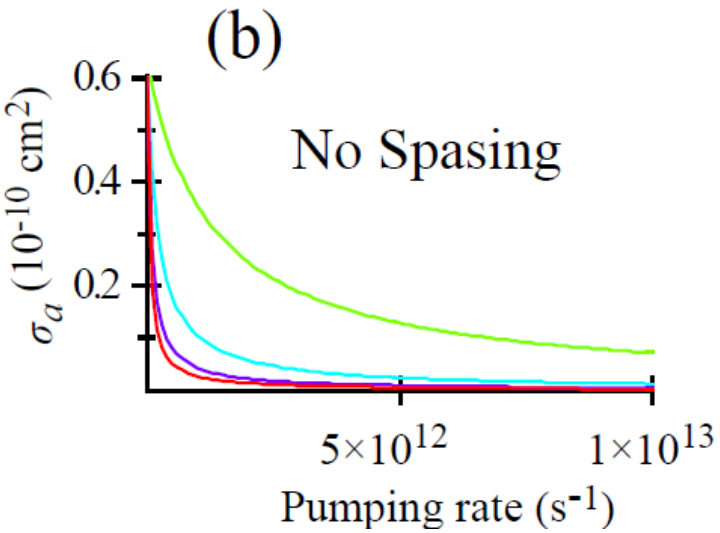


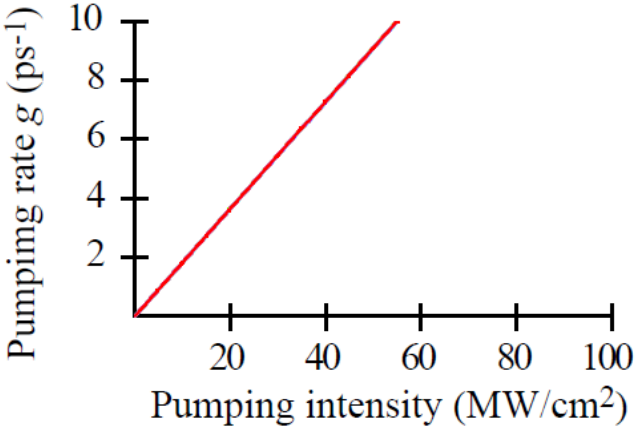


M. Javani, H. Koochaki, and M. Stockman
(In preparation)

Department of Physics and Astronomy
Georgia State University
Atlanta, GA 30303-3083

# Spaser Radiation Sensing of a Nanobubble Surrounding Spaser
## "Giant Spaser" Effect

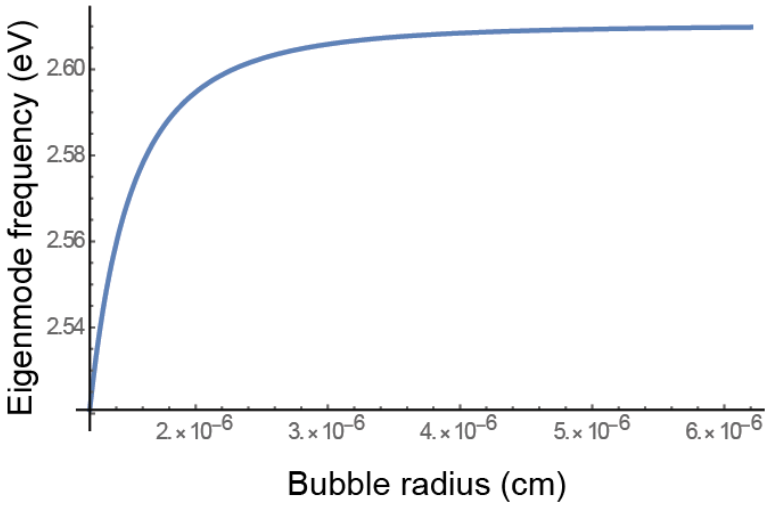


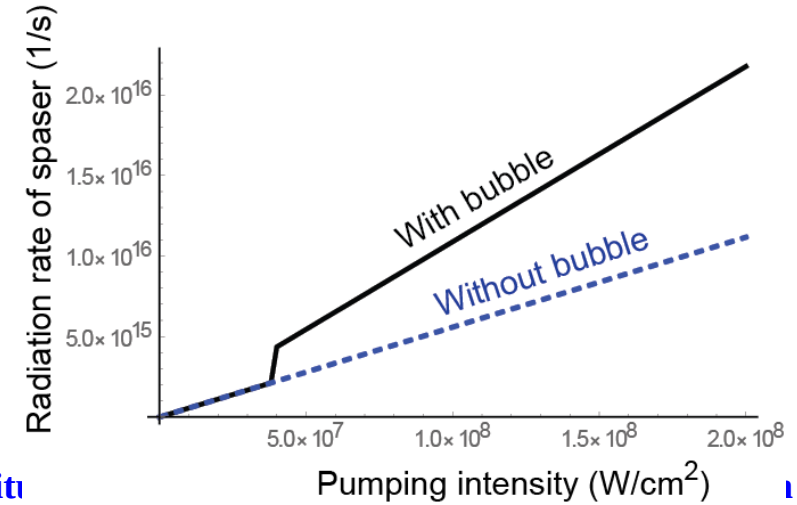

Department of Physics and Astronomy
Georgia State University
Atlanta, GA 30303-3083

nature COMMUNICATIONS

ARTICLE

Received 26 Jul 2016 | Accepted 30 Mar 2017 | Published 8 Jun 2017

DOI: 10.1038/ncomms15528 OPEN

# Spaser as a biological probe

Ekaterina I. Galanzha[1], Robert Weingold[1], Dmitry A. Nedosekin[1], Mustafa Sarimollaoglu[1], Jacqueline Nolan[1], Walter Harrington[1], Alexander S. Kuchyanov[2], Roman G. Parkhomenko[3], Fumiya Watanabe[4], Zeid Nima[4], Alexandru S. Biris[4], Alexander I. Plekhanov[2], Mark I. Stockman[5] & Vladimir P. Zharov[1]

[1] Arkansas Nanomedicine Center, University of Arkansas for Medical Sciences, Little Rock, Arkansas 72205, USA. [2] Institute of Automation and Electrometry of the Siberian Branch of the Russian Academy of Science, Koptyug Avenue 1, Novosibirsk 630090, Russia. [3] Nikolaev Institute of Inorganic Chemistry of the Siberian Branch of the Russian Academy of Science, Lavrentiev Avenue 3, Novosibirsk 630090, Russia. [4] Center for Integrative Nanotechnology Sciences, University of Arkansas at Little Rock, Little Rock, Arkansas 72204, USA. [5] Center for Nano-Optics and Department of Physics and Astronomy, Georgia State University, 29 Peachtree Center Avenue, Atlanta, Georgia 30302, USA. Correspondence and requests for materials should be addressed to V.P.Z. (email: zharovvladimirp@uams.edu).

# Spaser Label Radiation

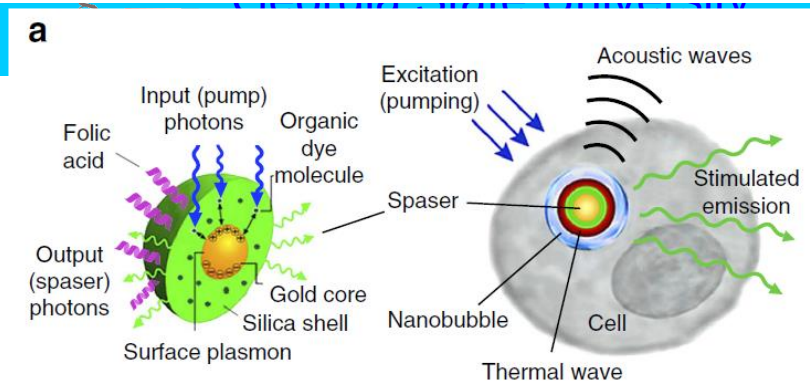


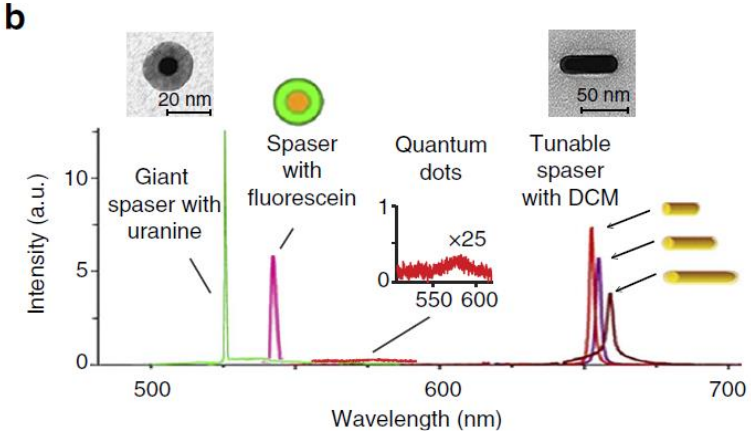


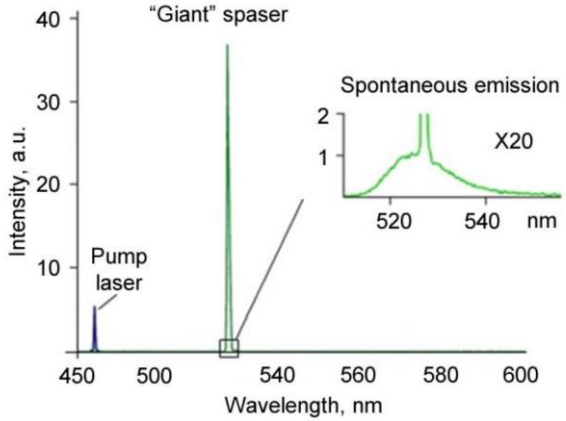


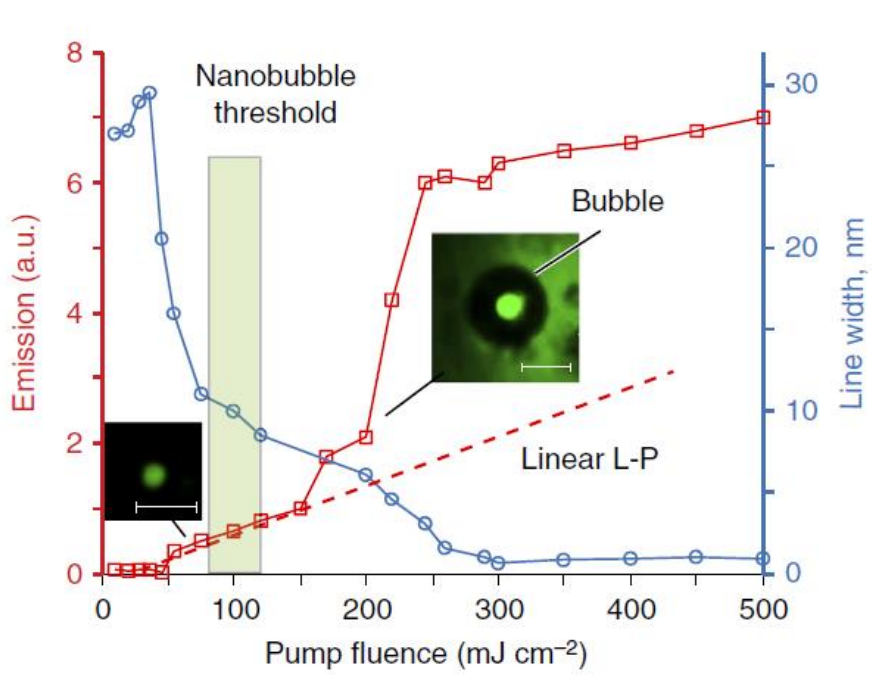


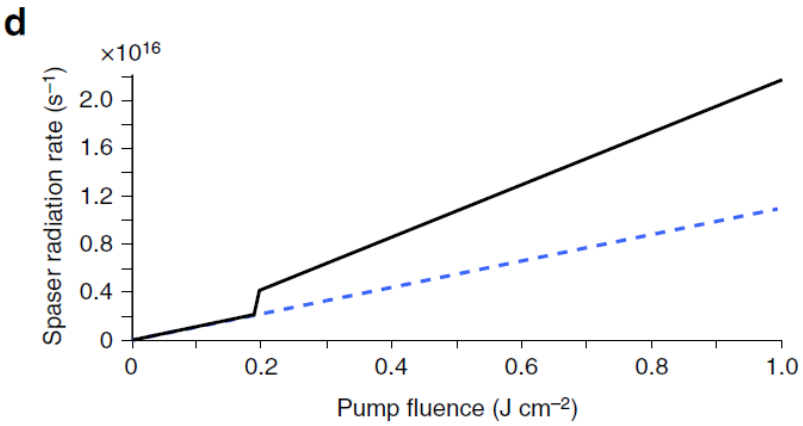

# Spaser Geometry and Elemental Composition

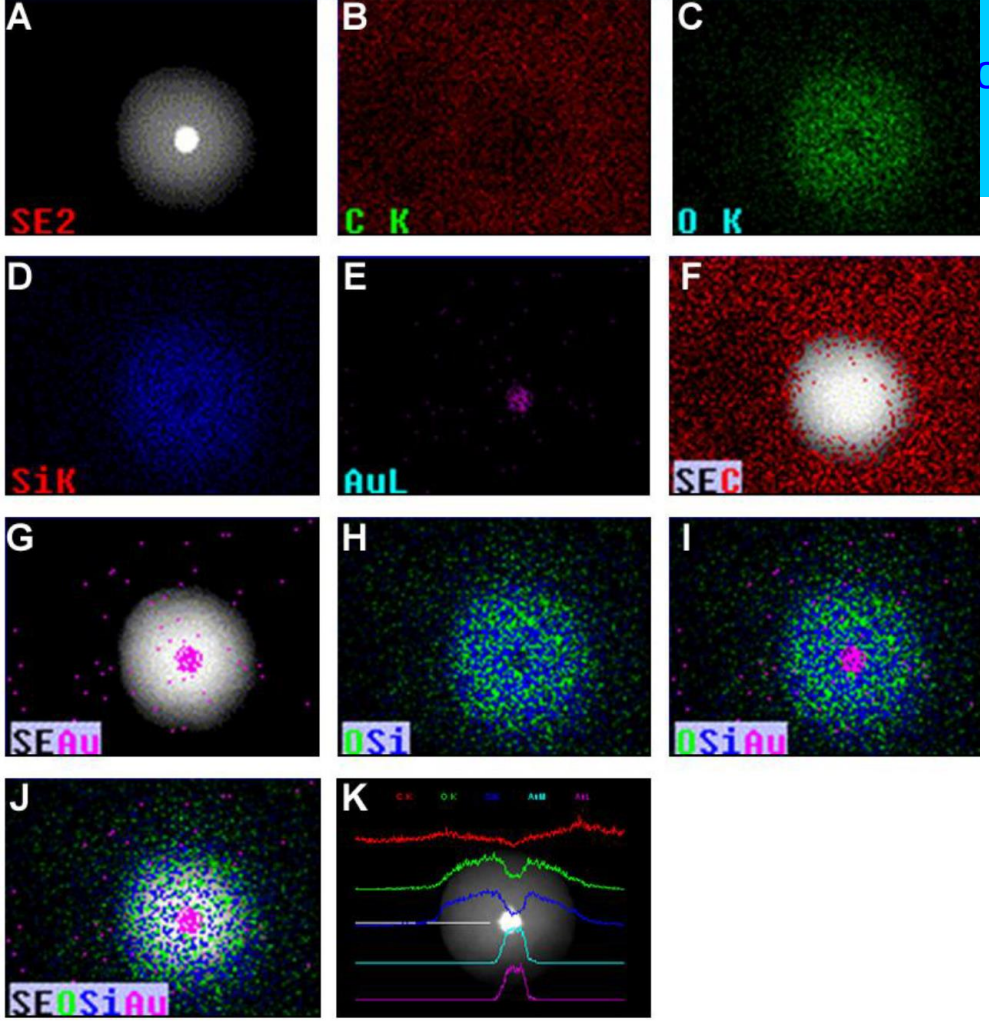


**Supplementary Figure 3 | Integration of imaging and elemental maps of a single spaser.** (**A**) STEM dark-field electron image taken with the x-ray maps. (**B**) C-K x-ray map. (**C**) O-K x-ray map. (**D**) Si-K x-ray map. (**E**) Au-L x-ray map. (**F**) Overlay of electron image with C-K X-ray (**A** and **B**). (**G**) Overlay of electron image with Au-L x-ray (**A** and **E**). (**H**) Overlay of O-K x-ray and Si-K x-ray (**C** and **D**). (**I**) Overlay of O-K x-ray, Si-K x-ray, and Au-L x-ray (**C**, **D**, and **E**). (**J**) Overlay of electron image with O-K x-ray, Si-K x-ray, and Au-M x-ray (**A**, with **C**, **D**, and **E**). (**K**) Elemental line scans across the center of this spaser (red: C-K, green: O-K, blue: Si-K, magenta: Au-L, and purple: Au-M intensities).

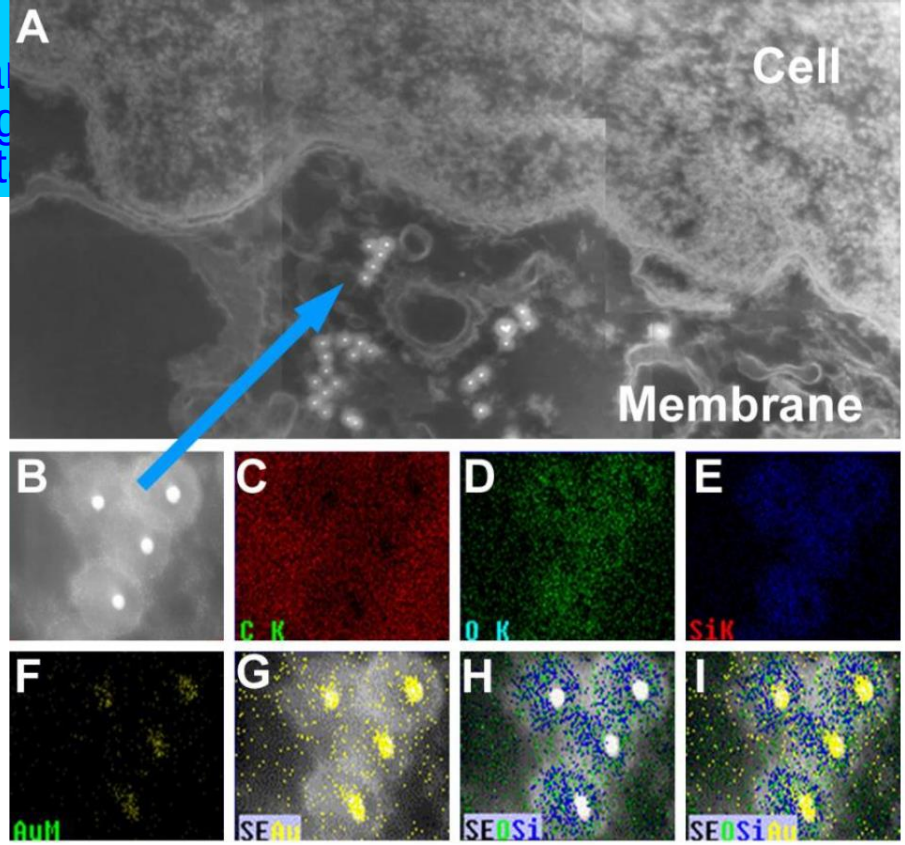


**Supplementary Figure 11 | Integration of imaging and elemental mapping of spasers in cancer cells**. **(A)** Composite of low magnification STEM dark field images spaser nanoparticles near a cell; **(B)** STEM dark field image taken with the x-ray maps. **(C)** C-K x-ray map. **(D)** O-K x-ray map. **(E)** Si-K x-ray map. **(F)** Au-M x-ray map. **(G)** Overlay of dark field image with Au-M x-ray map (**B** and **F**). **(H)** Overlay of dark field image with O-K x-ray map and Si-K x-ray map (**B, D,** and **E**). **(I)** Overlay of dark field image, O-K x-ray map, Si-K x-ray map, and Au-M x-ray map (**B, D**, **E,** and **F**). The elements with higher atomic numbers appear brighter in dark field images, while the elements with lower atomic numbers appear dark in bright field images (the contrast is reversed).

Department of Physics and Astronomy
Georgia State University
Atlanta, GA 30303-3083

# Spasers incide a Cell: Fluorescence, Electron Microscopy, and Phototermal Image

(**A-B**), Fluorescence image of breast cancer cells (MDA-MB-231) with a single spaser (**A**) and multiple (**B**) spasers. Pump parameters: wavelength 488 nm; pump pulse width 10 ns; beam diameter 20 μm; energy fluence 80 mJ/cm$^2$ (**A**), 150 mJ/cm$^2$ (**B**). Incubation time: 10 min (**A**) and 60 min (**B**). (**C**), TEM image of single and clustered spasers on a breast cancer cell (MDA-MB-231) membrane after 30 min cell incubation at 37 °C; **(D**), PT image of cancer cell labeled with spasers (false colors).

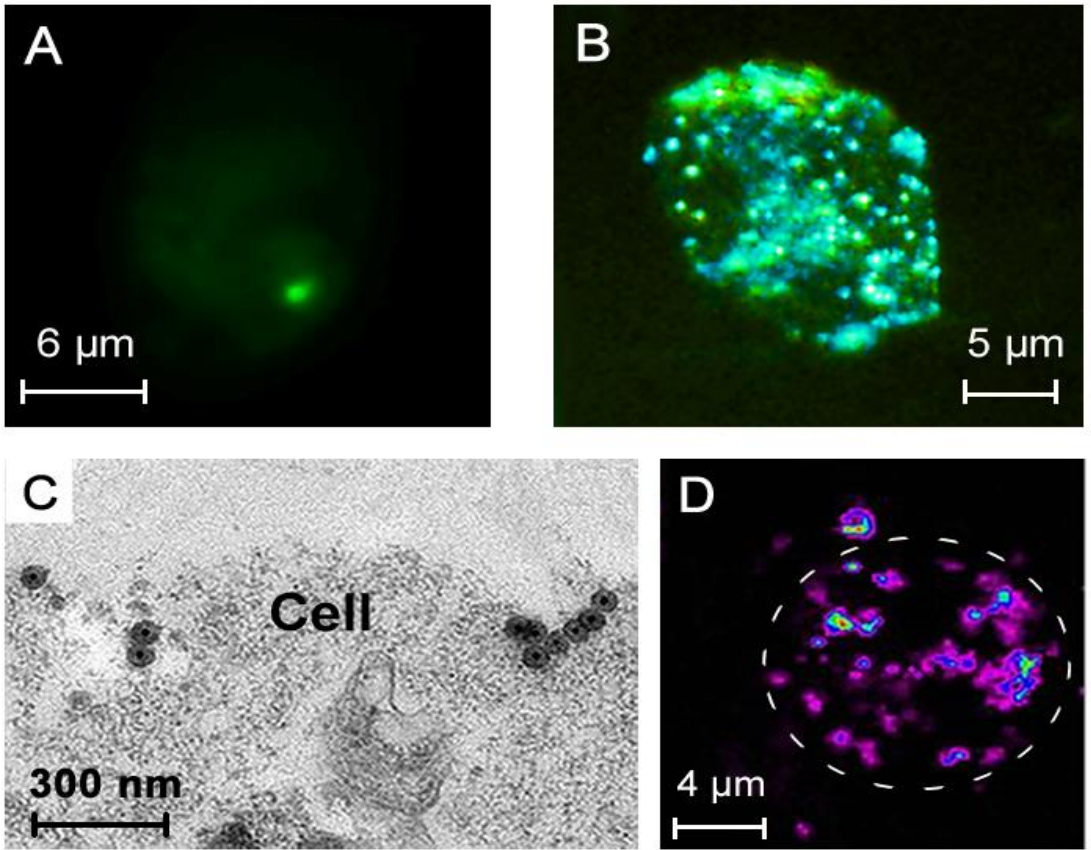

Department of Physics and Astronomy
Georgia State University
Atlanta, GA 30303-3083

# Spaser as an Efficient Biocompatible Theranostic Agent: Toxicity and Efficacy Tests

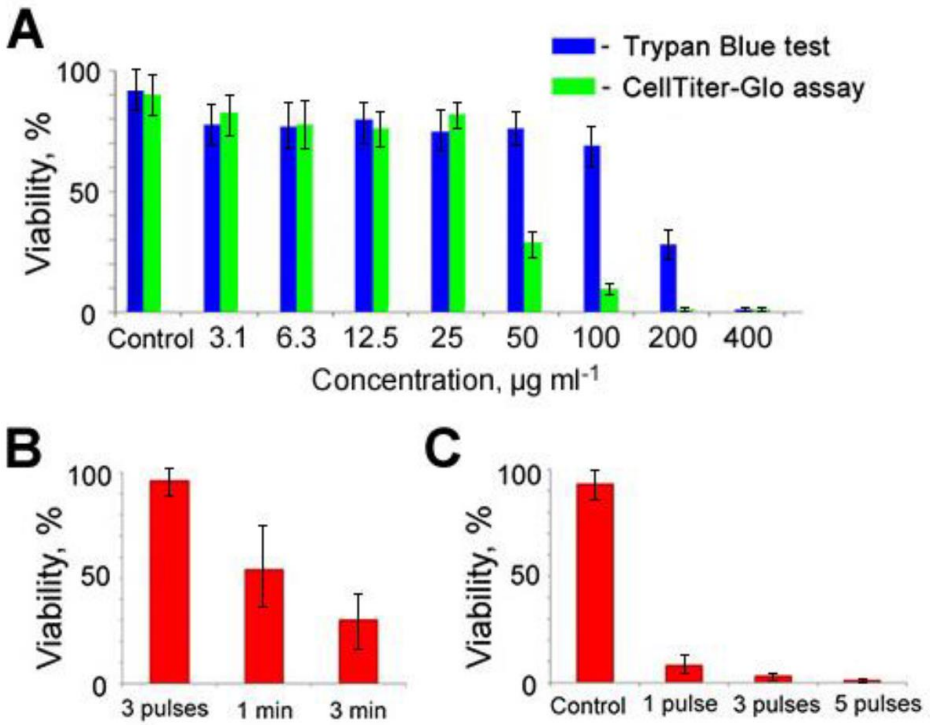


**Supplementary Figure 13 | Toxicity study**. **(A)** Cell viability tests for different spaser concentration using two various kits: Trypan Blue and Cell Titer-Glot. **(B)** Viability (Trypan Blue) test for the 3.1 μg $ml^{-1}$ concentration as a function of laser exposure time (3s [3 pulses], 1 min, and 3 min) at pulse rate of 1 Hz; **(C)** Viability (Trypan Blue) test for the 3.1 μg $ml^{-1}$ concentration as a function of laser pulse number (1, 3 and 5). It shows that even single laser pulse with a fluence of 500 mJ $cm^{-2}$ is sufficient for significant damage of cancer cells labeled by spasers. The average SD for each column is 15-20%.

Department of Physics and Astronomy
Georgia State University
Atlanta, GA 30303-3083

# Spaser as an Efficient Biocompatible Theranostic Agent: Efficacy and Selectivity Tests

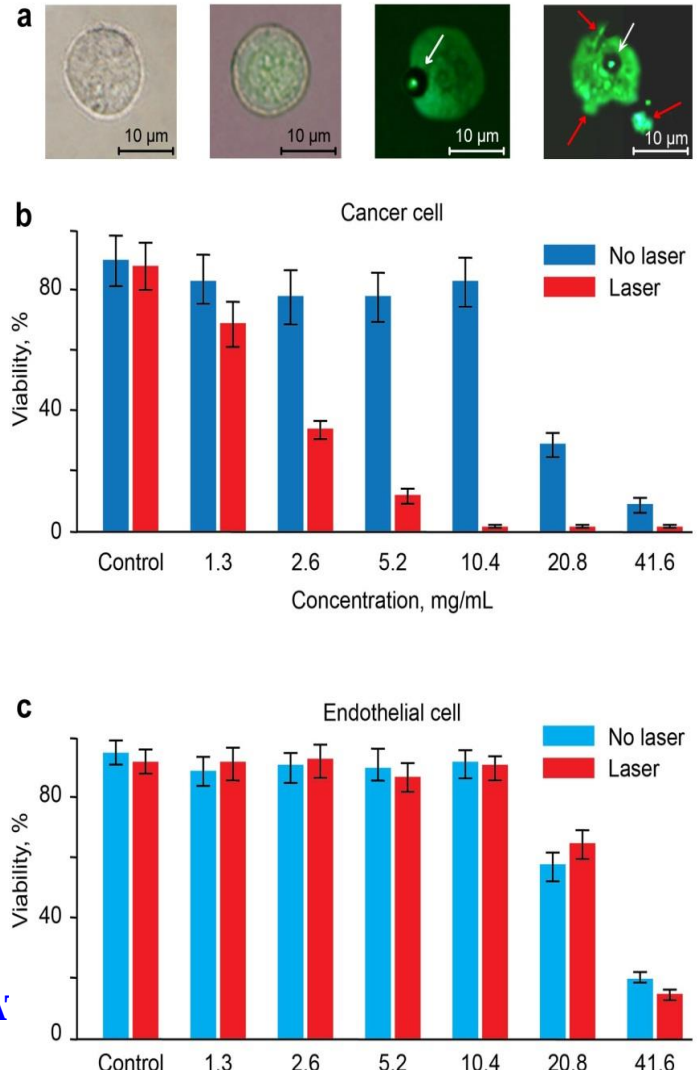


(**A**) Bright field of control cancer cell (MDA-MB-231) cell with no spasers (1), integration of fluorescent and bright field of the same cell labeled with spasers at a low concentration (2); fluorescent imaging of bubble formation (3, arrow) in a cell with a moderate spaser concentration (3); bubble formation (white arrow) leading to cell fragmentation (red arrows) at a high spaser concentration (4). (**B**) Cell viability tests for cancer cells (MDA-MB-231) at different spaser concentration using CellTiter-Glot assay before (blue) and after (red) laser irradiation (100 mJ/cm$^2$, 1 Hz, 3min). (**C**) Cell viability tests for endothelial cells (2H11) at different spaser concentrations using CellTiter-Glot assay before (blue) and after (red) laser irradiation (100 mJ/cm$^2$, 1 Hz, 3min). Standard deviations (SD) for each column are in the range of 15-20%.

Department of Physics and Astronomy
Georgia State University
Atlanta, GA 30303-3083

# Detection of Spasers and Labeled Cancer Cells *in vitro* and in Animal Model (Mouse) *in vivo*

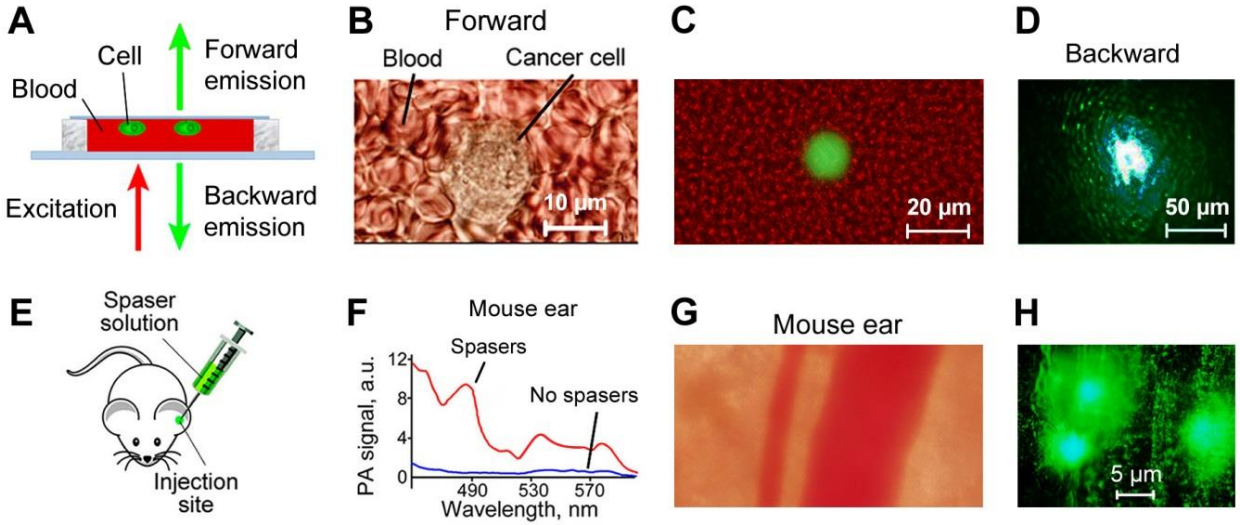


(**A**) Schematic of laser irradiation of cells in blood in slide. (**B-C**) Transmission (**B**) and combined fluorescence (**C**) image at energy fluence of 20 mJ/cm$^2$ (below the spasing threshold) of single cancer cell in human blood in slide in forward direction. (**D**) Fluorescence images of single cell in human blood at depth of 1 mm in backward direction at energy flounce of 120 mJ/cm$^2$ (above the spasing threshold). (**E**) Schematic of intradermal injection of spaser suspension into of mouse ear tissue. (**F**) PA spectral identification of spasers in ear tissue inside (red) and outside (blue) injection area using tunable optical parametric oscillator (OPO) with diameter of 15 μm and energy fluence of 20 mJ/cm$^2$. (**G- H**) Transmission (**G**) and fluorescence (**H**) images of mouse ear fragment with blood vessels and two spots with spasers. Laser pump parameters: wavelength, 488 nm**;** beam diameter: 50 μm**;** energy fluence intensity, 120 mJ/cm$^2$

Department of Physics and Astronomy
Georgia State University
Atlanta, GA 30303-3083

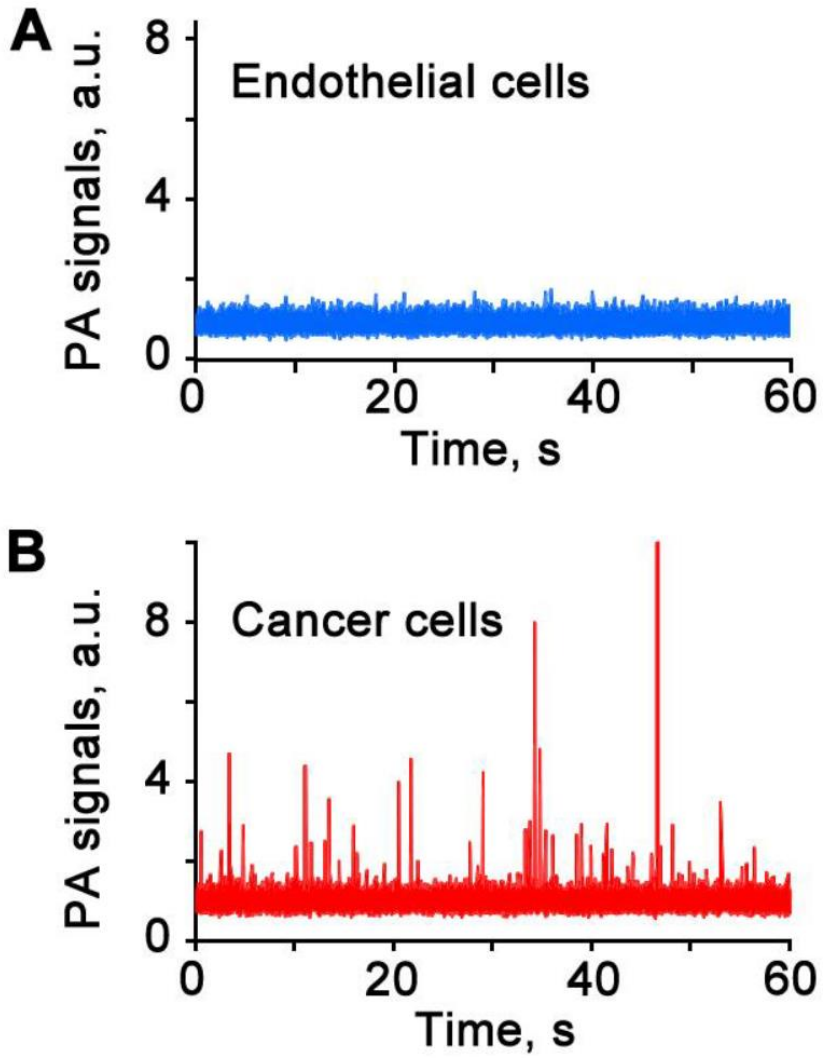


**Functionalized Spaser as a Selective Label**

**Supplementary Figure 12 | PA flow cytometry[6,7] of labeled cells *in vitro*.** PA signal traces of endothelial (**A**) and cancer (MDA-MB-231) cells (**B**) targeted by folic acid-conjugated spasers.

# The most important technological application: Information processing

P. Packan et al., in 2009 IEEE International Electron Devices Meeting (IEDM), *High Performance 32nm Logic Technology Featuring Second Generation High-K + Metal Gate Transistors (Baltimore, MD, 2009), Vol. IEDM09-662, p. 28.4.1-28.4.4*

**Abstract:**
A 32nm logic technology for high performance microprocessors is described. 2nd generation high-k + metal gate transistors provide record drive currents at the tightest gate pitch reported for any 32 nm or 28nm logic technology. NMOS drive currents are 1.62mA/um Idsat and 0.231mA/um Idlin at 1.0V and 100nA/um Ioff. PMOS drive currents are 1.37mA/um Idsat and 0.240mA/um Idlin at 1.0V and 100nA/um Ioff. The impact of SRAM cell and array size on Vccmin is reported.

**MOSFET US Patent**

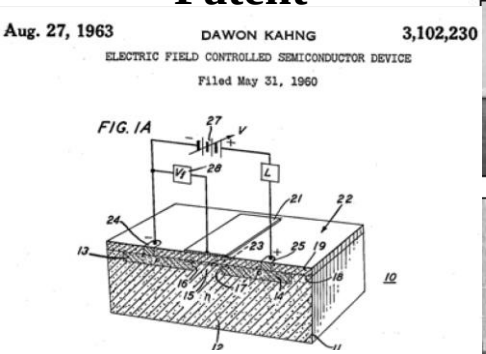


Speed ~ 100-300 GHz
Low resistance to ionizing radiation

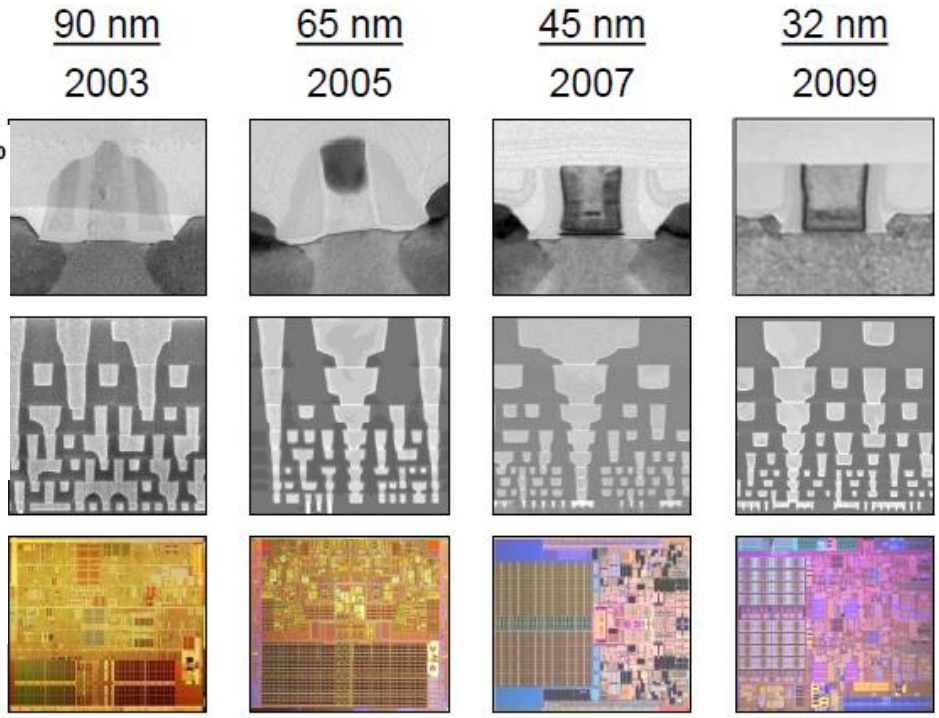


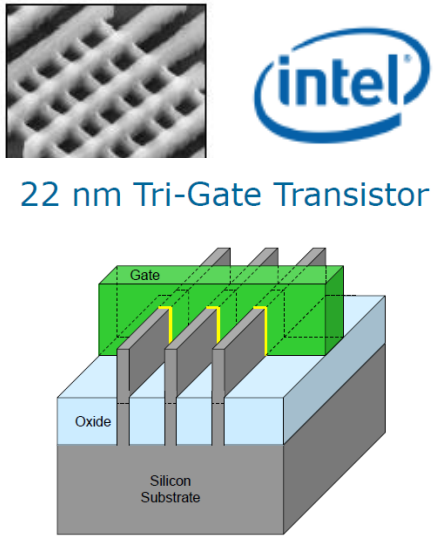


**Processor speed :**

$$f_{\max} = I_{\text{drive}} / \left( C_{\text{Intercon}} \Delta U \right) \sim 3 \text{ GHz}$$

**Transistor speed is not a limiting factor!**
**Charging the interconnects is.**

Department of Physics and Astronomy
Georgia State University
Atlanta, GA 30303-3083

Nanospaser with electric excitation ("pumping") does not exist as of today *yet*, but fundamentally it is entirely possible

**Concept of ~300 GHz processor unit with ~1% energy cost per flop**

**Today C-MOS Technology**

Electric interconnect (Copper wire)

$$\tau = RC \sim \varepsilon\sigma\frac{L^2}{r^2}$$

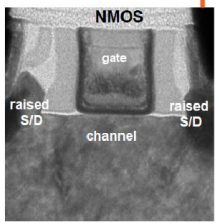


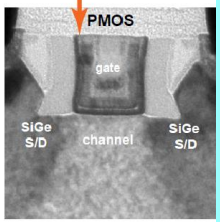


Charging time does not depend on scale

**Near-future C-MOS Technology with on-chip plasmonic interconnects**

Nanoplasmonic on-chip interconnect (Copper wire)

**Spaser pumped by transistor**

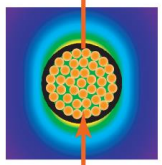

**Phototransistor** Ge

**No electric charging of interconnects!**

**C-MOS Transistors are not connected electrically**

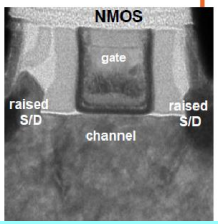


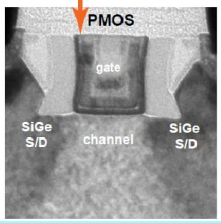


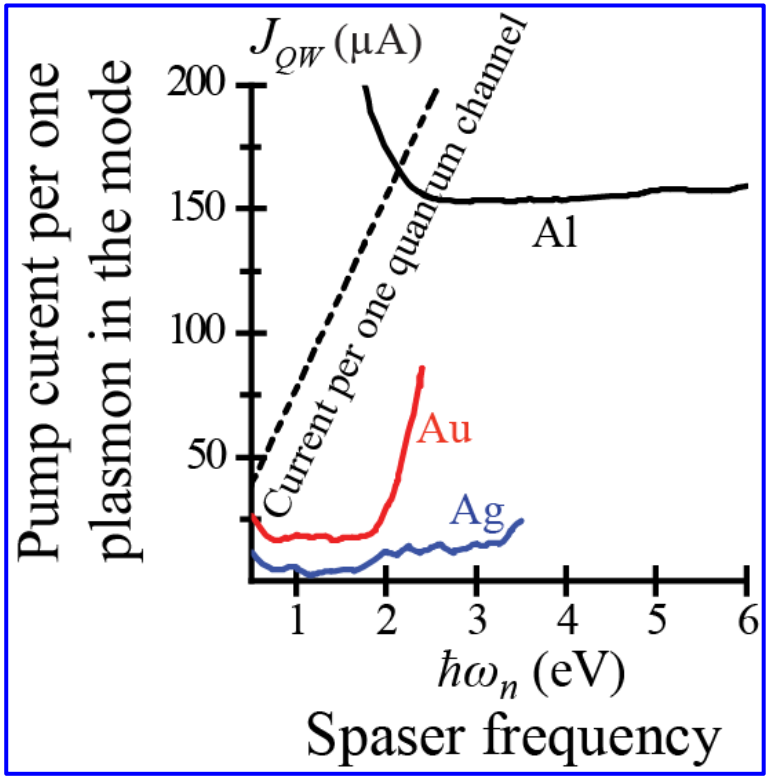


D. Li and M. I. Stockman, *Electric Spaser in the Extreme Quantum Limit*, Phys. Rev. Lett. **110**, 106803-1-5 (2013)

Department of Physics and Astronomy
Georgia State University
Atlanta, GA 30303-3083

## • CONCLUSIONS

**•Spasers are plasmonic nanolasers that have been demonstrated to generate in a wide range of optical frequencies: from near-UV to near-IR**

**•Various designs of spasers have been implemented incuding but not limited to:**

- **•metal core/gain shell**
- **•gain semiconductor nanorod over continuous metal nanofilm**
- **•metal/gain semiconductor/metal**

- **First application of spasers in explosives detection have been demonstrated**
- **Cancer diagnostics and therapeutics (theranostics) using spasers have been established**
- **For on chip communications, the spaser is the only realistic candidate as a source of optical near-field energy controlled by a transistor**

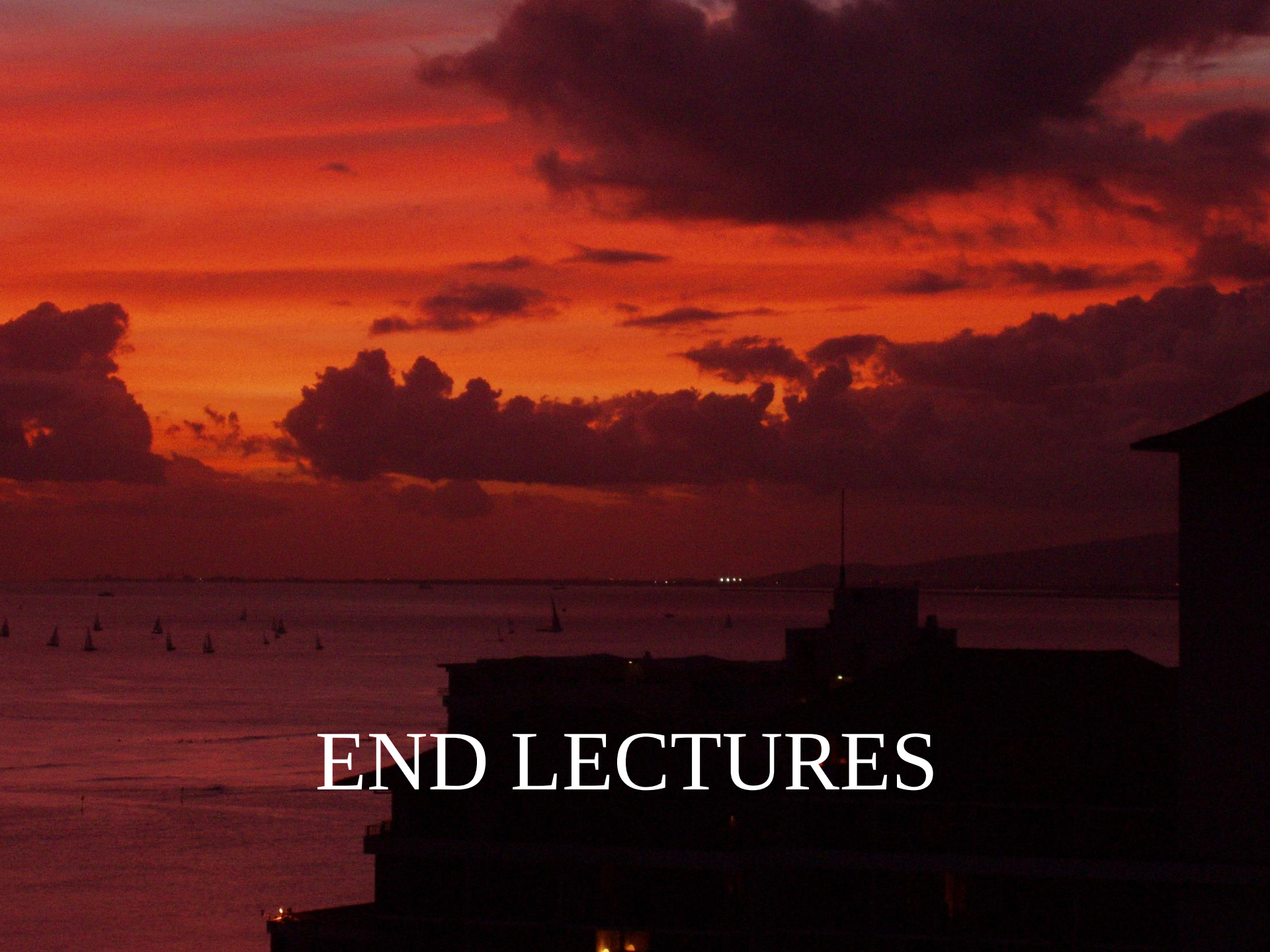
END LECTURES